2018

Stability analysis and robust control of power networks in stochastic environment

Sai Pushpak Nandanoori
Iowa State University

Stability analysis and robust control of power networks in stochastic environment

by

Sai Pushpak Nandanoori

A dissertation submitted to the graduate faculty

in partial fulfillment of the requirements for the degree of

DOCTOR OF PHILOSOPHY

Major: Electrical Engineering

Program of Study Committee:
Umesh Vaidya, Major Professor
Nicola Elia
Venkataramana Ajjarapu
Manimaran Govindarasu
Ananda Weerasinghe

The student author, whose presentation of the scholarship herein was approved by the program of study committee, is solely responsible for the content of this dissertation. The Graduate College will ensure this dissertation is globally accessible and will not permit alterations after a degree is conferred.

Iowa State University

Ames, Iowa

2018

TABLE OF CONTENTS

Page

LIST OF TABLES

Page

LIST OF FIGURES

Page

ABSTRACT

The modern power grid is moving towards a cleaner form of energy, renewable energy to meet the ever-increasing demand and new technologies are being installed in the power network to monitor and maintain a stable operation. Further, the interactions in the network are not anymore localized but take place over a system, and the control centers are located remotely, thus involving control of network components over communication channels. Further, given the rapid integration of wind energy, it is essential to study the impact of wind variability on the system stability and frequency regulation. Hence, we model the unreliable and intermittent nature of wind energy with stochastic uncertainty. Moreover, the phasor measurement unit (PMU) data from the power network is transmitted to the control center over communication channels, and it is susceptible to inherent communication channel uncertainties, cyber attacks, and hence, the data at the receiving end cannot be accurate. In this work, we model these communication channels with stochastic uncertainties to study the impact of stochastic uncertainty on the stability and wide area control of power network. The challenging aspect of the stability analysis of stochastic power network is that the stochastic uncertainty appears multiplicative as well as additive in the system dynamics.

The notion of *mean square exponential stability* is considered to study the properties of stochastic power network expressed as a networked control system (NCS) with stochastic uncertainty. We develop, necessary and sufficient conditions for mean square exponential stability which are shown in terms of the input-output property of deterministic or nominal system dynamics captured by the *mean square* system norm and variance of the channel uncertainty. For a particular case of single input channel uncertainty, we also prove a fundamental limitation result that arises in the mean square exponential stabilization of the continuous-time linear system. Overall, the theoretical contributions in this work generalize the existing results on stability analysis from discrete-time linear systems to continuous-time linear systems with multiplicative uncertainty. The stability

results can also be interpreted as a small gain theorem for continuous-time stochastic systems. Linear Matrix Inequalities (LMI)-based optimization formulation is provided for the computation of mean square system norm for stability analysis and controller synthesis.

An IEEE 68 bus system is considered, and the fragility of the decentralized load-side primary frequency controller with uncertain wind is shown. The critical variance value is shown to decrease with the increase in the cost of the controllable loads and with the rise in penetration of wind farms. Next, we model the power network with detailed higher order differential equations for synchronous generator (SG), wind turbine generator (WTG). The network power flow equations are expressed as algebraic equations. The resultant system is described by a detailed higher order nonlinear differential-algebraic model. It is shown that the uncertainty in the wind speed appears multiplicative in the system dynamics. Stochastic stability of such systems is characterized based on the developed results on mean square exponential stability. In particular, we study the stochastic small signal stability of the resultant system and characterize the critical variance in wind speeds, beyond which the grid dynamics becomes mean square unstable.

The power fluctuations in the demand side and intermittent generation (from renewables) cause frequency excursions from the nominal value. In this context, we consider the controllable loads which can vary their power to achieve frequency regulation based on the frequency feedback from the network. Two different load-side frequency controller strategies, decentralized and distributed frequency controllers are studied in the presence of stochastic wind. Finally, the time-domain simulations on an IEEE 39 bus system (by replacing some of the traditional SGs with WTG) are shown using the wind speeds modeled as stochastic as well as actual wind speeds obtained from the wind farm located near Ames, Iowa. It can be seen that, with an increase in the penetration of wind generation in the network, the network turns *mean square unstable*. Furthermore, we capture the mean square unstable behavior of the power network with increased penetration of renewables using the statistics of actual wind analytically and complement them through linear and nonlinear time domain simulations.

Finally, we analyze the vulnerability of communication channel to stochastic uncertainty on an IEEE 39 bus system and design a wide area controller that is robust to various sources of uncertainties that arise in the communication channels. Further, the PMU measurements and wide area control inputs are rank ordered based on their criticality.

CHAPTER 1. INTRODUCTION

1.1 Relevance of the Problem and Literature Review

The modern electric power grid is a perfect example of a cyber-physical system (CPS). The generators, loads, transmission lines constitute the physical part of CPS. The cyber components consist of a control center, sensors, actuators, and communication links connecting the physical part to the cyber part of the power network. This CPS paradigm combined with advancement in sensing and actuation technologies are increasingly viewed as critical components for improving the reliability and operability of modern power grid. For example, Phasor Measurement Units (PMUs) are playing a pivotal role in real-time monitoring and feedback control of power system (refer De La Ree et al. (2010)). The future power grid consists of renewable energy sources to meet the increasing demands and communication becomes important for the monitoring, control and stable operation of the power grid as discussed in Wang et al. (2011).

The problem of power system stability with traditional synchronous generation is extensively studied in Anderson and Fouad (2008); Sauer and Pai (1998a). Given the rapid integration of variable and intermittent wind energy, one needs to revisit this analysis to investigate the problem of power system stability. The presence of wind generation in the power system affects the grid in two crucial ways. First, the dynamics of a doubly-fed induction based wind generator differs significantly with the dynamics of a synchronous generator (refer Pulgar Painemal (2011)). Second, the input to the wind turbine generator, wind speeds is a stochastic resource in contrast to the controllable fuel source near a conventional generator.

Renewable energy sources such as wind and solar are free and abundant resources, but a cost is paid for their variability. The intermittent and unreliable nature of these renewables has to be compensated with other energy sources or demand response strategies to maintain power balance and thereby frequency regulation in the power network. For example, one can have questions like

how large a variation in wind velocities can be tolerated under normal operating conditions before it becomes unstable? This question is in contrast with transient stability analysis of the power grid where we determine if a power system can reach a post-fault stable state after losing a transmission line or a synchronous generator.

Impact of wind generation on the power system stability has been studied in different directions. In Slootweg and Kling (2003a), the authors have studied the effect of wind generation on power system oscillations by observing the movement of eigenvalues when the amount of wind generation is increased. Similarly, the authors in Gautam et al. (2009) investigate the transient and small signal stability of the power network with increased wind generation. Further, several probabilistic (refer Pan et al. (2016); Wang et al. (2016); Xu et al. (2005); Bian et al. (2016); Vicente et al. (2017); Rueda et al. (2009); Yuan et al. (2015)) and analytical methods (refer Bu et al. (2012)) have been reported in the literature which studies the effect of wind uncertainties on the small signal stability of the power network. A literature survey on various notions of stochastic stability of power networks can be found in Jiang et al. (2016).

By modeling the mechanical power input to the wind turbine as random, the authors in Yuan et al. (2015) have studied the stochastic small signal stability of the power network based on Ito calculus. In Wang et al. (2016), the authors model the wind speed as stochastic and propose an analytical method to analyze the probabilistic small signal stability of the power system. Considering uncertainty in demand as well as generation, Xu et al. (2005) gives a Monte Carlo based probabilistic small signal stability analysis using eigenvalue analysis. Using extensive Monte Carlo time-domain simulations, the stochastic transient stability of an islanded power network with random wind generation and random load models is studied under the case of contingencies in Vicente et al. (2017).

One of the important components of the smart grid vision is the active participation of loads for improved operation and performance of network power system at different time scales as discussed in staff report (2006). The technology is maturing to the point where the smart grid vision can be realized for actively controlling the loads to absorb not only the long-term variability or

uncertainty from renewable power generation but also short-term fluctuations. Moving away from the traditional way of onsetting the power imbalances in the network, in this work, we use the cost-effective, fast-acting resource, the controllable loads to compensate the power mismatch and regulate the frequency. The application of load-side control for frequency regulation falls in the latter category. With the potential benefits of active load control, there are increased research efforts towards the development of systematic analytical methods and optimization-based tools for distributed load control. Most of the literature on this topic primarily focus on stability properties of control algorithms developed for load-side frequency regulation and can be found in Trudnowski et al. (2006); Short et al. (2007); Molina-Garcia et al. (2011); Andreasson et al. (2013); Namerikawa and Kato (2011); Zhao et al. (2015). The availability of controllable loads and recent advancements in the communication between these devices and the system operator makes it a right choice for frequency regulation without trading off the end-user quality of service (refer Callaway and Hiskens (2011); Mathieu et al. (2013); Zhao et al. (2014a); Short et al. (2007); Donnelly et al. (2010); Zhang et al. (2013); Bashash and Fathy (2013)).

A primary frequency controller that utilizes controllable loads to regulate the frequency in the network is designed by Zhao et al. (2014b). In particular, Zhao et al. (2014b) proves the asymptotic stability of the primal-dual gradient system leading to the decentralized algorithm for load-side frequency control. The relevant literature on the topic of load-side frequency regulation primarily focus on stability properties of control algorithms developed as seen in Trudnowski et al. (2006); Short et al. (2007); Molina-Garcia et al. (2011); Andreasson et al. (2013); Namerikawa and Kato (2011); Zhao et al. (2015). In the absence of uncertain wind, several load-side primary frequency controller strategies are proposed in the literature. Discussion on the design of a decentralized load-side primary frequency controller can be found in Zhao et al. (2014a); Molina-Garcia et al. (2011); Trudnowski et al. (2006); Donnelly et al. (2010), optimal load control with neighborhood communication in Mallada et al. (2017), distributed control in Fan (2012); Andreasson et al. (2014, 2013); Dörfler et al. (2016), hierarchical distributed control in Lian et al. (2012) and a detailed survey on existing controllers is given in Shayeghi et al. (2009). Furthermore, it is important to

notice that the performance of the load-side frequency controller in the presence of stochastic wind is still an open problem.

The advancement in PMU technology leads to their wide usage for real-time monitoring and feedback control in the power system. Algorithms for real-time angle and voltage stability monitoring of network power system using high-resolution PMU data are proposed in Liu et al. (1994); Yan et al. (2011); Dasgupta et al. (2013, 2015). One important power system problem from CPS viewpoint of the power system is the control of inter-area oscillations as discussed in Chakrabortty and Khargonekar (2013); Singh et al. (2015); Drfler et al. (2014). Damping of inter-area oscillations requires exchanging PMU measurements over communication channels across wide areas for active feedback control (refer Terzija et al. (2011)). PMU devices measure the current and voltage phasor information from the buses at sample rates of up to 60 Hz. PMU data is a time synchronizing signal as per standards specified in IEEE C37.118 (refer Martin et al. (2014)). The packets of PMU data are sent through the TCP/IP communication channel to the control center for improved state estimation, monitoring, protection, and control.

Being aware of the potential benefits of the CPS paradigm, it is essential to analyze the vulnerability of cyber components against possible natural causes, calamities, and also intentional malicious activities. The reliability of cyber components can be severely limited by communication channel uncertainty in the form of packet drop, random delay, quantization error, sensors/actuators failure from natural causes, and most importantly intentional and malicious attack on cyber components. There are ongoing research efforts to provide guidelines for the quality and reliability of the data that need to be transmitted over the communication channel for feedback control. The stability of the power system can be affected in several ways such as through a cyber attack, natural faults, communication channel uncertainties and many others. Moreover, it is crucial in maintaining the voltage magnitude and frequency within the prescribed limits for smooth and stable operation of the power network. These scenarios can be studied with the system-theoretic framework by modeling the communication channels and renewable energy sources as stochastic. The results presented in this report are a step towards this direction.

In what follows, we discuss the approach we take to study the stability analysis of continuous-time stochastic power network.

1.2 Power System as a Networked Control System

The problem of stability analysis of continuous-time stochastic power network is studied by taking the approach of a networked control system (NCS). This NCS is a closed-loop power network with measurements and control signals traversing through the lengthy communication channels connecting the cyberspace and physical space. Besides, NCS can be easily modified by adding sensors, actuators, and controllers to them. Most of the systems with stochastic uncertainty can be represented in the general form of NCS, and the framework developed in this work can study the stochastic stability of NCS with uncertainty. In particular, we look at the problem of stochastic small-signal stability with renewable energy integration where the wind speeds are modeled stochastic, and the wide area control problem in power network with communication channel uncertainty.

The wind speeds to the wind turbine are modeled stochastic, and the stochastic uncertainty is shown to appear as a multiplicative parametric uncertainty in the system dynamics. Detailed higher order nonlinear differential-algebraic model is used to model the resultant system. It is shown that the stochastic uncertainty in the wind speeds appears parametric in the linearized power system dynamics. This stochastic power network is expressed as a networked control system with deterministic part of the system as a nominal system and uncertain wind speed in the feedback to the nominal system.

The problem of damping inter-area oscillations with wide area control of power network in the presence of communication channel uncertainty is expressed as a linear system with wide area control inputs and stochastic uncertainty in the measurements/communication. The resultant system is expressed as a networked control system by considering the mean of the uncertainties in the nominal system and zero mean uncertainties in the feedback. The measurements and control signals are in the form of packets of information. In the framework of an NCS, the authors in Singh et al. (2015) looks at stability analysis and control of inter-area oscillations in a power system where

the communication channel is modeled with time-delay and data dropouts. The wide area control of the power network in the presence of delayed communication channels is discussed in Wang et al. (2012); Chaudhuri et al. (2011); Dotta et al. (2009); Chaudhuri et al. (2004); Naduvathuparambil et al. (2002). More literature in this area can be found in the references within the above-cited papers. In contrast with the existing literature, it is important to emphasize that, we study the stability of continuous-time linear power network where the stochastic uncertainty appears multiplicative in the dynamics.

In the next section, we provide the literature survey and introduction on the stochastic stability analysis of continuous-time linear stochastic networked systems.

1.3 Networked Control System with Stochastic Uncertainty

The problem of stability analysis and control synthesis of systems in the presence of uncertainty has a rich, long history of literature. The literature in this area can be broadly divided into two parts. Classical robust control literature addresses this problem using norm bounds on uncertainty as discussed in Dullerud and Paganini (2013); Skogestad and Postlethwaite (2007). In this work, we study the robust control problem for continuous-time linear dynamics, where the uncertainty is modeled as a stochastic random variable. The stochastic uncertainty is assumed parametric and hence enters multiplicatively in the system dynamics. The analysis and control problem with stochastic multiplicative uncertainty has received renewed attention lately as a model for NCS with communication uncertainty.

Some of the classical results involving stochastic stability analysis and control problems are presented in Has'minskiĭ (1980). The work by Wonham (1967) is one of the earliest literature on this topic involving continuous-time dynamics with multiplicative measurement and control noise. Willems and Blankenship (1971) derive frequency domain-based stability criteria for continuous-time LTI system with state-dependent noise. Mclane (1971) study the LQR problem for continuous-time linear systems with state-dependent noise entering only in the state dynamics. Willems and Willems (1976) study mean square exponential stability analysis and static state feedback control

design for stochastic systems with state-dependent control noise. Also, Willems and Willems (1983) developed robust stabilization results for continuous and discrete-time uncertain LTI systems using state feedback control.

El Bouhtouri and Pritchard (1992, 1993) propose input-output operator approach for characterizing the stability radii and maximizing the stability radii using state feedback. Bernstein (1987) provides a comparison of necessary and sufficient conditions with dynamic and static output feedback controller involving stochastic multiplicative uncertainty, and deterministic norm bounded uncertainty respectively. Bernstein (1987) also provides a comprehensive survey of literature on this topic of stochastic stability analysis and control. Ghaoui (1995) gives a linear matrix inequality (LMI)-based mean square exponential stability result using static state feedback control for continuous-time LTI systems with state-dependent noise. Using input/output operator approach, a small-gain theorem for stochastic systems with state-dependent noise only affecting the state dynamics has been developed in Dragan et al. (1997). In contrast to these references, we develop mean square exponential stability analysis and synthesis results with stochastic multiplicative uncertainty, both at the input and output side of the plant (for example, the plant can be a power network). The problem formulation is general enough to address problems involving not only input-output channel uncertainty but also parametric stochastic uncertainty.

There is also extensive literature on this topic for systems involving nonlinear dynamics with multiplicative stochastic uncertainty. For example, authors in Deng et al. (2001); Deng and Krstić (2000) study the stability analysis and stabilization of nonlinear systems for stochastic uncertainty of unknown covariance by generalizing the results from Willems and Blankenship (1971); Wonham (1967) and Ghaoui (1995) to nonlinear dynamics. Lyapunov function-based approach for stability analysis and stabilization for a nonlinear stochastic system is proposed in Florchinger (1995). Generalization of stochastic positive real lemma for stochastic stability analysis and stabilization of nonlinear system in Lure form are addressed in Diwadkar et al. (2015). The references in the papers mentioned above further provide more literature review on stochastic system stability analysis.

Research activities in the area of NCS lead to the renewed interest in the analysis and design of systems with multiplicative uncertainty (refer L. Schenato and B. Sinopoli and M. Franceschetti and K. Poolla and S. Sastry (2007)). In particular, network systems with erasure or time-delay uncertainty in the input or output communication channel can be modeled as a system with multiplicative uncertainty. Issues related to fundamental limitations for stabilization and estimation of networked systems, i.e., largest tolerable channel uncertainty are addressed in Elia (2005); L. Schenato and B. Sinopoli and M. Franceschetti and K. Poolla and S. Sastry (2007); Tatikonda and Mitter (2004); N.C. Martins, M.A. Dahleh, and N.Elia (2006); N. Elia and J. N. Eisenbeis (2011); V. Gupta and B. Hassibi and R. M. Murray (2007). Fundamental limitation results are extended to nonlinear systems in Diwadkar and Vaidya (2013); Vaidya and Elia (2010). Similarly, the problem of fundamental limitations in linear and nonlinear consensus networks with stochastic interactions among network components are addressed in Diwadkar and Vaidya (2011); Vaidya and Elia (2012); Diwadkar et al. (2014); Diwadkar and Vaidya (2016); Elia et al. (2013); Diwadkar and Vaidya (2014). A small gain theorem for MIMO linear systems with multiplicative noise in the mean square sense is given in Lu and Skelton (2002). Bamieh (2012) considers the discrete-time system with correlated stochastic uncertainties and develops necessary, sufficient conditions for mean square exponential stability expressed in terms of the spectral radius of input-output linear matrix operator. However, all the above results are developed for discrete-time network dynamical systems.

The results in this work are inspired from Elia (2005) and can be viewed as a continuous-time counterpart of the discrete-time results developed in Elia (2005). Following Elia (2005), we provide a robust control-based framework for the analysis and synthesis of continuous-time linear networked systems with stochastic channel uncertainties. The developed framework is more general, and we apply it to study the mean square exponential stability of the power network with stochastic uncertainty.

The contribution of this work is summarized in the following section.

1.4 Contributions

In this work, we consider two different problems of interest in the power system community. First, the problem of stochastic small-signal stability and the performance of a load-side primary frequency controller in the presence of stochastic wind is considered. Second, the wide area control problem in the presence of measurement and control input uncertainties. Both these problems are formulated in the networked control system form, and the stochastic stability analysis for continuous-time linear networked systems is developed in this work. The challenging part of the investigation is that the stochastic uncertainty appears multiplicative in the system dynamics (i.e., uncertainty multiplies the system states). Necessary and sufficient conditions are developed for mean square exponential stability which is expressed in terms of the input-output property of deterministic or nominal system dynamics captured by the *mean square* system norm and variance of channel uncertainty. The stability results can also be interpreted as a small gain theorem for continuous-time stochastic systems. Linear Matrix Inequalities (LMI)-based optimization formulation is proposed for the computation of the mean square system norm. The LMI-based optimization formulation is used for the synthesis of a dynamic controller robust to input and output measurement noise. For a particular case of single input channel uncertainty, we propose a fundamental limitation result that arises in the mean square exponential stabilization of the continuous-time linear system. Furthermore, fundamental limitation result for mean square exponential stabilization expressed in terms of the unstable eigenvalues of the open-loop system is derived. By adopting density-based deterministic approach involving Fokker-Planck equation (refer Lasota and Mackey (1994)), we avoid the technical challenges associated with dealing with the stochastic calculus of stochastic differential equations. Overall, the theoretical contributions in this work generalize the existing results on stability analysis and controller synthesis from discrete-time linear systems given in Elia (2005) to continuous-time linear systems with multiplicative uncertainty.

We consider the problem of load-side frequency control in the power network with two different models. The first one considers a lower order model where the voltages corresponding to the renewable buses are modeled stochastically. We argue that renewable energy resources in the form

of wind and solar are the potential source of parametric uncertainty in network power system, where stochasticity in renewable energy resources will lead to stochastic bus voltages. We extended the primal-dual gradient system corresponding to the optimal load control problem developed in Zhao et al. (2014b) to incorporate the stochastic parametric uncertainty which appears multiplicative as well as additive. Developed mean square exponential stability framework is applied to study the stochastic stability of the networked power system and the critical variance of parametric stochastic uncertainty above which the system is mean square unstable is determined. In particular, we show the fragility of decentralized load-side primary frequency control algorithm proposed in Zhao et al. (2014b) in the presence of stochastic renewable energy sources. More specifically, we considered the IEEE 68 bus system and show that the decentralized load-side primary frequency control given in Zhao et al. (2014b) is extremely fragile to stochastic fluctuations in bus voltages corresponding to the renewables. Furthermore, we show that with an increase in the cost of the controllable loads, the value of the critical variance above which the system is unstable decreases. Furthermore, the critical variance value of Gaussian uncertainty also decreases with the increase in the penetration of the renewable energy resources in the power network. Finally, we propose a robust load-side primary frequency control algorithm to overcome the fragility of the decentralized control.

Next, we consider a detailed higher-order model of the power network with differential equations of synchronous machines, doubly fed induction generators (DFIG) as well as algebraic states at the generators and network power flow equations are considered. The input to the DFIGs, the intermittent and unreliable nature of wind speeds is modeled stochastic rather than the bus voltages. A load-side primary frequency controller is employed to regulate the frequency in the network in the presence of stochastic wind. The performance of the load-side primary frequency controller in the stochastic environment is studied on an IEEE 39 bus system. In particular, a discussion is made on the decentralized and control with neighborhood communication load-side primary frequency controller strategies with the stochastic wind. Furthermore, we identify the maximum allowable penetration in the wind generation while maintaining the stochastic small-signal stability using the actual wind speed data monitored near Ames, Iowa.

We further study the vulnerability of the power network to uncertainties in sensors and actuators such as PMUs and FACTS devices. The Gaussian uncertainty appears multiplicative in the power system dynamics which makes the analysis and control design challenging. In this scenario, the problem of designing a robust wide area control for damping the inter-area oscillations in a power network (with stochastic uncertainty) is studied. The power network with various sources of uncertainty is modeled as an NCS with stochastic uncertainty. The developed system theoretic framework is applied to analyze resiliency and design of robust mitigation strategies against vulnerabilities that arise from the cyber component of the power system. The framework allows us to characterize this loss of performance precisely and identify the critical value of stochastic uncertainty beyond which system losses stability. One of the unique features of our proposed modeling framework is that the stochastic uncertainties enter both additive and multiplicative in the system dynamics. The multiplicative nature of stochastic uncertainty allows us to use this framework to analyze vulnerabilities that appear parametric in the system dynamics such as a change in network topology or stochasticity in system parameters. Analytical bounds for the maximum tolerable variance for the noise in the communication channel without losing the stochastic stability of the network are computed. Our theoretical framework is also used to determine the most critical measurement/control input that can tolerate the least amount of noise variance. We further provide LMI-based optimization formulation to design a controller robust to communication channel noise. Simulation results are presented for IEEE 39 bus system whose communication channel is modeled as a Gaussian channel, and the PMU measurements are rank ordered based on their criticality.

1.5 Organization of this Report

This report is organized in the following way. We have presented the stochastic model of the power network in Chapter 2. Specifically, this chapter consists of a power network model with renewables modeled as stochastic and two different load-side primary frequency controller architectures are discussed. Chapter 3 consists of a power network model with stochastic uncertainty in the communication channels. In Chapter 4, we provide the theoretical framework on stability

analysis and controller synthesis of continuous-time linear stochastic networked systems to tackle the problems discussed in Chapter 2 and Chapter 3. The application of the developed framework to study the load-side frequency algorithms with uncertainty in renewables modeled in bus voltages is given in Chapter 5. In Chapter 6, we discuss the performance of the load-side primary frequency controller in the presence of stochastic wind and identify the maximum allowable wind generation in a given IEEE 39 bus system. The problem of wide area control in the presence of communication channel uncertainties has been addressed in Chapter 7 by applying the developed framework. Finally, we conclude this report in Chapter 8 by summarizing the results.

CHAPTER 2. STOCHASTIC UNCERTAINTY MODELING IN POWER NETWORKS

In this chapter, we show how we can model the power network with stochastic uncertainty and represent it in NCS form. Because of renewable integration into the grid, the intermittent and unreliable nature of clouds formation and wind speeds results in an uncertain generation at a solar farm or a wind farm (see Figure 2.1). In particular, we are interested in stochastic uncertainty

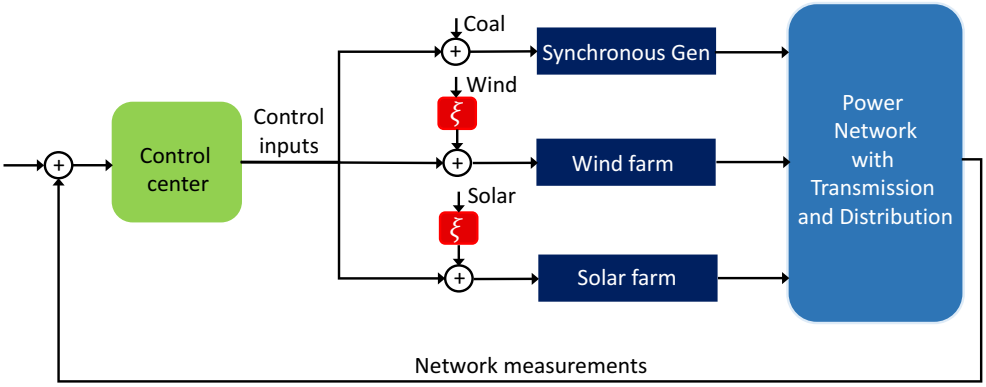

Figure 2.1 Power network with stochastic generation from solar and wind.

arising due to intermittent and unreliable nature of renewables and due to inherent communication channel uncertainties or because of faulty sensors and actuators. First, we consider the power network with wind farms and derive the stochastic power network model.

2.1 Modeling of Power Network with Uncertain Wind

Our primary objective is to study how the variability of wind affects the stability of a power system. To that end, we begin with a differential-algebraic system description of an entire power system. We adopt the *multi-machine power system model* from Pulgar Painemal (2011)[Chapter 4] for the same. Classically, the power network consists of synchronous generators, and we augment

it with Type-C wind turbines that are doubly-fed induction machines. The choice of Type-C, as opposed to others, is solely motivated by their popularity in the modern power system as described in Pulgar Painemal (2011). Our model and notation mirror that in Pulgar Painemal (2011).We assume at any bus, either a synchronous generator (SG) or a wind turbine generator modeled as a doubly-fed induction generator (DFIG) is available. A detailed discussion of types of wind turbine generators, their advantages and setbacks can be found in Pulgar Painemal (2011).

Let n_b be the number of buses in the power network with n_s synchronous generators and n_d doubly-fed induction generators. We only allow at most one generator to supply power at each bus. It can either be a *synchronous generator* (SG) or a *doubly-fed induction generator* (DFIG). Further, $V_i e^{j\theta_i}$ denote the (per phase) voltage at bus i. In the following, we describe the description of DA equations for SGs, DFIGs, and network algebraic equations. The DA model presented here is based on (Pulgar Painemal, 2011, Chapter 4) and one can refer (Pulgar Painemal, 2011, Chapter 4) for a detailed description of the model. We append the modeling of frequency dependent controllable and uncontrollable loads, frequency insensitive loads to the DA system and model the wind speeds to the DFIG as stochastic. We begin with the description of the dynamic model at SGs.

2.1.1 The Synchronous Generator at Node i

We utilize the so-called *two-axis* SG model as given in Sauer and Pai (1998b); Pulgar Painemal (2011). Its DAE description is given below.

$$\begin{aligned}\dot{x}_{SG_i} =& f_{SG_i}(x_{SG_i}, y_{SG_i}),\\ 0 =& g_{SG_i}(x_{SG_i}, y_{SG_i}),\end{aligned}$$

where

$$\begin{aligned}x_{SG_i} &= \begin{bmatrix} E'_{q_i} & E'_{d_i} & \delta_i & \omega_i & E_{fd_i} & R_{f_i} & V_{R_i} & P_{m_i}\end{bmatrix}^\top,\\ y_{SG_i} &= \begin{bmatrix} I_{d_i} & I_{q_i}\end{bmatrix}^\top,\\ T_{m_i} &= P_{m_i}\frac{\omega_s}{\omega_i},\end{aligned}$$

$$f_{SG_i} = \begin{pmatrix} \frac{1}{T'_{d0_i}}(-E'_{q_i} - (X_{d_i} - X'_{d_i})I_{d_i} + E_{fd_i}) \\ \frac{1}{T'_{q0_i}}(-E_{d_i} + (X_{q_i} - X'_{q_i})I_{q_i}) \\ \omega_i - \omega_s \\ \frac{\omega_s}{2H}(T_{m_i} - E_{d_i}I_{d_i} - E_{q_i}I_{q_i}) \\ \frac{1}{T_{E_i}}(-K_{E_i}E_{fd_i} + V_{R_i}) \\ \frac{1}{T_{F_i}}(-R_{f_i} + \frac{K_{F_i}}{T_{F_i}}E_{fd_i}) \\ \frac{K_{A_i}}{T_{A_i}}\left(-\frac{V_{R_i}}{K_{A_i}} + R_{f_i} - \frac{K_{F_i}}{T_{F_i}}E_{fd_i} + (V_{ref_i} - V_i)\right) \\ \frac{1}{T_{G_i}}(\omega_s - \omega_i) \end{pmatrix},$$

$$g_{SG_i} = \begin{pmatrix} -E'_{q_i} + X'_{d_i}I_{d_i} + V_i\cos(\theta_i - \delta_i) \\ E_{d_i} + X_{d_i}I_{q_i} + V_i\sin(\theta_i - \delta_i) \end{pmatrix}.$$

We remark that the above model is derived with an IEEE Type-I exciter, and a linear turbine-speed governor without a droop controller.

2.1.2 The Type-C Wind Turbine Generator at Node i

We adopt a zero-axis model for the DFIG from Pulgar Painemal (2011).[1] The DAEs describing the DFIG at node i is given below.

$$\dot{x}_{DFIG_i} = f_{DFIG_i}(x_{DFIG_i}, y_{DFIG_i}),$$
$$0 = g_{DFIG_i}(x_{DFIG_i}, y_{DFIG_i}),$$

[1] The dynamics of the flux linkages at the rotor and the stator are assumed to be much faster than the rotor angle dynamics, and hence, are represented by algebraic, and not, differential equations.

where

$$
\begin{aligned}
x_{DFIG_i} &= \begin{bmatrix} \omega_{r_i} & z_{1_i} & z_{2_i} & z_{3_i} & z_{4_i} \end{bmatrix}^\top, \\
y_{DFIG_i} &= \begin{bmatrix} V_{qr_i} & V_{dr_i} & I_{qr_i} & I_{dr_i} & I_{qs_i} & I_{ds_i} & P_{gen_i} & Q_{gen_i} \end{bmatrix}^\top, \\
T_{mD_i} &= \bar{B}\omega_b C_p \frac{v_{Wind}^3}{\omega_{r_i}}, \\
P_{ref_i} &= \begin{cases} \bar{C}\omega_{r_i}^3 & \text{if } w_{r_i} \leq w_{max} \\ P_{max} & \text{if } w_{r_i} > w_{max} \end{cases}, \\
s_i &= \frac{\omega_s - \omega_{r_i}}{\omega_s}, \\
Q_{ref_i} &= Q_{set},
\end{aligned}
$$

$$
f_{DFIG_i} = \begin{pmatrix} \frac{\omega_s}{2H_{D_i}} \left(T_{mD_i} - X_{m_i} I_{qs_i} I_{dr_i} + X_{m_i} I_{ds_i} I_{qr_i}\right) \\ K_{I1_i}(P_{ref_i} - P_{gen_i}) \\ K_{I2_i}(K_{P1_i}(P_{ref_i} - P_{gen_i}) + z_{1_i} - I_{qr_i}) \\ K_{I3_i}(Q_{ref_i} - Q_{gen_i}) \\ K_{I4_i}(K_{P3_i}(Q_{ref_i} - Q_{gen_i}) + z_{3_i} - I_{dr_i}) \end{pmatrix},
$$

$$
g_{DFIG_i} = \begin{pmatrix} -V_{qr_i} + K_{P2_i}(K_{P1_i}(P_{ref_i} - P_{gen_i}) + z_{1_i} - I_{qr_i}) + z_{2_i} \\ -V_{dr_i} + K_{P4_i}(K_{P3_i}(Q_{ref_i} - Q_{gen_i}) + z_{3_i} - I_{dr_i}) + z_{4_i} \\ -P_{gen_i} + V_i I_{qs_i} - (V_{qr_i} I_{qr_i} + V_{dr_i} I_{dr_i}) \\ -Q_{gen_i} + V_i I_{ds_i} \\ -V_i - R_{s_i} I_{qs_i} - X_{s_i} I_{ds_i} + X_{m_i} I_{dr_i} \\ -R_{s_i} I_{ds_i} + X_{s_i} I_{qs_i} - X_{m_i} I_{qr_i} \\ -V_{qr_i} + R_{r_i} I_{qr_i} - s_i X_{m_i} I_{ds_i} + s_i X_{r_i} I_{dr_i} \\ -V_{dr_i} + R_{r_i} I_{dr_i} + s_i X_{m_i} I_{qs_i} - s_i X_{r_i} I_{qr_i} \end{pmatrix}.
$$

We remark that our model includes a rotor speed (real power) controller and a reactive power (voltage) controller. Next, we describe the network algebraic equations.

2.1.3 Kirchhoff's Current Law over the Network

The algebraic equations for the network are described by

$$0 = g_{NW}(x, y),$$

where

$$x = \begin{bmatrix} x_{SG} \\ x_{DFIG} \end{bmatrix}, \quad y = \begin{bmatrix} y_{SG} \\ y_{DFIG} \\ y_{NW} \end{bmatrix}.$$

Here, $x_{SG} \in \mathbb{R}^{8n_s}$ is the concatenation of x_{SG_i}'s over all nodal SGs. Also, $y_{SG} \in \mathbb{R}^{2n_s}$, $x_{DFIG} \in \mathbb{R}^{5n_d}$, and $y_{DFIG} \in \mathbb{R}^{8n_d}$ are interpreted similarly. The algebraic states y_{NW} consists of complex voltages at every bus in the network. Hence, if there are n_b buses in the network, then $y_{NW} \in \mathbb{R}^{2n_b}$. One can write $g_{NW}(x, y)$ as the collection of $g_{NW_i}(x, y)$ for $i = 1, \ldots, n_b$, where

$$g_{NW_i}(x, y) = \begin{pmatrix} -\Re(\bar{I}_i) + \sum_{k=1}^{n_b} V_k(\hat{G}_{ik}\cos(\theta_k) - \hat{B}_{ik}\sin(\theta_k)) \\ -\Im(\bar{I}_i) + \sum_{k=1}^{n_b} V_k(\hat{B}_{ik}\cos(\theta_k) + \hat{G}_{ik}\sin(\theta_k)) \end{pmatrix}.$$

Here, $\Re(z), \Im(z)$ denote the real and imaginary parts of any complex number z. And, we have

$$\hat{G} = \Re(Y), \quad \hat{B} = \Im(Y),$$

Y is the admittance matrix of the network and $\Re$ and $\Im$ are interpreted entry wise. Each load bus is modeled with controllable as well as uncontrollable loads (refer Zhao et al. (2014a)). The uncontrollable frequency insensitive loads are assumed to be as constant power loads denoted by $P_{U_i} + jQ_{U_i}$ at any load bus i. The controllable load at any load bus i is denoted by P_{C_i}. The frequency in the power network is regulated by using the controllable load power as a design variable based on the frequency feedback. The discussion on the control design is reserved until Section 2.4.

At any load bus i, the current is given by

$$\bar{I}_i = -(\mathcal{R}_1^{oi} V_i^{pv} + P_{C_i}) V_i^{-1} e^{j\theta_i} + j\mathcal{R}_2^{oi} V_i^{qv-1} e^{j\theta_i},$$

where the load power can be expressed as

$$P_{Li} + jQ_{Li} = \mathcal{R}_1^{oi} V_i^{pv} + P_{C_i} + j\mathcal{R}_2^{0i} V_i^{qv}.$$

The choice of pv and qv will determine the type of load connected at bus i. The units of $\mathcal{R}_1^{oi}$ and $\mathcal{R}_1^{oi}$ are based on the choice of pv and qv. The uncontrollable load power is given by

$$P_{U_i} + jQ_{U_i} = \mathcal{R}_1^{oi} V_i^{pv} + j\mathcal{R}_2^{oi} V_i^{qv}.$$

2.1.4 Stochastic Wind Speed Modeling

Wind speed variation impacts the wind power output, and in turn, affects the power system dynamics. Simulations with forecasts of wind speed trajectories cannot capture the effect of that variation on grid stability, and even if they capture, it will result in misinterpretations due to the forecasting errors. In this work, our objective is to study the small signal stability (in the presence of load-side primary frequency controller) wrt the variations in the wind and identify the maximum allowable wind generation. In so doing, we model the wind speeds as a stochastic process which captures the variations in the wind speeds. Moreover, with the example of a recorded wind-speed data, we bring in the relevance of our work and the necessity to study the effect of variations on wind speeds on the grid stability. Consider the actual wind speeds (as shown in Fig. 2.2) recorded at a tower near the City of Ames, Iowa recorded in the early spring season on 10^{th} of April 2018 (refer Takle et al. (2018)). The wind speeds are recorded at every 1 second intervals for a period of 8 hours. Figure 2.3 shows the histogram of the wind speed data for the 8 hours. The red solid line in Fig. 2.3 corresponds to a Gaussian fit on that data. Therefore, for a short duration of time, the wind speed can be modeled as a Wiener process.

In this work, we model the (cubed) wind speed as the following stochastic process[2].

$$\vartheta_i^3 = \vartheta_{i_0}^3 + \sigma_i \xi_i \tag{2.1}$$

[2]See Pappala et al. (2009); Xu et al. (2005) for wind speed models via Gaussian distribution. Modeling ϑ_i^3 instead of ϑ_i through a Weiner process simplifies our exposition but however explains the instability from stochastic variations in wind.

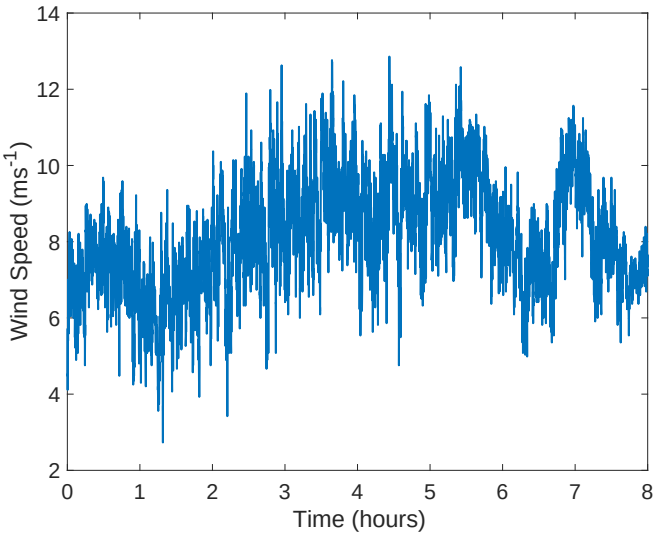

Figure 2.2 Real time wind speed data recorded at a resolution of 1 second from 10 AM to 6 PM (CDT) on April 10, 2018, observed at a height of 120 m near Ames, Iowa (refer Takle et al. (2018)).

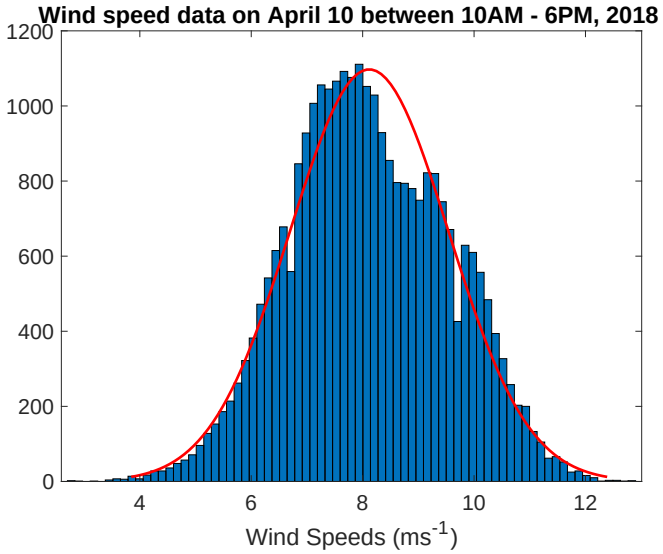

Figure 2.3 Gaussian fit on the real-time wind speed data as shown in Fig. 2.2.

for $\sigma_i > 0$, where ϑ_{i_0} represents the nominal wind speed, and $\xi_i =: \frac{d\Delta_i}{dt}$ denotes the time-derivative of a standard Wiener process Δ_i. The standard independent Wiener processes, $\Delta(t)$ satisfy,

(i) $\text{Prob}\{\Delta(0) = 0\} = 1$.

(ii) $\{\Delta(t)\}$ is a process with independent increments.

(iii) $\{\Delta(t) - \Delta(s)\}$ has a Gaussian distribution with $E[\Delta(t) - \Delta(s)] = 0$ and $E[(\Delta(t) - \Delta(s))^2] = |t - s|$.

Albeit simplistic, the wind speed model in (2.1) is sufficient to illustrate the (small-signal) stability concerns stemming from the stochasticity in wind speed.

With the wind speed model in (2.1), the mechanical torque to the DFIG at bus i becomes

$$T_{mD_i} = \bar{B}\omega_b C_p \frac{1}{\omega_r}(\vartheta_{i_0}^3 + \sigma_i \xi_i), \tag{2.2}$$

that further yields

$$\frac{d\omega_{ri}}{dt} = \frac{\omega_s}{2H_{D_i}} \left(\bar{B}\omega_b C_p \frac{1}{\omega_r}(\vartheta_{i_0}^3 + \sigma_i \xi_i) - X_{m_i} I_{qs_i} I_{dr_i} + X_{m_i} I_{ds_i} I_{qr_i} \right). \tag{2.3}$$

The uncertainty in wind speed in (2.3) enters multiplicatively in the system dynamics, i.e., ξ_i describes a parametric uncertainty in the vector field f_{DFIG}. In the presence of random wind, the dynamics of the DFIG at bus i can be expressed as

$$\begin{aligned} \dot{x}_{DFIG_i} &= f_{DFIG_i}(x_{DFIG_i}, y_{DFIG_i}, \xi_i), \\ 0 &= g_{DFIG_i}(x_{DFIG_i}, y_{DFIG_i}). \end{aligned}$$

2.1.5 DAE Model for the Power System

Collecting the DAEs for the SGs, stochastic DAEs of DFIGs, and algebraic equations of the network, we arrive at the following stochastic DAE that govern the dynamics of the stochastic power system.

$$\begin{aligned} \dot{x} &= f(x, y, \xi), \\ 0 &= g(x, y, P_C). \end{aligned} \tag{2.4}$$

where $x \in \mathbb{R}^n$, $y \in \mathbb{R}^{n_{alg}}$, with $n := 8n_s + 5n_d$ and $n_{alg} := 2n_s + 8n_d + n_{bus}$ denotes the number of dynamic and algebraic states respectively. Further,

$$f = \begin{bmatrix} f_{SG} \\ f_{DFIG} \end{bmatrix}, \quad g = \begin{bmatrix} g_{SG} \\ g_{DFIG} \\ g_{NW} \end{bmatrix}.$$

The stochastic nonlinear representation of the power system described in Eq. (2.4) is linearized around a nominal operating point (x_0, y_0) to obtain the following linear system.

$$\dot{x} = A(\xi)x + By, \tag{2.5}$$

$$0 = Cx + Dy + EP_C, \tag{2.6}$$

where

$$A = \frac{\partial f}{\partial x},\ B = \frac{\partial f}{\partial y},\ C = \frac{\partial g}{\partial x},\ D = \frac{\partial g}{\partial y},\ E = \frac{\partial g}{\partial P_C}.$$

The stochastic linearization of DAEs is followed by applying the results from Imkeller and Lederer (2002). Basically, the idea there is to transform the stochastic differential equations (SDEs) to random differential equations (RDEs) using a stationary coordinate change, referred to as Cohomology and then locally linearized. This local linearization result is a classic analogue of classical Hartman-Grobman Theorem (refer Strand (1970); Imkeller and Lederer (2002)). Once again, using cohomology, the stationary coordinate change, the linear random differential equations are converted to linear stochastic differential equations. The interested readers are referred to Imkeller and Lederer (2002) for a detailed description of linearization of stochastic differential equations. This entire process of linearization based on the work of Imkeller and Lederer (2002) is shown in Fig. 2.4.

Basically, the reason to study the system in the RDE space is due to the properties of solutions of RDEs. Existence and uniqueness of the solution to RDEs can be proved under a given hypothesis. An RDE can be interpreted as a non-autonomous ordinary differential equation and unlike SDEs can be analyzed pathwise with deterministic calculus (refer Han and Kloeden (2017)). The solution

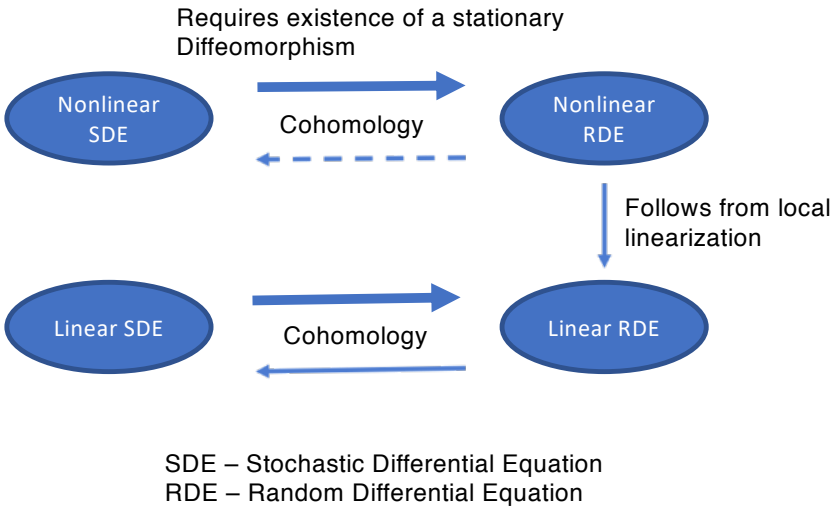

Figure 2.4 Pictorial representation of the process of linearization of nonlinear SDE which leads to a linear SDE (refer Imkeller and Lederer (2002))

of SDEs is not differentiable while the solution of RDEs is. SDEs are dealt with using Itô theory or density function based approach. Further the main result of (Imkeller and Lederer, 2002, Theorem 4.1) is to establish a connection between the cocycle generated by SDEs and RDEs using the stationary coordinate change, cohomology.

Notice that after the linearization of DAEs, the uncertainty in f appears in the system matrix A parametrically. In the case where D is invertible, the algebraic states can be expressed in terms of the dynamic states as $y = -D^{-1}Cx - D^{-1}EP_C$. Then, the differential equation Eq. (2.5) is given by

$$\dot{x} = \left(A(\xi) - BD^{-1}C\right)x - BD^{-1}EP_C. \tag{2.7}$$

The deterministic part and stochastic part of the system Eq. (2.7) can be separated as follows.

$$\dot{x} = \mathcal{A}x + \sum_{\ell=1}^{m} \sigma_\ell \mathcal{B}_\ell \mathcal{C}_\ell x \xi_\ell + \mathcal{E}P_C, \tag{2.8}$$

where m are the number of uncertainties in the network. In this case, as the uncertainty is modeled only in wind speed input to DFIGs, we have $m = n_d$. Further, $\mathcal{A}$ is the deterministic part of

$(A(\xi) - BD^{-1}C)$. Here, $\mathcal{B}_\ell$ and $\mathcal{C}_\ell$ are column and row vectors, respectively and $\mathcal{E} = -BD^{-1}E$. Moreover, $\mathcal{B}_\ell$ is sparse, with nonzero entries corresponding to the ω_r states of the DFIGs. The case is similar for $\mathcal{C}_\ell$.

The stochastic power network in Eq. (2.8) is shown to be in the form of NCS. We study this problem using two different approaches. The first involves a lower order model where the bus voltages corresponding to the renewable buses are modeled stochastically. And the second approach models the detailed higher-order model of the power network where the input to the DFIGs, the wind speeds are modeled stochastically. In both the cases, we show the fragility of the decentralized load-side primary frequency controller. More discussion on these results and other control strategies will follow in the forthcoming sections.

With the wind speed being modeled as a stochastic process, the resultant dynamics of the Type-C wind turbine generator is stochastic. Precisely, the mechanical input to DFIG, T_{mD} is stochastic and hence the state ω_r is stochastic. This reflects in P_{ref}, the reference power input to the DFIG is stochastic. Hence, P_{gen}, the power generated by the DFIG is stochastic. When the power injected into the grid is stochastic, the terminal voltages, V are stochastic. In this case, we are interested in the frequency regulation of the power grid with the help of controllable loads. In doing so, we modify the power system model with wind uncertainty to incorporate the controllable loads and also reduce the DAE model to simplify the analysis. Due to the uncertainty in wind availability, we have seen above that the terminal voltages at the renewable buses are uncertain. Therefore, in the load-side frequency model, we model the stochastic uncertainty in the voltages. Next, we describe the optimal load control (OLC) problem in a power network to achieve frequency regulation. First, we describe the deterministic OLC problem and then model it with stochastic uncertainty in the voltages which appear multiplicative in the system dynamics.

2.2 Introduction to Optimal Load Control Problem

In this section, we first discuss briefly the deterministic load-side frequency control model as developed in Zhao et al. (2014b). We refer the readers to Zhao et al. (2014b) for more detailed

discussion on this model. The basic idea behind the load-side frequency control is to control the loads, so that, the system-wide frequency can be regulated following a small change in power injection at one of the system bus. The load control comes at a cost and is measured by the aggregate disutility of the loads. The objective is to regulate the system frequency while minimizing the aggregate disutility of the loads.

To set up the problem, consider a power network as a graph network with generator and load buses as nodes and transmission lines as edges. Let the sets $\mathcal{G}, \mathcal{L}$, and $\mathcal{E}$ respectively, denote the set of generator nodes, set of load nodes, and the set containing network edges. The cardinalities of sets $\mathcal{G}, \mathcal{L}$, and $\mathcal{E}$ are denoted by n_g, n_l, and n_e respectively. Let $\mathcal{N}$ denote the set of generator and load nodes and its cardinality is given by n, where $n = n_g + n_l$. The dynamic network model for regulating system frequency using load can be written as follows (we refer to Zhao et al. (2014b) for various assumptions leading to this model).

$$\begin{aligned} \dot{\omega}_j =& -\frac{1}{M_j}(P_{L_j} + P_{C_j} - P_{U_j} + P_j^{out} - P_j^{in}),\ \forall j \in \mathcal{G} \\ 0 =& P_{L_j} + P_{C_j} - P_{U_j} + P_j^{out} - P_j^{in},\ \ \forall j \in \mathcal{L} \\ \dot{P}_{F_{ij}} =& W_{ij}(\omega_i - \omega_j),\ \ \forall (i,j) \in \mathcal{E} \end{aligned} \tag{2.9}$$

where ω_j is the frequency deviation at j^{th} bus,

$$W_{ij} := 3\frac{|V_i||V_j|}{X_{ij}}\cos(\theta_i^0 - \theta_j^0), \quad P_j^{out} := \sum_{k:j\to k} P_{F_{jk}}, \quad P_j^{in} := \sum_{i:i\to j} P_{F_{ij}}.$$

The terms, P_j^{out}, P_j^{in} are the total branch power flows out and into bus j respectively. Further, V_i, θ_i^0 are the voltage and nominal phase angle at bus i, and X_{ij} is the reactance of the line connecting the buses i and j. Three types of loads are distinguished in the above model namely, frequency-sensitive, frequency-insensitive but controllable, and uncontrollable loads. The quantity, P_{L_j} models the frequency-sensitive load and is assumed to be of the form $P_{L_j} = D_j\omega_j$, i.e., it responds linearly to frequency deviation. Further, P_{U_j} incorporates the part of load which is frequency-insensitive and uncontrollable and P_{C_j} models the load which is frequency-insensitive but controllable. Note that, in Zhao et al. (2014b), the notations for these various types of loads are denoted by $d_j, \hat{d}_j, P_j^m$. We have changed them here to avoid any conflicts in the notations with previous chapters.

The DAE model is given in Eq. (2.9) considered for load-side frequency control can be related to the most general DAE from given in Eq. (2.4) without uncertainty as follows. The PI controllers for real and reactive power in the DAE model (2.4) are neglected and the quasi-steady-state assumption made on the network power flow equations is not valid anymore. The quasi-steady-state assumption on the power flow essentially means that the power flow is not varying much in the transmission lines and it is modeled by an algebraic equation. But, here in the load-side frequency control model, the quasi-steady state assumption is not considered and hence, we have a dynamic equation describing the power flow in the network. Specifically, the network algebraic equations are given in subsection 2.1.3 are actually current balance equations and they are converted to power balance equations by multiplying with voltage and taking the time-derivative to obtain the dynamic equation for power flow as shown in Eq. (2.9). The resultant model for load-side frequency control is what has been described in Zhao et al. (2014b).

The objective is to design a feedback controller $P_{C_j}(\omega(t), P_F(t))$ for the controllable loads, so that, frequency can be regulated following disturbance, i.e., the system (2.9) is globally asymptotically stable. In Zhao et al. (2014b), an alternate optimization-based approach is proposed for adjusting the controllable load, P_{C_j}. The design of feedback controller, $P_{C_j}(\omega(t), P_F(t))$, is posed as an optimal load control (OLC) problem and the feedback controller is derived as a distributed algorithm to solve the OLC. The optimization problem for OLC is formulated as follows.

$$\min_{\underline{P_C} \le P_C \le \overline{P_C}, P_L} \quad \sum_{j \in \mathcal{N}} \left(c_j(P_{C_j}) + \frac{1}{2D_j} P_{L_j}^2 \right) \tag{2.10}$$

$$\text{subject to} \quad \sum_{j \in \mathcal{N}} (P_{C_j} + P_{L_j}) = \sum_{j \in \mathcal{N}} P_{U_j} \tag{2.11}$$

where $c_j(P_{C_j})$ is the cost on controllable load at bus j, when it is changed by P_{C_j} and $P_{L_j} := \hat{D}_j \omega_j$ denotes the frequency deviation, ω_j of the frequency sensitive load at bus j. The change in either generator or load power at bus j is denoted by P_{U_j} and each load always satisfy $-\infty < \underline{P_C} \le P_C \le \overline{P_C} < \infty$. Furthermore, the cost function c_j at every bus j is assumed to be strictly convex and twice continuously differentiable on $[\underline{P_C}, \overline{P_C}]$. A dual to the OLC problem (2.10)-(2.11) which can

be solved or implemented with a distributed architecture is written as

$$\max_{\nu} \quad \sum_{j\in\mathcal{N}} \Phi_j(\nu_j) \tag{2.12}$$

$$\text{subject to} \quad \nu_i = \nu_j, \quad \forall (i,j) \in \mathcal{E}, \tag{2.13}$$

where $c_j^{'}(\nu_j)$ is the derivative of the cost function

$$\begin{aligned}\Phi_j(\nu_j) =& c_j(P_{C_j}(\nu_j)) - \nu_j P_{C_j}(\nu_j) - \frac{1}{2} D_j \nu_j^2 + \nu_j P_{U_j},\\ d_j(\nu_j) =& \left[c_j^{'-1}(\nu_j)\right]_{\underline{P_{C_j}}}^{\overline{P_{C_j}}}.\end{aligned}$$

Note that Φ_j is only a function of ν_j, the dual variable, and all ν_j are constrained to be equal at optimality. After some change of variables, it can be shown that the primal-dual gradient system corresponding to optimization problem (2.12)-(2.13) takes the form as given below (refer Zhao et al. (2014b)).

$$\dot{\omega}_j = -\frac{1}{M_j}(P_{L_j} + P_{C_j} - P_{U_j} + P_j^{out} - P_j^{in}), \forall j \in \mathcal{G}, \tag{2.14}$$

$$0 = P_{L_j} + P_{C_j} - P_{U_j} + P_j^{out} - P_j^{in}, \forall j \in \mathcal{L}, \tag{2.15}$$

$$\dot{P}_{F_{ij}} = W_{ij}(\omega_i - \omega_j), \forall (i,j) \in \mathcal{E}, \tag{2.16}$$

$$P_{L_j} = D_j \omega_j, \forall j \in \mathcal{N}, \tag{2.17}$$

$$P_{C_j} = \left[c_j^{'-1}(\omega_j)\right]_{\underline{P_{C_j}}}^{\overline{P_{C_j}}}, \ \forall j \in \mathcal{N}. \tag{2.18}$$

Now, we assume that there are no controllable loads located at a generator bus and then rewrite the above primal-dual gradient system shown in Eqs. (2.14)-(2.18) in compact form.

$$\dot{\omega}_G = -M_G^{-1}\left(D_G \omega_G - P_{U_G} + E_G P_F\right), \tag{2.19}$$

$$0 = D_L \omega_L + \hat{D} u - P_{U_L} + E_L P_F, \tag{2.20}$$

$$\dot{P}_F = W(E_G^{\top} \omega_G + E_L^{\top} \omega_L), \tag{2.21}$$

where $\omega_G \in \mathbb{R}^{n_g}$, $\omega_L \in \mathbb{R}^{n_l}$, $P_F \in \mathbb{R}^{n_e}$ and u is the controllable load input with $P_C = \hat{D}u$. Observe that M_G, D_G, D_L are diagonal matrices corresponding to the inertia and damping values

at generators and loads respectively. The weight matrix, $W \in \mathbb{R}^{n_e \times n_e}$ is defined as a diagonal matrix with entries W_{ij} for all $(i,j) \in \mathcal{E}$. The matrices E_G and E_L are the incidence matrices corresponding to generator and load buses respectively.

The control input to be designed is denoted by u. The matrix $\hat{D}$, is a diagonal matrix and it contains the information of location of the controllable loads. The entries of $\hat{D}$ matrix are defined as shown below.

$$\hat{D}_{ii} = \begin{cases} 1, & \text{if there is a controllable load} \\ 0, & \text{otherwise.} \end{cases} \tag{2.22}$$

Clearly, we have

$$\omega := \begin{bmatrix} \omega_G \\ \omega_L \end{bmatrix} \in \mathbb{R}^{n_g+n_l}, \quad P_U := \begin{bmatrix} P_{U_G} \\ P_{U_L} \end{bmatrix} \in \mathbb{R}^{n_g+n_l}, \quad E := \begin{bmatrix} E_G \\ E_L \end{bmatrix} \in \mathbb{R}^{(n_g+n_l)\times n_e},$$

The algebraic equation corresponding to states ω_L can be eliminated and the differential algebraic system describing the optimal load control problem can be defined with purely differential equations. From, Eq. (2.20), we have

$$\omega_L = D_L^{-1}\left(P_{U_L} - \hat{D}u - E_L P_F\right). \tag{2.23}$$

Substituting the algebraic state in Eq. (2.19) and Eq. (2.21), we obtain

$$\dot{\omega}_G = -M_G^{-1}\left(D_G\omega_G - P_{U_G} + E_G P_F\right), \tag{2.24}$$

$$\dot{P}_F = W\left(E_G^\top \omega_G + E_L^\top D_L^{-1}(P_{U_L} - \hat{D}u - E_L P_F)\right). \tag{2.25}$$

In the following section, we motivate the stochastic dynamic network model using uncertain and intermittent nature of wind energy.

2.2.1 Stochastic Renewables and Parametric Uncertainty

In this subsection, we show how the parametric uncertainty enters in the power system dynamics. We motivate the parametric uncertainty in the power system dynamics through the presence of renewables where the intermittent nature of wind energy resource is modeled as a stochastic random

variable. The network power system with parametric uncertainty and ignoring the controllable loads can be modeled as a set of differential algebraic equations (DAEs) written as follows:

$$\dot{x} = f(x, y, \xi) \tag{2.26}$$

$$0 = g(x, y) \tag{2.27}$$

where, x are the dynamic states corresponding to generator angular velocities, generator excitation voltages, states of local PI controllers at each generator, power across the transmission lines, etc., and y are the network as well as generator algebraic states corresponding to the induced voltages, currents, bus angles, etc. and ξ denotes the stochastic parametric uncertainty.

The network power system model with renewable wind energy resources will consist of conventional synchronous generators as well as doubly fed induction generators (DFIG). We refer the readers to Pulgar Painemal (2011) for more detailed discussion on the deterministic modeling of network power system with renewable wind generation.

Under the assumption that $\frac{\partial g}{\partial y} \neq 0$, implicit function theorem can be applied to network algebraic equation (2.27) to eliminate the algebraic state y by expressing the algebraic state $y = h(x)$. In the presence of stochastic uncertainty in the algebraic equation, an argument involving center manifold based reduction for stochastic system and singular perturbation theory for stochastic system (refer Arnold (2013); Berglund and Gentz (2003)), the algebraic states, y can be expressed as a stochastic function of states x, i.e., $y = h(x, \xi)$. Using this in Eq. (2.26), more generally we obtain,

$$\dot{x} = f(x, h(x, \xi), \xi).$$

This system is linearized as discussed in Section 2.1.5 at a nominal operating point to obtain a linear stochastic system, where the stochastic uncertainty enters the linearized system parametrically.

In the following, we show how the stochastic uncertainty in the algebraic states propagates into the network power system. One of the algebraic states that are of particular interest to us is the bus voltages. It is clear that uncertainty in renewables will cause the power generated to fluctuate and henceforth, voltage fluctuates. As the availability of wind energy is uncertain, the terminal voltages are random. Apart from voltages, there are other network parameters that one

can assume to be uncertain and hence modeled as a stochastic random variable. For example, the frequency-sensitive loads can be assumed to be uncertain, i.e., $\hat{P}_{C_j} = (D_o + D_1\xi)\omega_j$, where ξ is the stochastic uncertainty. Note that, the uncertainty is assumed to be parametric, where the damping coefficient is changing over time. The loads are constantly turned on and off in the grid and thereby changing the effective damping coefficient of the frequency-sensitive loads.

Similarly, the frequency-insensitive uncontrollable loads can also be uncertain. However, in this chapter, we mainly focus on bus voltages being uncertain and analyze the impact of stochastic voltage fluctuations on the system (mean square exponential) stability. Suppose, $\hat{n}_g < n_g$ generators in the power network are now replaced with a renewable energy source. As we are modeling the voltages at renewable buses to be stochastic, the voltages at buses connecting the renewables are also stochastic. Let $\mathcal{M}$ be the set of a pair of buses whose voltages are stochastic and its cardinality be denoted by $m < n_e$, where n_e is the number of total links in the network. Under the assumption that the nominal voltages are 1 p.u., stochastic voltage fluctuations are modeled as follows:

$$|V_i||V_j| = 1 + \sigma_\ell \xi_\ell \ \ \forall (i,j) \in \mathcal{M} \tag{2.28}$$

where $\xi_\ell := \frac{d\Delta_\ell}{dt}$ is the Gaussian uncertainty with standard deviation σ_ℓ and Δ_ℓ is the standard Wiener process. We use unique index ℓ to identify and denote the edge pair $(i,j) \in \mathcal{M}$ and hence $\ell = 1, \ldots, m$.

Furthermore ξ_ℓ is assumed to be independent of ξ_k for $\ell \neq k$. For simplicity of presentation, we assume all the links in the network whose voltages are modeled with Gaussian uncertainty have the same variance, σ^2.

Remark 1. *Notice that instead of assuming individual bus voltages to be random, we assume product of voltages to be random. This is a modeling assumption and is made to avoid technical difficulty that arises while multiplying two stochastic processes.*

2.3 Load-side Frequency Control Model with Stochastic Uncertainty in Bus Voltages

Following the modeling of stochastic voltages as shown in (2.28), we write the stochastic link weight as follows

$$W_{ij} = 3\frac{(1+\sigma\xi_\ell)}{X_{ij}}\cos(\theta_i^0 - \theta_j^0).$$

Define $W_{ij}^0 := 3\frac{1}{X_{ij}}\cos(\theta_i^0 - \theta_j^0)$, and hence, we have

$$W_{ij} = W_{ij}^0 + \sigma W_{ij}^0 \xi_\ell. \tag{2.29}$$

Substituting Eq. (2.29) in Eq. (2.24) and Eq. (2.25), we obtain the following stochastic power network model.

$$\begin{aligned}\dot{\omega}_G =& -M_G^{-1}(D_G\omega_G - P_{U_G} + E_G P_F)\\ \dot{P}_F =& (W^0 + \sigma W^0 \circ \xi)\left(E_G^\top \omega_G + E_L^\top D_L^{-1}(P_{U_L} - E_L P_F - \hat{D}u)\right)\end{aligned} \tag{2.30}$$

where W^0 is a diagonal matrix with entries W_{ij}^0 for all $(i,j) \in \mathcal{E}$, ξ is a diagonal matrix with zeros, $\xi_1, \ldots, \xi_{m-1}$ and ξ_m. The nonzero entries of ξ correspond to the links given in set $\mathcal{M}$. The symbol, $\circ$ denotes the element-wise matrix multiplication. To represent the system (2.30) in standard robust control form (refer to Figure. 4.1), we rewrite the system equation in slightly different form by choosing the states as

$$\bar{x} := \begin{bmatrix}\omega_G \\ P_F\end{bmatrix}.$$

Then, we have

$$\dot{\bar{x}} = \bar{A}\bar{x} + b + \sigma\sum_{\ell=1}^{m}\bar{B}_\ell(\bar{C}_\ell\bar{x} + \bar{H}_\ell)\xi_\ell + \bar{B}u + \sigma\sum_{\ell=1}^{m}\tilde{H}_\ell u\xi_\ell,$$

where,

$$\bar{A} = \begin{bmatrix} -M_G^{-1}D_G & -M_G^{-1}E_G \\ W^0E_G^\top & -W^0E_L^\top D_L^{-1}E_L \end{bmatrix}, \quad b = \begin{bmatrix} M_G^{-1}P_{U_G} \\ W^0E_L^\top D_L^{-1}P_{U_L} \end{bmatrix},$$
$$\bar{B}_\ell = \begin{bmatrix} 0 \\ e_\ell \end{bmatrix}, \quad \bar{C}_\ell = \begin{bmatrix} (W^0E_G^\top)_\ell & -(W^0E_L^\top D_L^{-1}E_L)_\ell \end{bmatrix},$$
$$\bar{H}_\ell = \begin{bmatrix} (W^0E_L^\top D_L^{-1}P_{U_L})_\ell \end{bmatrix}, \quad \tilde{H}_\ell = \begin{bmatrix} -(W^0E_L^\top D_L^{-1}\hat{D})_\ell \end{bmatrix},$$
$$\bar{B} = \begin{bmatrix} 0 \\ -W^0E_L^\top D_L^{-1}\hat{D} \end{bmatrix},$$

with $e_\ell \in \mathbb{R}^m$ being a vector of all zeros except for 1 in the ℓ^{th} location. Chose $\bar{x}^*$, such that, $A\bar{x}^* + b = 0$ and define $v = \bar{x} - \bar{x}^*$ to shift the equilibrium of the deterministic system to origin. Then, we have

$$\dot{v} = \bar{A}v + \sigma \sum_{\ell=1}^{m} (\bar{B}_\ell \bar{C}_\ell v + \tilde{H}_\ell u)\xi_\ell + \sigma \sum_{\ell=1}^{m} \bar{B}_\ell (\bar{H}_\ell + \bar{C}_\ell \bar{x}^*)\xi_\ell + \bar{B}u \tag{2.31}$$

Due to the singularity of the matrix $\bar{A}$, we do the transformation on system (2.31) to separate the null space and range space of $\bar{A}$. Let $\mathcal{N}_s(\bar{A})$ and $\mathcal{R}_s(\bar{A})$ denotes the set of vectors which span the null space and range space of $\bar{A}$. Let n_u be the dimension of null space of $\bar{A}$ and n be the dimension of range space of $\bar{A}$.

Then, define the transformation matrix, $V = \begin{bmatrix} \mathcal{N}_s(\bar{A}) & \mathcal{R}_s(\bar{A}) \end{bmatrix}$, and using V, we define

$$\begin{bmatrix} r \\ x \end{bmatrix} := V^\top v.$$

Pre-multiplying system (2.31) with the transformation matrix V, we obtain

$$\begin{bmatrix} 0 & A_{rx} \\ 0 & A_{xx} \end{bmatrix} := V^\top \bar{A} V, \quad \begin{bmatrix} 0 & (V^\top \bar{B}_\ell \bar{C}_\ell V)_{rx} \\ 0 & (V^\top \bar{B}_\ell \bar{C}_\ell V)_{xx} \end{bmatrix} := V^\top \bar{B}_\ell \bar{C}_\ell V,$$
$$\begin{bmatrix} (V^\top \tilde{H}_\ell)_r \\ (V^\top \tilde{H}_\ell)_x \end{bmatrix} := V^\top \tilde{H}_\ell, \quad \begin{bmatrix} (V^\top \bar{B})_r \\ (V^\top \bar{B})_x \end{bmatrix} := V^\top \bar{B},$$

Defining,

$$B_1^\ell := (V^\top \bar{B}_\ell \bar{C}_\ell V)_{xx}, \quad B_2^\ell = (V^\top \tilde{H}_\ell)_x, \quad A := A_{xx},$$
$$H_\ell := (V^\top \bar{B}_\ell (\bar{C}_\ell u^* + \bar{H}_\ell))_{xx}, \quad B := (V^\top \bar{B})_x,$$

we write Eq. (2.31) in the transformed coordinates as follows

$$\begin{aligned}\dot{r} =& A_{rx}x + (V^\top \bar{B})_r u + \sigma \sum_{\ell=1}^{m} (V^\top \bar{B}_\ell \bar{C}_\ell V)_{rx} x \xi_\ell + \sigma \sum_{\ell=1}^{m} (V^\top \bar{B}_\ell (\bar{H}_\ell + \bar{C}_\ell x^*))_{rx} \xi_\ell \\ &+ \sigma \sum_{\ell=1}^{m} (V^\top \tilde{H}_\ell)_r u \xi_\ell \qquad (2.32)\\ \dot{x} =& Ax + Bu + \sigma \sum_{\ell=1}^{m} B_1^\ell x \xi_\ell + \sigma \sum_{\ell=1}^{m} B_2^\ell u \xi_\ell + \sigma \sum_{\ell=1}^{m} H_\ell \xi_\ell, \qquad (2.33)\end{aligned}$$

where $x \in \mathbb{R}^n$ and $r \in \mathbb{R}^{n_u}$. We notice that the z dynamics is completely driven by x dynamics, control input and noise processes whereas, x dynamics is not influenced by z dynamics. Hence, the necessary condition for the stability of the above system of equations (2.32)-(2.33) is that, x dynamics be stable. Therefore, we look at the stochastic stability analysis of the system (2.33).

We next study the small-signal stability of the power network modeled with detailed higher order DAEs and stochastic wind as shown in 2.1.5 and arrive at Eq. (2.8). Load-side primary frequency control is proposed to minimize the frequency excursions from the nominal due to the intermittent generation. Two different load-side primary frequency control strategies are discussed.

2.4 Load-Side Primary Frequency Control

The frequency excursions caused by the mismatch between generation and demand can be subdued by designing a frequency controller. In this work, we have considered the controllable loads and as the name suggests, they can vary the load power to achieve the power balance in the network and thus maintains the frequency close to the nominal value. As the controllable loads are providing the grid services such as frequency regulation in contrast to the governor based control, this type of control is referred to as load-side primary frequency control. This type of control mechanism is under debate for several decades and is now emerging as a strong alternative to governor based

primary frequency control (refer Callaway and Hiskens (2011)). The load-side primary frequency control benefits from features such as speed of operation, no additional installation cost, availability of controllable loads (for instance, residential loads such as electric water heaters, air conditioners, commercial loads such as HVAC systems, etc.) among others and suffers from privacy issues and additional added communication infrastructure (based on the control architecture). Achieving optimal load control is beyond the scope of this work and can be referred to Zhao et al. (2014b, 2013).

From Section 2.1.3, we recall that each load is modeled with controllable as well as uncontrollable loads. The uncontrollable loads are subject to change with respect to time and the variability of uncontrollable power is also a source of power mismatch in the network. In the ensuing, we discuss two different control strategies of interest to achieve frequency regulation using controllable loads. The baseline power at any bus is the load power at that bus without any load modulation. In this context, we discuss the following decentralized controller.

2.4.1 Decentralized Control

The decentralized load-side primary frequency controller in this work follows closely with the one discussed in Trudnowski et al. (2006). The real power modulation at every bus i is given by

$$\Delta P_{C_i} = K_i \Delta\omega_i \tag{2.34}$$

where

- ΔP_{C_i} - Real power modulation at bus i in percent with respect to baseline loading at bus i
- $\Delta\omega_i$ - Error in frequency at bus i measured in Hz
- K_i - Proportional control gain [percentage/Hz]

The frequency range in which this controller provides frequency regulation depends on the choice of the proportional control gain. For example, when $K_i = 50$ and suppose the frequency at bus i went down by 0.005 Hz. Let the load at bus i be 740 kW. Then, using the formula (2.34), we can obtain how much percentage of the load has to be cut down to increase the frequency back to

nominal. By (2.34), we obtain that 2.5% of load has to be modulated, i.e., the new load at bus i will be 738.15 kW. The numerical values provided in the above example are only for an understanding purpose. Similarly, the control gains at every bus are defined based on the availability of the proportion of controllable loads.

One of the advantages of this type of controller is the non-necessity of the additional communication from individual buses to the centralized control. However, as each the controller at each bus is acting independently, there will be transients in the system before reaching steady state. Nevertheless, these transients can be attenuated by considering the additional frequency measurements from the neighborhood buses which results in a control with neighborhood information. A similar optimal load control with neighborhood communication control can be found in Zhao et al. (2013).

2.4.2 Control with Neighboring Communication

Let $\mathcal{N}_i$ be the set of collection of buses neighboring the bus i. Then the real power modulation based on the control with neighboring communication can be given by

$$\Delta P_{C_i} = \sum_{j \in \mathcal{N}_i} K_{ij} \Delta \omega_j. \tag{2.35}$$

The above-discussed control strategies are implemented on an IEEE 39 bus system with wind generation in Section 6. The motivation behind considering these control strategies is to achieve a better frequency regulation with the existing resources.

All the notations used in this section are summarized in Appendix 8.2.

Next, we describe the modeling of power network with communication channel uncertainty which arises in the wide area control of the power network. Wide area control is used to damp the inter-area oscillations that occur in a power network. For wide area control, measurement signals are transferred across distance over communication channels measured from the sensors, phasor measurement units (PMUs). Moreover, the wide area control inputs are also sent over communication channels to the power network.

CHAPTER 3. POWER SYSTEM MODEL WITH COMMUNICATION CHANNEL UNCERTAINTY

In the modern electric power grid, PMUs are the most important measuring devices, and they can also be used as a protective relay. Further, FACTS devices are power electronic based static devices in electric power grid which can enhance controllability and increase power transfer capability in the network. Due to their functionality, PMUs and FACTS devices play an essential role in monitoring and maintaining the stability of the power network. All the control and sensing signals are sent over the communication channels (cyber layer), and these communication channels are subjected to a natural source of uncertainty. Furthermore, these communication channels will be an ideal target of cyber attack where the attacker could tamper the data transmitted over them.

We begin with the deterministic power system model which is borrowed from Sauer and Pai (1998b).

3.1 Power System Dynamic Model

The multi-machine differential algebraic equation (DAE) model for power system dynamics is given by

1. Differential algebraic equations describing the generator,

2. Algebraic equations describing the network power flow.

We consider $n_g + n_l$ bus power system model with n_g generator buses, n_l load buses and assuming there are n_e transmission lines in the network.

Differential algebraic equations at generator i

$$\begin{aligned}
\frac{d\delta_i}{dt} &= \omega_i - \omega_s, \\
\frac{d\omega_i}{dt} &= \frac{T_{m_i}}{M_i} - \frac{E'_{q_i} I_{q_i}}{M_i} - \frac{(X_{q_i} - X'_{d_i})}{M_i} I_{d_i} I_{q_i} - \frac{D_i(\omega_i - \omega_s)}{M_i}, \\
\frac{dE'_{q_i}}{dt} &= -\frac{E'_{q_i}}{T'_{do_i}} - \frac{(X_{d_i} - X'_{d_i})}{T'_{do_i}} I_{d_i} + \frac{E_{fd_i}}{T'_{do_i}}, \\
\frac{dE_{fd_i}}{dt} &= -\frac{E_{fd_i}}{T_{A_i}} + \frac{K_{A_i}}{T_{A_i}}(V_{ref_i} - V_i), \\
0 &= V_i \sin(\delta_i - \theta_i) + R_{s_i} I_{d_i} - X_{q_i} I_{q_i}, \\
0 &= E'_{q_i} - V_i \cos(\delta_i - \theta_i) - R_{s_i} I_{q_i} - X'_{d_i} I_{d_i}, \\
&\text{for} \quad i = 1, \ldots, n_g.
\end{aligned}$$

The network equations corresponding to the real and reactive power at generator and load buses are shown below.

Network algebraic equations

$$\begin{aligned}
I_{d_i} V_i \sin(\delta_i - \theta_i) + I_{q_i} V_i \cos(\delta_i - \theta_i) + P_{L_i}(V_i) - \sum_{k=1}^{n_e} V_i V_k Y_{ik} \cos(\theta_i - \theta_k - \alpha_{ik}) = 0, \\
I_{d_i} V_i \cos(\delta_i - \theta_i) - I_{q_i} V_i \sin(\delta_i - \theta_i) + Q_{L_i}(V_i) - \sum_{k=1}^{n_e} V_i V_k Y_{ik} \sin(\theta_i - \theta_k - \alpha_{ik}) = 0, \\
\text{for} \quad i = 1, \ldots, n_g, \\
P_{L_i}(V_i) - \sum_{k=1}^{n_e} V_i V_k Y_{ik} \cos(\theta_i - \theta_k - \alpha_{ik}) = 0, \\
Q_{L_i}(V_i) - \sum_{k=1}^{n_e} V_i V_k Y_{ik} \sin(\theta_i - \theta_k - \alpha_{ik}) = 0, \\
\text{for} \quad i = n_g + 1, \ldots, n_g + n_l.
\end{aligned}$$

The respective states and parameters in the power network are described in Appendix 8.2.

By linearizing the DAEs at an equilibrium point, we obtain the small-signal model of the power network. We determine the equilibrium point from the power flow analysis as shown in Sauer and Pai (1998b); Chakrabortty and Khargonekar (2012). A power system stabilizer (PSS), which acts as a local controller at the generator is designed based on the small-signal model as shown in

Chakrabortty and Khargonekar (2012). The input to the PSS controller is $\omega_i(t)$ and PSS output, $V_{ref_i}(t)$, is fed to the fast acting exciter at the generator. A Type-I PSS given in Jabr et al. (2010) is considered here which consists of a wash-out filter and two phase-lead filters. The transfer function of PSS is given by

$$\frac{\Delta V_{ref_i}(s)}{\Delta \omega_i(s)} = k_{pss} \frac{(1+sT_{num})^2}{(1+sT_{den})^2} \frac{sT_w}{1+sT_w} \tag{3.1}$$

where k_{pss} is the PSS gain, T_w is the time constant of wash-out filter and T_{num}, T_{den} are time constants of phase-lead filter with $T_{num} > T_{den}$. Now, define the PSS states at all generators as $x_{pss} = [x_{pss_1}^\top \cdots x_{pss_{n_g}}^\top]^\top$, where $x_{pss_i} = [\Delta V_{ref_i}, \Delta \dot{V}_{ref_i}, \Delta \ddot{V}_{ref_i}]^\top$. Now, by appending the PSS dynamics with the generator dynamics and eliminating the algebraic states by kron-reducing the system, we obtain a reduced order dynamic model as shown below.

$$\Delta \dot{x}_p = \bar{A} \Delta x_p + E_1 \Delta \tilde{u} \tag{3.2}$$

where $\Delta x_p \in \mathbb{R}^{7n_g}$ and $\Delta \tilde{u} \in \mathbb{R}^{n_g}$. For a clear explanation of this model description, we refer the readers to Chakrabortty and Khargonekar (2012). In this work, we focus on using this model to study the inter-area oscillations and to design a robust wide-area controller with PMU measurements subject to communication channel uncertainties.

The problem of inter-area oscillations in a power network is well-studied, and one can find a summary of the work on this topic in Rogers (2012). We try to give a brief idea behind the cause and consequences of these inter-area oscillations. In the presence of poor damping in the power network or weak transmission lines, the system tends to group into coherent areas that are oscillating against each other at low frequencies. Those oscillations in the range of 0.1-1 Hz are referred to as inter-area oscillations. These oscillations are undesirable as they hinder the goal to achieve optimal power flow in the power network and in some cases, the oscillations become unstable leading to blackouts or cascading failures. Although PSS is present at each generator, its effect is limited to a local area and does not damp inter-area oscillations that are taking place in the entire power network. Therefore, it is imperative for us to design a controller with measurements of the whole network. Such a controller is called wide area controller, and it achieves the inter-area

oscillation damping in the power network by inducing additional damping in the network. This additional damping is induced in the network by controlling the power electronic devices, referred to Flexible AC Transmission Systems (FACTS) devices located in the power network. FACTS devices use the wide area measurements from PMUs and change the real and reactive power injections into the network. One such FACTS device we model in this work is SVC - Static VAr Compensator. An SVC is a shunt device and supplies reactive power to the bus to control its voltage. For the detailed modeling of the FACTS devices in the system dynamics, we refer the reader to Chakrabortty and Khargonekar (2012); Pushpak and Vaidya (2016).

As the power transfer depends on bus voltage, the addition of a shunt device is modeled into the swing dynamics. We assume the availability of the shunt device, SVC at each bus. The small-signal model of the power network with the FACTS devices is given by

$$\begin{aligned} \Delta\dot{x}_p &= A_p\Delta x_p + B_p\Delta u_p \\ y_p &= C_p\Delta x_p \end{aligned} \tag{3.3}$$

where $\Delta x_p \in \mathbb{R}^{7n_g}$, $\Delta u_p \in \mathbb{R}^{3n_g}$ and $y_p \in \mathbb{R}^{3n_g}$. For simplicity, we define, $n := 7n_g$, $d := 3n_g$, $m := 2d$ and we stick to these notations hereafter in this chapter. The output matrix we are dealing with here is not the power system output matrix, it is in fact the matrix corresponding to the PMU locations (sensors) in the network. Hence, the entries of the output matrix, C_p depends on the availability of PMUs.

3.2 Power System with Wide Area Control

The state space system (3.3) describes the reduced power network model with PSS and FACTS devices. PMUs are placed at different buses in the network to continuously relay the data at that bus to the control center. The PMU measurements from the power network are transferred to the control center through a communication channel. Similarly, all the control inputs to the generators, FACTS devices from the control center are sent through a communication network. While the generators, loads, and transmission lines constitute the physical part of the power network, the sensing using PMUs, control center, and communication channel connecting the physical power

grid to control center constitute the cyber component of the power network. Together, they define a cyber-physical power system. In Fig. 3.1, we show the cyber-physical split of the power system. The cyber component of the power system is subjected to various forms of uncertainties. The source of uncertainties could be natural such as faulty sensors or actuators, packet drops, and random delay in communication channels. Furthermore, malicious attack or intentional tampering of data on the cyber component can also be modeled as uncertainty.

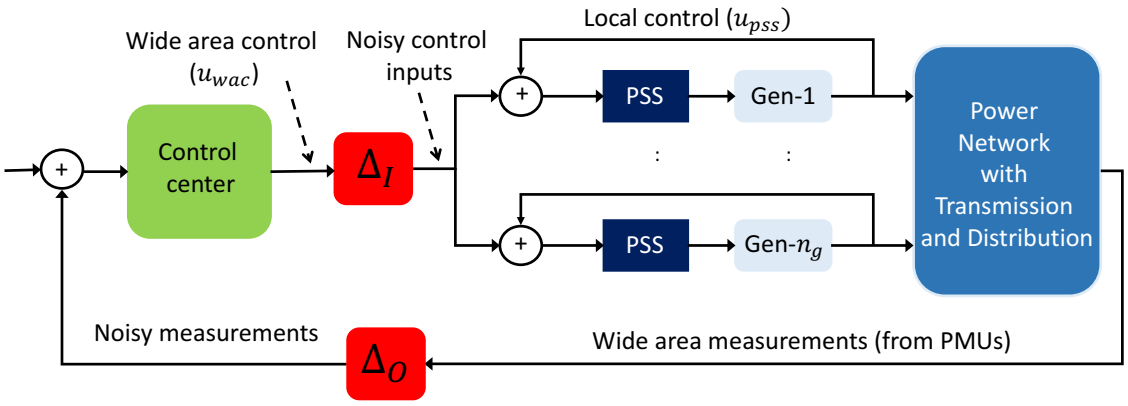

Figure 3.1 Feedback control of power network with stochastic uncertainty

Stochastic uncertainty-based channel uncertainty model provides a unified framework to model various sources of uncertainty arising from the cyber component of power grid. In the following discussion, we present stochastic uncertainty-based model for the cyber-physical power system. We discuss both continuous and discrete-time models for cyber-physical power system specifically motivated with regard to accommodating two different forms of channel uncertainties. The physical part of the power system in continuous-time is given in Eq. (3.3) and is denoted by $\mathbb{P}$. After dropping the Δ in front of the state variable and control input, we rewrite Eq. (3.3) as

$$\mathbb{P}: \begin{cases} \dot{x}_p = A_p x_p + B_p u_p \\ y_p = C_p x_p \end{cases} \tag{3.4}$$

The cyber component consists of controller dynamics and the communication channels connecting the physical power grid with the controller. The controller dynamics for the cyber component is

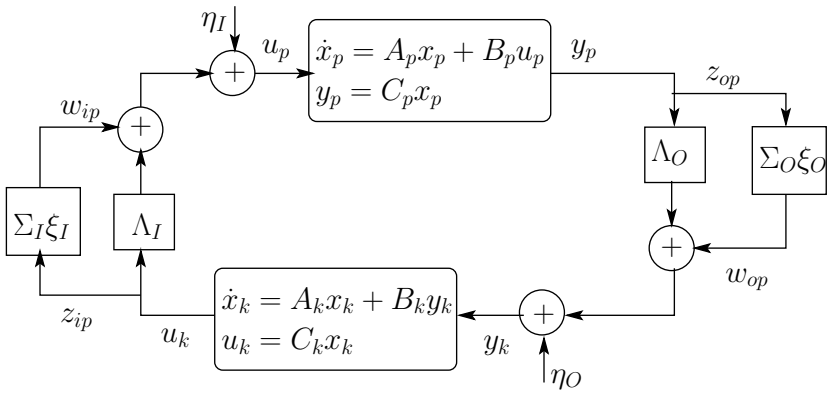

Figure 3.2 Power network interacting with controller over stochastic communication channels.

denoted by $\mathbb{K}$ and is written as follows:

$$\mathbb{K} : \begin{cases} \dot{x}_k = A_k x_k + B_k y_k \\ u_k = C_k x_k \end{cases} \tag{3.5}$$

where $x_k \in \mathbb{R}^n$ are the controller states, $y_k \in \mathbb{R}^d$, and $u_k \in \mathbb{R}^d$ are the controller input and output respectively. The physical power grid interacts with the controller over the communication channels where the output of the physical system, y_p interacts with the input of the controller, y_k, over the output communication channels and the output of the controller, u_k interacts with the input of the physical system, u_p over input communication channels (refer to Fig. 3.2).

Next, we show the modeling of the stochastic channel between the power network and the control center. To generalize this set-up, we also consider a zero mean additive uncertainty in the communication channels.

3.3 Communication Channel Modeling with Stochastic Uncertainty

For continuous-time network power system model with wide area control, we assume that the output of the plant is connected to the input of the controller over a Gaussian uncertain channel and it is assumed to be affected by multiplicative as well as additive uncertainty. In particular, we

separate the mean and zero mean (stochastic part) of the multiplicative uncertainty (as shown in Eq. (4.11)) and is expressed as

$$y_k = (\Lambda_O + \Sigma_O \xi_O)\, y_p + H_O \eta_O$$

where $\xi_O = \frac{d\Delta_O}{dt}$ and $\eta_O = \frac{d\zeta_O}{dt}$ are the multiplicative and additive stochastic uncertainties in the output channel respectively. The matrices, Λ_O, Σ_O denote the mean and standard deviation of the multiplicative uncertainty and they are defined as

$$\Lambda_O := \operatorname{diag}\left(\lambda_O^1, \ldots, \lambda_O^d\right), \quad \Sigma_O := \operatorname{diag}\left(\sigma_O^1, \ldots, \sigma_O^d\right).$$

Further,

$$H_O := \operatorname{diag}\left(H_O^1, \ldots, H_O^d\right),$$
$$\frac{d\Delta_O}{dt} := \operatorname{diag}\left(\frac{d\Delta_O^1}{dt}, \ldots, \frac{d\Delta_O^d}{dt}\right), \quad \frac{d\zeta_O}{dt} := \operatorname{diag}\left(\frac{d\zeta_O^1}{dt}, \ldots, \frac{d\zeta_O^d}{dt}\right),$$

where $\Delta_O^1(t), \ldots, \Delta_O^d(t)$ and $\zeta_O^1(t), \ldots, \zeta_O^d(t)$ are independent standard Wiener processes. It is assumed that the additive uncertainty and multiplicative uncertainty in the output channel are assumed to be uncorrelated. More specifically, the standard Wiener processes, $\Delta_O^\ell(t)$ and $\zeta_O^\ell(t)$ for $\ell = 1, \ldots, d$, are independent.

Similarly, the input of the plant is connected to the output of the controller over a channel with Gaussian uncertainty as follows,

$$u_p = (\Lambda_I + \Sigma_I \xi_I)\, u_k + H_I \eta_I,$$

where $\xi_I = \frac{d\Delta_I}{dt}$ and $\eta_I = \frac{d\zeta_I}{dt}$ are the multiplicative and additive uncertainties in the input channel respectively. The matrices, Λ_I, Σ_I are the mean and standard deviation of the multiplicative uncertainty and are defined as

$$\Lambda_I = \operatorname{diag}\left(\lambda_I^1, \ldots, \lambda_I^d\right), \quad \Sigma_I = \operatorname{diag}\left(\sigma_I^1, \ldots, \sigma_I^d\right).$$

Further,

$$H_I := \operatorname{diag}\left(H_I^1, \ldots, H_I^d\right),$$

$$\frac{d\Delta_I}{dt} = \text{diag}\left(\frac{d\Delta_I^1}{dt}, \ldots, \frac{d\Delta_I^d}{dt}\right), \quad \frac{d\zeta_I}{dt} := \text{diag}\left(\frac{d\zeta_I^1}{dt}, \ldots, \frac{d\zeta_I^d}{dt}\right),$$

where $\Delta_I^1(t), \ldots, \Delta_I^d(t)$ and $\zeta_I^1(t), \ldots, \zeta_I^d(t)$ are independent standard Wiener processes. It is assumed that the additive uncertainty and multiplicative uncertainty in the input channel are assumed to be uncorrelated, ie., the standard Wiener processes, $\Delta_I^\ell(t)$ and $\zeta_I^\ell(t)$ for $\ell = 1, \ldots, d$, are independent. Moreover, the input and output channel uncertainties are assumed uncorrelated.

3.4 Network Power System in Robust Control Form

The power system dynamical model derived in subsection 3.1, wide area control model from subsection 3.2, and channel uncertainty model from subsection 3.3 can all be combined to model the power system with communication channel uncertainty in robust control form with stochastic uncertainty. Note that standard robust control form consists of the nominal deterministic system in feedback interconnection with norm-bounded deterministic uncertainty. Stability analysis and controller synthesis results are well established in Dullerud and Paganini (2013); Skogestad and Postlethwaite (2007) for this standard framework. The novelty of our framework is that we have extended the stability analysis and controller synthesis from standard robust control theory with norm-bounded deterministic uncertainty to stochastic uncertainty in the feedback loop (refer to Fig.4.1).

The basic idea behind writing the power system in standard robust control form is by separating the non-zero mean part of the stochastic channel uncertainty and including it in the deterministic part or the nominal power system dynamics. To achieve this, we introduce two new variables namely disturbance signal $w_1 \in \mathbb{R}^d$, $w_2 \in \mathbb{R}^d$ and control variables $z_1 \in \mathbb{R}^d$ and $z_2 \in \mathbb{R}^d$. Concerning Fig. 3.2, the control and disturbance variables are related as follows:

$$z_{op} = y_p, \quad z_{ip} = u_k, \quad w_{op} = \Sigma_O \frac{d\Delta_O}{dt} z_{op}, \quad w_{ip} = \Sigma_I \frac{d\Delta_I}{dt} z_{ip}.$$

We re-enumerate the input and output uncertainties,

$$\Delta_I^1(t), \ldots, \Delta_I^d(t), \Delta_O^1(t), \ldots, \Delta_O^d(t)$$

as

$$\Delta_1(t), \Delta_2(t), \ldots, \Delta_m(t),$$

since $m := 2d$. Similarly, re-enumerate the processes, $\zeta_I(t), \zeta_O(t)$.

The nominal power system dynamics, denoted by $\mathbb{G}$, now consists of feedback interconnection of power network and wide area control with nonzero mean part of the stochastic uncertainty in the feedback channel. We denote it by $\mathbb{G} := \mathcal{F}(\mathbb{P}, \mathbb{K})$. The nominal system has the following state space form.

$$\mathbb{G} : \begin{cases} \dot{x} = Ax + Bw \\ z = Cx \end{cases} \tag{3.6}$$

where

$$x = \begin{bmatrix} x_p \\ x_k \end{bmatrix} \in \mathbb{R}^{2n}, z = \begin{bmatrix} z_{op} \\ z_{ip} \end{bmatrix} \in \mathbb{R}^m, w = \begin{bmatrix} w_{op} \\ w_{ip} \end{bmatrix} \in \mathbb{R}^m, C := \begin{bmatrix} C_p & 0 \\ 0 & C_k \end{bmatrix}, B := \begin{bmatrix} 0 & B_p \\ B_k & 0 \end{bmatrix},$$

$$A := \begin{bmatrix} A_p & B_p \Lambda_I C_k \\ B_k \Lambda_O C_p & A_k \end{bmatrix}.$$

Similarly, defining

$$\frac{d\zeta}{dt} = \begin{bmatrix} \frac{d\zeta_I}{dt} \\ \frac{d\zeta_O}{dt} \end{bmatrix}, \quad \frac{d\Delta}{dt} := \begin{bmatrix} \Sigma_O \frac{d\Delta_O}{dt} & 0 \\ 0 & \Sigma_I \frac{d\Delta_I}{dt} \end{bmatrix}, \quad H := \begin{bmatrix} B_p H_I & 0 \\ 0 & B_k H_O \end{bmatrix},$$

we can write the feedback interconnection of nominal system, $\mathbb{G}$ with the multiplicative uncertainty $\frac{d\Delta}{dt}$ and additive uncertainty $\frac{d\zeta}{dt}$, as $\mathcal{F}\left(\mathbb{G}, \frac{d\Delta}{dt}\right)$.

$$\mathcal{F}\left(\mathbb{G}, \frac{d\Delta}{dt}\right) : \begin{cases} \dot{x} = Ax + Bw + H\frac{d\zeta}{dt} \\ z = Cx \\ w = \frac{d\Delta}{dt} z \end{cases} \tag{3.7}$$

In this chapter, we have modeled the power system dynamics with stochastic uncertainty arising due to

1. presence of unreliable and intermittent availability of wind energy
2. a cyber attack on the communication channels or inherent communication channel uncertainties

Further, we have shown the stochastic power network model can be written in a networked control system form. In the next chapter, we develop stability analysis and controller synthesis results that can be applied to analyze the stochastic stability of the power network. The results we presented in the next chapter are more general and can be applied to any continuous-time stochastic linear networked systems.

CHAPTER 4. STOCHASTIC STABILITY ANALYSIS AND CONTROLLER SYNTHESIS

In this chapter, we lay the foundation for the analysis of linear continuous-time stochastic networked systems and provide the results for stability analysis and controller synthesis formulation of such systems. The results developed in this chapter are more general and are applied to study the stochastic stability of the power network and design controller robust to stochastic uncertainty. We start this chapter by recalling some of the concepts and definitions related to stochastic differential equations (SDE) from Lasota and Mackey (1994). In this work, rather than looking at the evolution of individual trajectories, we look at the flow of densities where the initial density function corresponds to the initial states. This intuitive approach is discussed in Chapter 1 of Lasota and Mackey (1994).

4.1 Preliminaries and Definitions

This section consists of preliminaries and definitions behind the density function based approach for the analysis of stochastic differential equations (SDE's). Consider the following linear SDE with stochastic multiplicative uncertainty,

$$\dot{x} = Ax + \sum_{\ell=1}^{m} \sigma_\ell B_\ell x \xi_\ell \tag{4.1}$$

where $x \in \mathbb{R}^n$, for $\ell = 1, \ldots, m$, $\xi_\ell = \frac{d\Delta_\ell}{dt}$ with $\Delta_1, \ldots, \Delta_m$ being the standard independent Wiener process (Brownian motion) and $\sigma_\ell > 0$, for $\ell = 1, \ldots, m$.

Notation 2. *In the following, $x(t)$ is used to denote the solution of system (4.1) defined in the sense of Itô and notation x is used to describe the states. We refer the readers to Lasota and Mackey (1994)[Theorem 11.5.1] for technical assumptions leading to existence and uniqueness of solution to SDE (4.1). It is important to emphasize that these assumptions are satisfied by (4.1).*

Next, we state the following stability definition for system (4.1).

Definition 3. *[Mean Square Exponentially Stable] System (4.1) is mean square exponentially stable, if there exists positive constants β_1 and β_2, such that,*

$$E[x(t)^\top x(t)] \leq \beta_1 \exp(-\beta_2 t) E[x(0)^\top x(0)], \quad \forall\ x(0) \in \mathbb{R}^n.$$

We now consider the following SDE with multiplicative as well as additive stochastic uncertainty.

$$\dot{x} = Ax + \sum_{\ell=1}^{m} \sigma_\ell B_\ell x \xi_\ell + H\eta, \tag{4.2}$$

where $x \in \mathbb{R}^n$, $H \in \mathbb{R}^n$, and for $\ell = 1, \ldots, m$, $\xi_\ell = \frac{d\Delta_\ell}{dt}$, $\eta = \frac{d\zeta}{dt}$ with $\Delta_1, \ldots, \Delta_m, \zeta$ being the standard independent Wiener process (Brownian motion). It is assumed that the standard Wiener process, ζ is uncorrelated with the processes, $\Delta_1, \ldots, \Delta_m$. We now define the notion of bounded moment stability for system (4.2).

Definition 4. *[Second Moment Bounded] System (4.2) is said to be second moment bounded if there exists a positive constant β, such that,*

$$\lim_{t\to\infty} E[x(t)^\top x(t)] \leq \beta,\ \forall\ x(0) \in \mathbb{R}^n.$$

Instead of analyzing the individual trajectories, $x(t)$, we adopt density-based approach as proposed in Lasota and Mackey (1994) towards the analysis of stochastic system (4.2). In particular, the density function $\psi(x,t)$ for the stochastic process $x(t)$ satisfies

$$\text{Prob}\{x(t) \in B\} = \int_B \psi(z,t) dz \ \text{ for any set } \ B \subset \mathbb{R}^n.$$

The density function, $\psi(x,t)$ is obtained as a solution of a linear partial differential equation, known as the Fokker-Planck (FP) equation, also called the Kolmogorov forward equation (refer Lasota and Mackey (1994)[Theorem 11.6.1]). The FP equation is defined as follows

$$\frac{\partial \psi}{\partial t} = \frac{1}{2} \sum_{i,j=1}^{n} \frac{\partial^2}{\partial x_i \partial x_j} \left(\sum_{\ell=1}^{m} \sigma_\ell^2 (b_\ell^i x)(b_\ell^j x) + h_i h_j \right) \psi - \sum_{i=1}^{n} \frac{\partial}{\partial x_i} (a_i x) \psi, \quad t > 0,\ x \in \mathbb{R}^n, \tag{4.3}$$

where a_i, b_ℓ^i are the i^{th} rows of A, B_ℓ respectively and h_i is the i^{th} entry of H in Eq. (4.2).

Remark 5. *The coefficients, $\sum_{\ell=1}^{m}\sigma_\ell^2(b_\ell^i x)(b_\ell^j x)+h_i h_j$, $a_i x$ satisfy the uniform parabolicity condition and hence they are regular (refer (Lasota and Mackey, 1994, Definition 11.7.2)). Based on these properties of coefficients, the solution of FP equation satisfies following bounds (refer Lasota and Mackey (1994)[Theorem 11.7.1]),*

$$|\psi|,\left|\frac{\partial\psi}{\partial t}\right|,\left|\frac{\partial\psi}{\partial x_i}\right|,\left|\frac{\partial^2\psi}{\partial x_i\partial x_j}\right|\leq \bar{K}t^{-(n+2)/2}\exp\left(-\frac{1}{2}\bar{\delta}|x|^2/t\right),$$

where $\bar{K}$ and $\bar{\delta}$ are positive constants and are function of bounds that appear in the uniform parabolicity condition and bounds on the initial density function, $\psi(x,0)$.

These bounds on ψ and its derivatives allow us to multiply the FP equation (4.3) with any increasing function that increases more slowly than $\exp(-\frac{1}{2}|x|^2)$. The resultant function is decreasing and we can integrate term by term in order to compute moments of $\psi(x,t)$. It is known, for the case of a linear system driven by additive white noise process, if the initial density function, $\psi(x,0)$, is Gaussian, then $\psi(x,t)$ remains Gaussian for all future time t. Hence, for linear systems with additive white noise forcing, the infinite dimensional FP equation can be replaced with the finite dimensional equation for the evolution of the mean and covariance. In the following lemma, we show the covariance evolution for system (4.2) with multiplicative noise is closed and does not depend upon higher order moments.

Lemma 6. *Define the covariance matrix,*

$$\bar{Q}(t)=E[x(t)x(t)^\top|\psi]:=\int_{\mathbb{R}^n}xx^\top\psi(x,t)dx,$$

and $\bar{Q}(0):=\bar{Q}_0<\infty$, then $\bar{Q}(t)$ satisfies the following matrix differential equation (MDE) for system (4.2).

$$\dot{\bar{Q}}=\bar{Q}A^\top+A\bar{Q}+\sum_{\ell=1}^{m}\sigma_\ell^2 B_\ell\bar{Q}B_\ell^\top+HH^\top. \tag{4.4}$$

Proof. Consider the quadratic function, $V(x)=x^\top Px$, for any $P=P^\top>0$ that is increasing. Then,

$$E[V|\psi]:=\int_{\mathbb{R}^n}V(x)\psi(x,t)dx.$$

Taking the time derivative on both sides and after simplification, we obtain (refer Lasota and Mackey (1994)[Theorem 11.9.1])

$$\frac{dE[V|\psi]}{dt} = \int_{\mathbb{R}^n} \left\{ \frac{1}{2} \sum_{i,j=1}^{n} \left[\sum_{\ell=1}^{m} \sigma_\ell^2 (b_\ell^i x)(b_\ell^j x) + h_i h_j \right] \frac{\partial^2 V}{\partial x_i \partial x_j} + \sum_{i=1}^{n} (a_i x) \frac{\partial V}{\partial x_i} \right\} \psi(x,t) dx = E[\mathcal{L}V|\psi] \tag{4.5}$$

where,

$$\mathcal{L}V = x^\top \left(A^\top P + PA + \sum_{\ell=1}^{m} \sigma_\ell^2 B_\ell^\top P B_\ell \right) x + H^\top P H. \tag{4.6}$$

The time derivative of $E[V|\psi]$ is obtained by doing integration by parts where we make use of Remark 5. In particular, we make use of the fact that the products, $\psi V, \frac{\partial \psi}{\partial x_i} V, \psi \frac{\partial V}{\partial x_i}$ vanish exponentially as $|x| \to \infty$ and hence, the higher order moments become zero. By substituting Eq. (4.6) in Eq. (4.5), and using the linearity of trace, expectation and commutativity inside trace, we obtain,

$$\frac{d(\mathrm{tr}(E[xx^\top|\psi]P))}{dt} = \mathrm{tr}\left(\left(A^\top P + PA + \sum_{\ell=1}^{m} \sigma_\ell^2 B_\ell^\top P B_\ell \right) E[xx^\top|\psi] + HH^\top P \right).$$

By definition of expectation, $E[xx^\top|\psi] = \bar{Q}$, we have,

$$\mathrm{tr}(\dot{\bar{Q}}P) = \mathrm{tr}\left(\left(\bar{Q}A^\top + A\bar{Q} + \sum_{\ell=1}^{m} \sigma_\ell^2 B_\ell \bar{Q} B_\ell^\top + HH^\top \right) P \right).$$

This can be rewritten in terms of an inner product as

$$\left\langle \dot{\bar{Q}} - (\bar{Q}A^\top + A\bar{Q} + \sum_{\ell=1}^{m} \sigma_\ell^2 B_\ell \bar{Q} B_\ell^\top + HH^\top), P \right\rangle = 0.$$

Since, $P > 0$, we have

$$\dot{\bar{Q}} = \bar{Q}A^\top + A\bar{Q} + \sum_{\ell=1}^{m} \sigma_\ell^2 B_\ell \bar{Q} B_\ell^\top + HH^\top.$$

Furthermore, for $H = 0$, we obtain the covariance propagation equation for the system (4.1) without additive noise. □

Lemma 7. *The system (4.1) is mean square exponentially stable if and only if system (4.2) is second moment bounded.*

Proof. Let $\phi : \mathbb{R}^{n\times n} \to \mathbb{R}^{n^2}$ be a bijective operator (refer Costa et al. (2006)[Chapter 2]) which converts a matrix into a column vector. Then, applying the operator, ϕ on both sides of MDE's, Eq. (4.1) and Eq. (4.2), they can be written as linear vector differential equations.

$$\dot{\vartheta} = \mathscr{A}\vartheta, \tag{4.7}$$

$$\dot{\bar{\vartheta}} = \mathscr{A}\bar{\vartheta} + \mathscr{B}, \tag{4.8}$$

where $\vartheta = \phi(Q), \bar{\vartheta} = \phi(\bar{Q})$, $\mathscr{B} = (G \otimes G)\phi(I) \in \mathbb{R}^{n^2}$ and

$$\mathscr{A} = A \oplus A + \sum_{k=1}^{p} \sigma_k^2 (B_k \otimes B_k) \in \mathbb{R}^{n^2\times n^2},$$

where I is the identity matrix of size $n \times n$ and $\otimes$ denotes the Kronecker product, $\oplus$ is the Kronecker sum.

Necessity: The mean square exponential stability of system (4.1) yields stability of system (4.7), that is, $\mathscr{A}$ is Hurwitz. Since $\mathscr{A}$ is Hurwitz, the steady state value of $\bar{\vartheta}$ is given by

$$\lim_{t\to\infty} \bar{\vartheta}(t) = \lim_{t\to\infty} \phi(\bar{Q}(t)) = -\mathscr{A}^{-1}\mathscr{B}.$$

Now, taking the inverse ϕ operator, we obtain,

$$\lim_{t\to\infty} E[x(t)x(t)^\top|\psi] = -\phi^{-1}(\mathscr{A}^{-1}\mathscr{B}),$$

where $\phi^{-1}(\mathscr{A}^{-1}\mathscr{B})$ is finite. Therefore, system (4.2) is second moment bounded.

Sufficiency: If system (4.2) is second moment stable, then $\lim_{t\to\infty} \bar{Q}(t)$ is a finite value. Then, we have

$$\lim_{t\to\infty} \bar{Q}(t) = \lim_{t\to\infty} \phi^{-1}(\vartheta(t)) = \lim_{t\to\infty} \phi^{-1}(e^{\mathscr{A}t}\vartheta(0) + (e^{\mathscr{A}t} - I)\mathscr{A}^{-1}\mathscr{B}),$$

where I is the identity matrix. The limit on the right-hand side is finite, if and only if $\mathscr{A}$ is Hurwitz, which implies system (4.7) is stable and hence system (4.1) is mean square exponentially stable. □

4.2 Stochastic Uncertainty Modeling

In this section, we discuss how the stochastic uncertainty enters into the system dynamics. The problem set-up (as shown in Figure. 4.1) follows closely with the one used in Elia (2005) for mean

square exponential stability analysis of a discrete-time network. The dynamics of the plant are described by

$$\mathbb{P}: \begin{cases} \dot{x}_p &= A_p x_p + B_p u_p \\ y_p &= C_p x_p \end{cases}, \tag{4.9}$$

where $x_p \in \mathbb{R}^n, u_p \in \mathbb{R}^d$, and $y_p \in \mathbb{R}^q$ are the plant state, input, and output, respectively. Here, in this work, the plant of interest is the power network. The state space model for the plant is assumed to be stabilizable, detectable, and strictly proper. Similarly, the controller dynamics are assumed to be strictly proper with the following state space model.

$$\mathbb{K}: \begin{cases} \dot{x}_k &= A_k x_k + B_k y_k \\ u_k &= C_k x_k \end{cases}, \tag{4.10}$$

where $x_k \in \mathbb{R}^n, y_k \in \mathbb{R}^q$, and $u_k \in \mathbb{R}^d$. The assumption on the controller dynamics being strictly proper is essential, since it allows us to study the case where the uncertainties enter at both input and output channels (for more explanation, please refer to Subsection 4.2.1). If the uncertainty enters only at the input or the output channel, then one can consider the controller dynamics which is not strictly proper, such as in Pushpak et al. (2015).

The output of the plant before reaching the controller is affected by stochastic uncertainty and is given by $y_k = \Xi_O y_p$. Similarly, the input to the plant from controller is affected by stochastic uncertainty which is $u_p = \Xi_I u_k$. The output (Ξ_O) and input (Ξ_I) channel uncertainties can be separated into mean and zero mean part as shown below.

$$\Xi_O = \Lambda_O + \Sigma_O \frac{d\Delta_O}{dt}, \qquad \Xi_I = \Lambda_I + \Sigma_I \frac{d\Delta_I}{dt}, \tag{4.11}$$

where $\Lambda_{I(O)}$ are the mean part of the input (output) channel uncertainty, $\Sigma_{I(O)}$ are the standard deviation of the input (output) channel uncertainty, and $\Delta_{I(O)}$ denotes the vector valued independent Wiener processes. The corresponding matrices are defined as

$$\begin{aligned} &\Lambda_O := \mathrm{diag}(\lambda_O^1, \ldots, \lambda_O^q), \quad \Lambda_I := \mathrm{diag}(\lambda_I^1, \ldots, \lambda_I^d), \\ &\Sigma_O := \mathrm{diag}(\sigma_O^1, \ldots, \sigma_O^q), \quad \Sigma_I := \mathrm{diag}(\sigma_I^1, \ldots, \sigma_I^d), \\ &\frac{d\Delta_O}{dt} := \mathrm{diag}\left(\frac{d\Delta_O^1}{dt}, \ldots, \frac{d\Delta_O^q}{dt}\right), \quad \frac{d\Delta_I}{dt} := \mathrm{diag}\left(\frac{d\Delta_I^1}{dt}, \ldots, \frac{d\Delta_I^d}{dt}\right). \end{aligned}$$

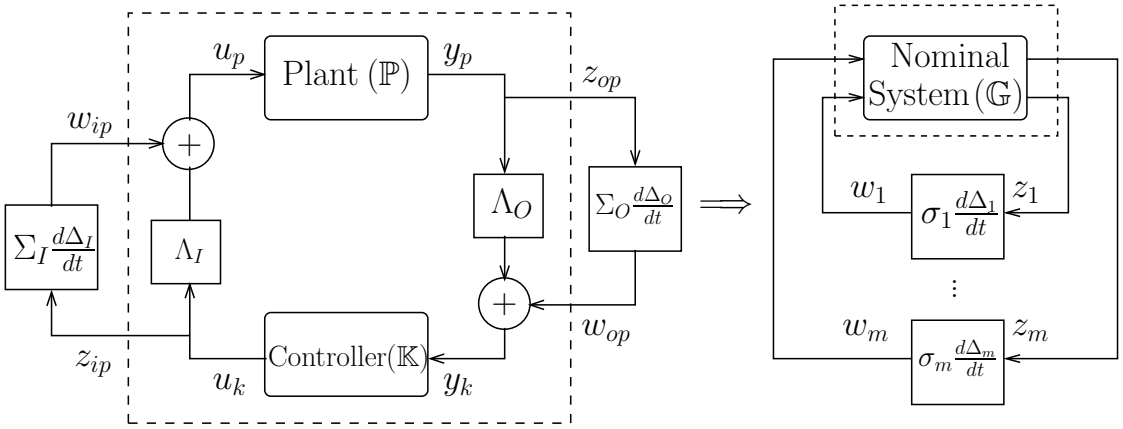

Figure 4.1 a) MIMO plant and controller with stochastic uncertainty in the input and output channels b) MIMO nominal system with stochastic uncertainty in the feedback

Both the input and output channel uncertainties are assumed to be uncorrelated.

Figure 4.1a consists of MIMO plant and controller interacting through uncertain inputs and outputs. The nominal part of this stochastic closed-loop system ($\mathbb{G}$) is the deterministic part of the stochastic closed-loop system which consists of MIMO plant ($\mathbb{P}$), controller ($\mathbb{K}$) and the mean part of the uncertainties (Λ_O, Λ_I). This nominal part, denoted by $\mathbb{G} = \mathcal{F}(\mathbb{P}, \mathbb{K})$, which is essentially the feedback interconnection of plant and controller interacting through the mean part of uncertain channels and is shown inside the dotted line in Figure. 4.1a. Now, the nominal system in Figure. 4.1a, interacts with the stochastic uncertainty via the disturbance ($w_{op} \in \mathbb{R}^q$ and $w_{ip} \in \mathbb{R}^d$) and control signals ($z_{op} \in \mathbb{R}^q$ and $z_{ip} \in \mathbb{R}^d$). The disturbance and control signals are

$$w_{op} = \Sigma_O \frac{d\Delta_O}{dt} z_{op}, \quad w_{ip} = \Sigma_I \frac{d\Delta_I}{dt} z_{ip},$$

$$\text{and } z_{op} = y_p = C_p x_p, \quad z_{ip} = u_k = C_k x_k.$$

The nominal system has the following state space form.

$$\mathbb{G} : \begin{cases} \dot{x} &= Ax + Bw \\ z &= Cx \end{cases}, \tag{4.12}$$

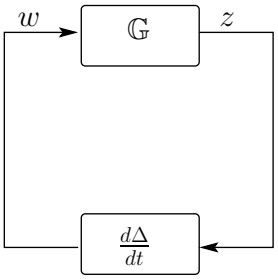

Figure 4.2 Nominal system with stochastic uncertainty

where $m = d + q$, $x = \begin{bmatrix} x_p \\ x_k \end{bmatrix} \in \mathbb{R}^{2n}$, $z = \begin{bmatrix} z_{op} \\ z_{ip} \end{bmatrix} \in \mathbb{R}^m$, $w = \begin{bmatrix} w_{op} \\ w_{ip} \end{bmatrix} \in \mathbb{R}^m$, $C = \text{diag}(C_p, C_k)$,

$$A = \begin{bmatrix} A_p & B_p \Lambda_I C_k \\ B_k \Lambda_O C_p & A_c \end{bmatrix}, \quad B = \begin{bmatrix} 0 & B_p \\ B_k & 0 \end{bmatrix}.$$

Finally, this nominal system, $\mathbb{G}$ interacting with stochastic uncertainty, $\frac{d\Delta}{dt}$ can be written in the standard robust control form, $\mathcal{F}(\mathbb{G}, \frac{d\Delta}{dt})$ as shown in Figure. 4.1b, where the stochastic uncertainty, $\frac{d\Delta}{dt} = \text{diag}\Big(\sigma_1 \frac{d\Delta_1}{dt}, \ldots, \sigma_m \frac{d\Delta_m}{dt}\Big)$. We show the nominal part of the stochastic closed-loop system inside the dotted line in Figure. 4.1b and for clarity, the individual uncertain channels are shown in feedback. Thus, the resultant stochastic closed-loop system (stochastic MIMO system) has number of feedback connections equal to the number of uncertainties. We now re-enumerate the input and output uncertainties, $\Delta_I^1, \ldots, \Delta_I^d$, $\Delta_O^1, \ldots, \Delta_O^q$ as $\Delta_1, \Delta_2, \ldots, \Delta_m$, where $m = d+q$. The closed-loop system, $\mathcal{F}(\mathbb{G}, \frac{d\Delta}{dt})$ has the following state space form and is shown in Fig. 4.2.

$$\begin{aligned} \dot{x} &= Ax + Bw \\ z &= Cx \\ w &= \tfrac{d\Delta}{dt} z := \begin{bmatrix} \Sigma_O \frac{d\Delta_O}{dt} & 0 \\ 0 & \Sigma_I \frac{d\Delta_I}{dt} \end{bmatrix} z \end{aligned} \tag{4.13}$$

where $\frac{d\Delta}{dt} = \text{diag}\Big(\sigma_1 \frac{d\Delta_1}{dt}, \ldots, \sigma_m \frac{d\Delta_m}{dt}\Big)$.

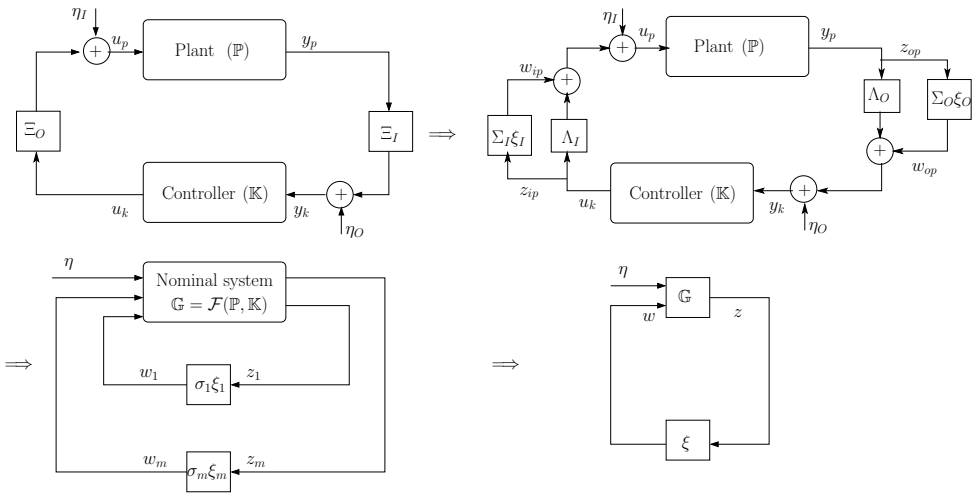

Figure 4.3 Two interconnected systems, plant and controller with multiplicative as well as additive uncertainty expressed as a nominal system interacting with uncertainty.

Remark 8. *Although we arrive at system (4.13) given in standard robust control form with input and output channel uncertainties, the framework is general enough to model stochastic parametric uncertainty in system plant, A_p, matrix.*

Given any interconnected system with stochastic uncertainty, it can written in the robust control form as shown in Fig. 4.3.

Before we conclude this section, we show mathematically that choosing a proper controller will lead to a multiplication of white noise processes which may not be a white noise process.

4.2.1 Stochastic Uncertainty Modeling with Proper Controller

The choice of strictly proper controller is necessary for our formulation to model the stochastic uncertainty in both input and output channels. In this work, the stochastic uncertainty entering the input and output channel is assumed to be uncorrelated, and these stochastic uncertainties (white noise) in the feedback loop will multiply when they traverse around the loop. While the multiplication of two white noise process is well defined, the resulting process might not be white noise, and hence the FP equation for the evolution of density cannot be defined.

In the following, we now show mathematically the choice of a proper controller (but NOT strictly proper) will lead to the multiplication of the white noise process in the closed-loop system.

Consider the state space of a strictly proper plant:

$$\mathbb{P}: \begin{cases} \dot{x}_p &= A_p x_p + B_p u_p \\ y_p &= C_p x_p \end{cases},$$

and the state space of a proper controller:

$$\mathbb{K}: \begin{cases} \dot{x}_k &= A_k x_k + B_k y_k \\ u_k &= C_k x_k + D_k y_k \end{cases},$$

and this feedback interconnection of plant and controller are connected through the uncertain channels as shown in Figure. 4.4.

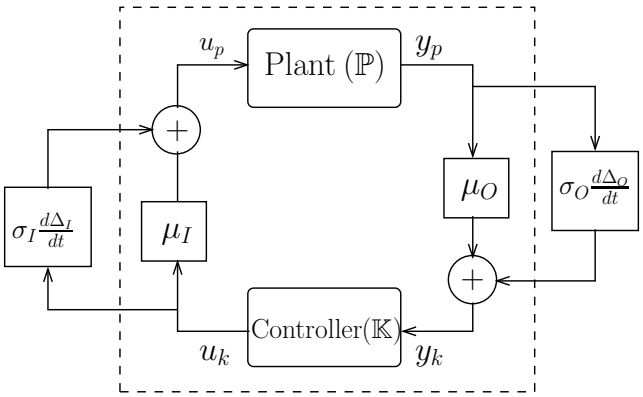

Figure 4.4 Plant and controller with uncertainty in feedback

The input to the controller and the input to the plant are given by:

$$u_p = \left(\mu_I + \sigma_I \frac{d\Delta_I}{dt}\right) u_k,$$
$$y_k = \left(\mu_O + \sigma_O \frac{d\Delta_O}{dt}\right) y_p,$$

where $\xi_O = \frac{d\Delta_O}{dt}, \xi_I = \frac{d\Delta_I}{dt}$ with ξ_O, ξ_I being the white noise processes and Δ_O, Δ_I are the independent standard Wiener processes. Now, the closed-loop system is given by

$$\begin{aligned}
\dot{x}_p =& (A_p + \mu_I\mu_O B_p D_k C_p)x_p + \mu_I B_p C_k x_k + \mu_I\sigma_O B_p D_k C_p x_p \xi_O + \sigma_I B_p C_k x_k \xi_I \\
&+ \sigma_I\mu_O B_p D_k C_p x_p \xi_I + \sigma_I\sigma_O B_p D_k C_p x_p \xi_O \xi_I, \\
\dot{x}_k =& A_k x_k + B_k(\mu_O + \sigma_O\xi_O)C_p x_p.
\end{aligned}$$

Notice that, the white noise processes are multiplying in the above closed-loop system (the term marked in red color). This multiplication can be avoided when we consider strictly proper controller or uncertainty in either input or output channels. If the uncertainty is assumed either at the input side or output side (but not on both sides) of the plant, then we can consider the controller to be a proper system. Stability analysis and controller synthesis results for the case with uncertainty either at the input or at the output case without strictly proper assumption on the controller dynamics have been shown in Pushpak et al. (2015).

In the next section, we derive necessary and sufficient conditions for mean square exponential stability of system (4.13).

4.3 Mean Square Stability Analysis

We first extend the notion of mean square norm for discrete-time system from Elia (2005) to continuous-time system. The mean square norm will be used to analyze the mean square stability of system (4.13) i.e., the feedback interconnection $\mathcal{F}(\mathbb{G}, \frac{d\Delta}{dt})$. However, the norm itself is defined for nominal system $\mathbb{G}$ with multiple inputs and outputs.

Definition 9. *[Mean Square Norm] The mean square norm for nominal system, $\mathbb{G}$, is defined as follows,*

$$\| \mathbb{G} \|_{MS} = \max_{i=1,\ldots,m} \sqrt{\sum_{j=1}^{m} \| G_{ij} \|_2^2},$$

where the system, G_{ij} denotes the transfer function of the nominal system corresponding to the input j and output i and $\| G_{ij} \|_2$ denotes the standard $\mathcal{H}_2$ norm.

Remark 10. *In the definition of mean square norm given above, number of inputs and outputs to the nominal system depend on number of uncertainties in the input and output channels. For example, in Figure. 1, there are d inputs, q outputs respectively and hence, there are* $d + q := m$ *feedback channels in the stochastic closed-loop system shown in Figure. 4.1b.*

The stochastic interconnected system (4.13) can be written as system (4.1) for which, the mean square exponential stability given in Definition 3 applies. We make the following assumption on the feedback interconnected system (4.13).

Assumption 11. *(a) The deterministic system* (4.12) *denoted by* $\mathbb{G}$ *is internally stable, that is, A is Hurwitz and moreover,* $\mathbb{G}$ *is considered to be stabilizable, detectable and strictly proper.*

(b) The initial state of the system $\mathbb{G}$*, denoted by* $x(0)$ *has bounded variance and is independent from* $\Delta_i(t)$ *for each* $i \in \{1, \ldots, m\}$*.*

These assumptions are common in the control literature (for example, refer Elia (2005); Dullerud and Paganini (2013)). To investigate the stochastic stability of the feedback interconnection $\mathcal{F}(\mathbb{G}, \frac{d\Delta}{dt})$, it is necessary condition that the system $\mathbb{G}$ is internally stable, i.e., if the system $\mathbb{G}$ is not internally stable, then the feedback interconnection is mean square unstable. Without internal stability, we cannot analyze the mean square stability of the entire system. In particular, when the system $\mathbb{G}$ is internally stable, one can determine the maximum tolerable variance of the stochastic uncertainty.

Stabilizability and detectability are again very standard assumptions in the control literature as shown in Elia (2005); Dullerud and Paganini (2013) and they are in fact weaker assumptions than controllability and observability. Moreover, the results we provide in this manuscript are based on $\mathcal{H}_2$ norm computation of this deterministic system. The assumption on stabilizability and detectability is required in the design of controller and for the computation of $\mathcal{H}_2$ norm (refer Dullerud and Paganini (2013)). Furthermore, the assumption on strictly proper nature of plant and controller is to avoid the product of two white noise processes (which is defined, but the resultant

process might not be white noise, refer Subsection 4.2.1), when the loop is closed. Finally, the assumption on initial condition is to avoid the complexity of math due to correlations.

The following theorem provides necessary and sufficient conditions for the mean square exponential stability of the interconnected system (4.13).

Theorem 12. *Under Assumption 11, the feedback interconnected system* (4.13) *shown in Figure. 4.1b is mean square exponentially stable, if and only if, there exists a* $P > 0$*, such that, it satisfies*

$$A^\top P + PA + \sum_{\ell=1}^{m} \sigma_\ell^2 C_\ell^\top B_\ell^\top P B_\ell C_\ell < 0. \tag{4.14}$$

Proof. Sufficiency: The covariance propagation equation for the feedback interconnected system with uncertainty is

$$\dot{Q}(t) = Q(t)A^\top + AQ(t) + \sum_{\ell=1}^{m} \sigma_\ell^2 B_\ell C_\ell Q(t) C_\ell^\top B_\ell^\top. \tag{4.15}$$

This covariance propagation equation is a matrix differential equation and follows from Lemma 6. To achieve mean square exponential stability, $Q(t)$ should converge to zero exponentially. To show this, we construct the Lyapunov function $V(Q(t)) = \mathrm{tr}(Q(t)P)$, where $P > 0$. Then,

$$\dot{V}(Q(t)) = \mathrm{tr}\Big((Q(t)A^\top + AQ(t) + \sum_{\ell=1}^{m} \sigma_\ell^2 B_\ell C_\ell Q(t) C_\ell^\top B_\ell^\top)P\Big).$$

Then, we obtain, $\dot{V}(Q(t)) = \mathrm{tr}(-Q(t)M)$ for some positive matrix $M > 0$. Since $M > 0$, there exits an $\alpha := \frac{\lambda_{min}(M)}{\lambda_{max}(P)} > 0$, such that $\alpha P \leq M$. Therefore, $\dot{V}(Q(t)) \leq -\alpha V(Q(t))$ and it follows, system (4.13) is mean square exponentially stable.

Necessity: Let $\phi : \mathbb{R}^{n\times n} \to \mathbb{R}^{n^2}$ be a bijective operator as shown in Costa et al. (2006)[Chapter 2] which converts a matrix into a column vector. Assume, system (4.13) to be mean square exponentially stable. Then, we know, the covariance matrix, $Q(t)$, converges exponentially to zero. This implies, we have a stable evolution for $\vartheta(t) = \phi(Q(t)) \in \mathbb{R}^{n^2}$ with the following dynamics,

$$\dot{\vartheta}(t) = \mathscr{A}\vartheta(t), \tag{4.16}$$

where $\mathscr{A} = A \oplus A + \sum_{\ell=1}^{m} \sigma_\ell^2 (B_\ell C_\ell \otimes B_\ell C_\ell)$. Stability of system (4.16) implies $\mathscr{A}$ is Hurwitz and hence $\mathscr{A}^\top$ is also Hurwitz. Therefore, the evolution, $\dot{r}(t) = \mathscr{A}^\top r(t)$ is stable and satisfies the following matrix differential equation,

$$\dot{R}(t) = A^\top R(t) + R(t)A + \sum_{\ell=1}^{m} \sigma_\ell^2 C_\ell^\top B_\ell^\top R(t) B_\ell C_\ell \tag{4.17}$$

which is also stable, where $R(t) = \phi^{-1}(r(t))$. Let $R(0) > 0$, and $R(t)$ denote the solution for Eq. (4.17). Since $R(t)$ satisfies the stable first order linear differential equation, the function $P(t) = \int_0^t R(\tau) d\tau$ has a finite value. Integrating on both sides of Eq. (4.17) and simplifying, we obtain

$$\dot{P}(t) - R(0) = A^\top P(t) + P(t)A + \sum_{\ell=1}^{m} \sigma_\ell^2 C_\ell^\top B_\ell^\top P(t) B_\ell C_\ell.$$

Observing that Eq. (4.17) is stable, as $t \to \infty$, we obtain,

$$A^\top P + PA + \sum_{\ell=1}^{m} \sigma_\ell^2 C_\ell^\top B_\ell^\top P B_\ell C_\ell = -R(0),$$

where $P := \lim_{t\to\infty} P(t)$. The result now follows by noticing that $R(0) > 0$. □

The ensuing result gives an alternative representation of the inequality given in Eq. (4.14), which is helpful in writing the LMI-based optimization for computing the mean square norm of system $\mathbb{G}$. The following lemmas, theorems, and their proofs can be viewed as the continuous-time counterpart of the discrete-time results from Elia (2005).

Lemma 13. *The inequality, Eq. (4.14) holds, if and only if, there exists a $\mathcal{Q} > 0$, and $\alpha_\ell > 0$ for every $\ell = 1, 2, \ldots, m$, such that*

$$\begin{aligned} &A\mathcal{Q} + \mathcal{Q}A^\top + \sum_{\ell=1}^{m} B_\ell \alpha_\ell B_\ell^\top < 0, \\ &\alpha_\ell > \sigma_\ell^2 C_\ell \mathcal{Q} C_\ell^\top, \quad \ell = 1, 2, \ldots, m. \end{aligned} \tag{4.18}$$

Proof. The dual inequality equivalent to Eq. (4.14) is

$$A\mathcal{Q} + \mathcal{Q}A^\top + \sum_{\ell=1}^{m} \sigma_\ell^2 B_\ell C_\ell \mathcal{Q} C_\ell^\top B_\ell^\top < 0, \tag{4.19}$$

where $\mathcal{Q} > 0$. Observe the straight forward substitution leads to a sufficiency condition. In showing the necessary part, for some matrix $M > 0$, the inequality (4.19) can be rewritten as

$$A\mathcal{Q} + \mathcal{Q}A^\top + \sum_{\ell=1}^{m} \sigma_\ell^2 B_\ell C_\ell \mathcal{Q} C_\ell^\top B_\ell^\top + M = 0. \tag{4.20}$$

Since we have, $\sum_{\ell=1}^{m} B_\ell B_\ell^\top \geq 0$, there exists $\epsilon(M) := \epsilon > 0$, such that

$$0 \leq \epsilon \sum_{\ell=1}^{m} B_\ell B_\ell^\top < M.$$

Using this in Eq. (4.20), we get

$$\begin{aligned} &A\mathcal{Q} + \mathcal{Q}A^\top + \sum_{\ell=1}^{m} \sigma_\ell^2 B_\ell C_\ell \mathcal{Q} C_\ell^\top B_\ell^\top + \epsilon \sum_{\ell=1}^{m} B_\ell B_\ell^\top < 0, \\ \Rightarrow &A\mathcal{Q} + \mathcal{Q}A^\top + \sum_{\ell=1}^{m} \left(\epsilon + \tilde{\sigma}_\ell^2 C_\ell \mathcal{Q} C_\ell^\top \right) B_\ell B_\ell^\top < 0. \end{aligned}$$

Define $\alpha_\ell = \epsilon + \sigma_\ell^2 C_i \mathcal{Q} C_\ell^\top$ and we obtain,

$$\begin{aligned} &A\mathcal{Q} + \mathcal{Q}A^\top + \sum_{\ell=1}^{m} B_\ell \alpha_\ell B_\ell^\top < 0, \\ &\alpha_\ell > \sigma_\ell^2 C_\ell \mathcal{Q} C_\ell^\top \ \text{ for } \ \ell = 1, 2, \ldots, m. \end{aligned}$$

□

In the ensuing result, a LMI-based optimization formulation is provided for the computation of mean square system norm.

Lemma 14. *Suppose A is Hurwitz and let $\theta > 0$ be a diagonal matrix. Then, we obtain,*

$$\begin{aligned} \| \theta^{-1} \mathbb{G} \theta \|_{MS}^2 = &\inf_{\mathcal{P}>0, \mathcal{S}>0, \gamma} \gamma \\ &\text{subject to } \ \mathcal{S}_{\ell\ell} < \gamma, \ \ell = 1, 2, \ldots, m, \\ &\begin{bmatrix} A^\top \mathcal{P} + \mathcal{P} A & \mathcal{P} B \theta \\ \theta B^\top \mathcal{P} & -I \end{bmatrix} < 0, \\ &\begin{bmatrix} \theta \mathcal{S} \theta & C \\ C^\top & \mathcal{P} \end{bmatrix} > 0. \end{aligned}$$

Proof. For the system, $\theta^{-1}\mathbb{G}\theta$, the mean square exponential stability conditions can be equivalently written as, there exists a $\mathcal{Q} > 0$, such that, it satisfies the following inequalities.

$$A\mathcal{Q} + \mathcal{Q}A^\top + \sum_{\ell=1}^{m} B_\ell \theta_{\ell\ell}^2 B_\ell^\top < 0, \tag{27}$$

$$\gamma_\ell \theta_{\ell\ell}^2 > C_\ell \mathcal{Q} C_\ell^\top, \quad \ell = 1, 2, \ldots, m, \tag{28}$$

where $\theta_{\ell\ell}$'s are the diagonal elements of θ. The column vector, B_ℓ's are the columns of B matrix and the row vector, C_ℓ's are the rows of C matrix. Now, multiply on both sides of inequality (27) by $\mathcal{Q}^{-1} := \mathcal{P}$, and writing it in compact form, we obtain

$$A^\top\mathcal{P} + \mathcal{P}A + \mathcal{P}B\theta\theta^\top B^\top\mathcal{P}^\top < 0. \tag{29}$$

Further, the element wise inequalities shown in Eq. (28) can be written in compact form as a linear matrix inequality as shown below.

$$\begin{aligned} &\theta\mathcal{S}\theta > C\mathcal{P}^{-1}C^\top, \\ &\mathcal{S}_{\ell\ell} < \gamma_\ell, \quad \ell = 1, 2, \ldots, m. \end{aligned} \tag{30}$$

Now rewriting Eqs. (29), (30) using Schur compliments, the computation for $\mathcal{H}_2$ norm problem can be written as an LMI optimization problem as shown below.

$$\begin{aligned} \| \theta^{-1}\mathbb{G}\theta \|_2^2 = \inf_{\gamma_\ell, \mathcal{S}>0, \mathcal{P}>0} & \sum_\ell \gamma_\ell \\ \text{subject to} \\ & \begin{bmatrix} A^\top\mathcal{P} + \mathcal{P}A & \mathcal{P}B\theta \\ \theta B^\top\mathcal{P} & -I \end{bmatrix} < 0, \\ & \begin{bmatrix} \theta\mathcal{S}\theta & C \\ C^\top & \mathcal{P} \end{bmatrix} > 0, \\ & \mathcal{S}_{\ell\ell} < \gamma_\ell, \quad \ell = 1, 2, \ldots, m. \end{aligned}$$

Now, the cost is modified to obtain the result by observing the difference between $\| \mathbb{G} \|_{MS}^2 = \max_{\ell=1:m} \mathcal{S}_{\ell\ell}$ and $\| \mathbb{G} \|_2^2 = \sum_{\ell=1}^{m} \mathcal{S}_{\ell\ell}$. □

The computation of $\mathcal{H}_2$ norm problem as an LMI optimization problem is not new and has been discussed in Dullerud and Paganini (2013), Scherer et al. (1997). A similar result for the discrete-time case has been discussed in Elia (2005).

The following theorem is the main result in this section and provides equivalent necessary, sufficient conditions for mean square exponential stability of feedback interconnected system (4.13). In fact, the results of the following theorem can be viewed as a stochastic counterpart of the small gain theorem for the continuous-time system. We apply this result to study the stochastic power network as discussed in Chapter 2.

Theorem 15. *Under Assumption 11, consider the feedback interconnected system (4.13) as shown in Figure. 4.1b. Then, the following stability conditions for mean square exponential stability are equivalent.*

(a) The feedback interconnection of nominal system $\mathbb{G}$ with stochastic uncertainty, $\frac{d\Delta}{dt}$ is mean square exponentially stable.

(b) There exists a $\mathcal{Q} > 0$ and $\alpha_\ell > 0$, for every $\ell = 1, \ldots, m$, satisfying the LMI given in Eq. (4.18).

(c) $\rho(\tilde{G}\tilde{\Sigma}) < 1$,

where ρ stands for the spectral radius of a matrix and $\tilde{\Sigma} = \text{diag}(\sigma_1^2, \cdots, \sigma_m^2)$,

$$\tilde{G} = \begin{bmatrix} \| G_{11} \|_2^2 & \ldots & \| G_{1m} \|_2^2 \\ \vdots & \ddots & \vdots \\ \| G_{m1} \|_2^2 & \ldots & \| G_{mm} \|_2^2 \end{bmatrix}.$$

Further, for $\sigma_1^2 = \cdots = \sigma_m^2 = \sigma^2$, the feedback interconnection is mean square exponentially stable if and only if

$$\sigma^2 \inf_{\theta > 0, \theta - diag} \| \theta^{-1} \mathbb{G} \theta \|_{MS}^2 < 1.$$

Proof. $(a) \Leftrightarrow (b)$ This follows by combining the results from Theorem 12 and Lemma 13.

$(b) \Leftrightarrow (c)$ This result follows by distributing the system to single input single output systems and using the spectral radius definition of nonnegative matrices discussed in Horn and Johnson (2012).

In the special case of all variances to be the same, the result follows from Lemma 14 and by choosing

$$\theta = \text{diag}(\sqrt{\alpha_1}, \sqrt{\alpha_2}, \ldots, \sqrt{\alpha_m}).$$

□

Here, the mean square norm is computed for the transformed system $\theta^{-1}\mathbb{G}\theta$. The scaling factor, θ, ensures the mean square norm with respect to all inputs and outputs is the same. Hence, for a SISO system, the scaling factor, θ, does not come into play. Moreover, in the case for a SISO system, the mean square norm is equal to the standard $\mathcal{H}_2$ norm.

Remark 16. *The equivalent condition (c) from Theorem 15 can be used to determine the maximum tolerable variance of uncertainty, σ^* above which the feedback interconnection will be mean square exponentially unstable. In particular, the critical σ^* is given by*

$$\sigma^* = \frac{1}{\sqrt{\inf_{\theta>0,\theta-diag} \parallel \theta^{-1}\mathbb{G}\theta \parallel^2_{MS}}}.$$

The results derived until here provide a framework for determining the largest variance of channel uncertainty. However, the variance value itself must be computed numerically. We do not have the analytic expression for the largest variance value expressed in terms of characteristics of the open-loop system dynamics. Later, in the simulation section, we show the variance value is a function of both the open-loop unstable poles and zeros. Therefore, in the next section, for a special class of systems, single input system with full state feedback, we show analytically, the maximum variance that can be tolerated by the nominal system with state feedback controller.

In the following, we summarize how the stochastic system with multiplicative uncertainty is written in a form that is standard in robust control theory.

(a) The original system consists of feedback interconnection of plant dynamics, denoted by $\mathbb{P}$, with the controller, $\mathbb{K}$, where the plant is connected to the controller through input and output channel with uncertainty. The uncertainty in the input and output channels are written as mean plus stochastic (i.e., zero mean) part. In particular, the input and output channel uncertainty, Ξ_I and Ξ_O respectively are written as

$$\Xi_I = \Lambda_I + \Sigma_I \frac{d\Delta_I}{dt}, \quad \Xi_O = \Lambda_O + \Sigma_O \frac{d\Delta_O}{dt},$$

where $\Lambda_{I(O)}$ are the mean part of the input (output) channel uncertainty, $\Sigma_{I(O)}$ are the variance of the input (output) channel uncertainty, and $\Delta_{I(O)}$ denotes the vector-valued independent Wiener processes. The resultant system is a stochastic system with multiplicative uncertainty.

(b) Next, we combine the plant dynamics, the controller dynamics, and the mean part of the channel uncertainties (as shown inside the dotted box in Figure. 4.1a to construct the mean or nominal closed-loop system denoted by $\mathbb{G} := \mathcal{F}(\mathbb{P}, \mathbb{K})$).

(c) Finally, the nominal closed-loop system $\mathbb{G}$ interacts with the *zero* mean input and output channel uncertainty through the disturbance signal, w, and control signal, z. We stack all the input and output channel uncertainties as $\Delta_1, \ldots, \Delta_m$ where $m = p+q$ (i.e., sum of input and output channel uncertainties) to close the uncertainty loop over the nominal dynamics $\mathbb{G}$ as shown in Figure. 4.1b. This closed-loop system is denoted by $\mathcal{F}(\mathbb{G}, \frac{d\Delta}{dt})$. Now, we can analyze the mean square exponential stability of this closed-loop system by applying Theorem 15.

4.3.1 Fundamental Limitations in a Single Input Case

In this section, we discuss the fundamental limitations in the mean square stabilization for a special case, single input system with full state feedback. The channel uncertainty is assumed at input side only. With single uncertainty in the feedback loop, the mean square system norm is reduced to standard $\mathcal{H}_2$ norm. Furthermore, using one of the standard results from robust control theory given in Rotea (1993), we know using the full state feedback measurements, the

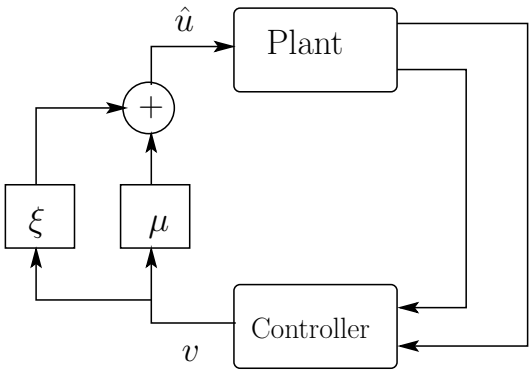

Figure 4.5 Single input system with full state feedback and uncertainty in the input channel

optimal $\mathcal{H}_2$ performance obtained from static and dynamic controllers are the same. Hence, to find the controller giving optimal $\mathcal{H}_2$ norm, it is enough to restrict the search to the class of static controllers. With some abuse of notation, we write the single-input LTI system (as shown in Figure. 4.5) with input channel uncertainty as follows.

$$\begin{aligned} \dot{x} &= A_o x + B\hat{u},\ \hat{u} = (\mu + \sigma\xi)v \\ v &= Kx, \end{aligned} \tag{4.21}$$

where $\hat{u} \in \mathbb{R}$, $\mu \neq 0$ and σ are the mean and standard deviation of the white noise process, $\xi = \frac{d\Delta}{dt}$, with Δ being the standard Wiener process. System matrix, A_o correspond to the open-loop system. We now make the following assumption.

Assumption 17. *Assume all the eigenvalues of A_o are in the right-half plane, i.e., $-A_o$ is Hurwitz and the pair (A_o, B) is stabilizable.*

Since, A_o has all eigenvalues on the right hand side, the stabilizability of pair (A_o, B) is equivalent to controllability of (A_o, B). Further, the pair $(A_o, \mu B)$ is also controllable and there exists a stabilizing controller K such that $A := A_o + \mu BK$ is Hurwitz. The objective here is to design a state feedback controller, so the closed-loop system is mean square exponentially stable with maximum tolerable variance, σ_*^2.

Theorem 18. *Consider the stabilization problem for single-input full state feedback LTI system with channel uncertainty at the input side (refer Figure. 4.5) shown in Eq. (4.21). Under Assumption 17, system (4.21) is mean square exponentially stable, if and only if,*

$$2\frac{\sigma^2}{\mu^2}\sum_i \lambda_i(A_o) < 1.$$

Proof. The system (4.21) with plant, state-feedback controller and uncertain input channel are written in closed-loop form as

$$\dot{x} = Ax + \sigma BKx\xi. \tag{4.22}$$

This closed-loop system (4.22) can be further written as a SISO system with nominal system $\mathbb{G}$ and stochastic uncertainty, ξ in the feedback. The system matrices of the nominal system, $\mathbb{G}$ are

$$\begin{pmatrix} A_o + \mu BK & B \\ K & 0 \end{pmatrix}.$$

This follows by noticing that the disturbance (w) and control (z) signals are given by $w = \xi z$ and $z = Kx$ respectively. We recall that the mean square norm for the SISO system (4.22) is equivalent to $\mathcal{H}_2$ norm of the system (4.22). Based on this, we first show the necessity part.

Necessity: From Theorem 15, we know that the necessary condition for mean square exponential stability is, $\sigma^2 \parallel \mathbb{G} \parallel_2^2 < 1$. The $\mathcal{H}_2$ norm of $\mathbb{G}$, i.e., $\parallel \mathbb{G} \parallel_2$, is given by $B^\top PB$ where $P > 0$, and is obtained from

$$(A_o + \mu BK)^\top P + P(A_o + \mu BK) + K^\top K = 0. \tag{4.23}$$

Now, the optimal K satisfying Eq. (4.23) is obtained by minimizing the left hand side (lhs) of Eq. (4.23), i.e., by taking the derivative of lhs of Eq. (4.23) w.r.t K and equating it to zero which yields, $K = -\mu B^\top P$. Using this optimal K in Eq. (4.23), we obtain,

$$A_o^\top P + PA_o - \mu^2 PBB^\top P = 0.$$

Further, we rewrite this equation by multiplying and dividing the last term with $\sigma^2 B^\top PB$ to obtain

$$A_o^\top P + PA_o - \frac{\mu^2}{\sigma^2}\frac{PBB^\top P}{B^\top PB}\sigma^2 B^\top PB = 0. \tag{4.24}$$

Now, using the given relation, $\sigma^2 B^\top PB < 1$ from mean square exponential stability, we can rewrite Eq. (4.24) as

$$A_o^\top P + PA_o - \frac{\mu^2}{\sigma^2}\frac{PBB^\top P}{B^\top PB} < 0. \tag{4.25}$$

Since, $P > 0$, pre and post multiplying Eq. (4.25) by $P^{-\frac{1}{2}}$ on both sides, we obtain,

$$P^{-\frac{1}{2}}A_o^\top P^{\frac{1}{2}} + P^{\frac{1}{2}}A_o P^{-\frac{1}{2}} - \frac{\mu^2}{\sigma^2}\frac{P^{\frac{1}{2}}BB^\top P^{\frac{1}{2}}}{B^\top PB} < 0. \tag{4.26}$$

Now, taking trace on both sides of Eq. (4.26) and using the properties of trace, we have, $2\text{tr}(A_o) < \frac{\mu^2}{\sigma^2}$.

Sufficiency: It is enough to show, $\sigma^2 B^\top PB < 1$, where $P > 0$ satisfies Eq. (4.23). Consider Eq. (4.23) and choose $K = -\mu B^\top P$ to rewrite Eq. (4.23) as

$$A_o^\top P + PA_o - \mu^2\frac{PBB^\top P}{B^\top PB}B^\top PB = 0. \tag{4.27}$$

Pre and post multiplying Eq. (4.27) by $P^{-\frac{1}{2}}$ on both sides and then taking trace on both sides, we obtain,

$$2tr(A_o) - \mu^2 tr(B^\top PB) = 0. \tag{4.28}$$

Given, $2\frac{\sigma^2}{\mu^2}tr(A_o) < 1$. Then, Eq. (4.28) simplifies to $\mu^2 B^\top PB < \frac{\mu^2}{\sigma^2}$ and hence the result follows. □

In the next section, we discuss the controller synthesis formulation when all the uncertainties in the input and output channels are considered to be same, i.e., $\sigma_1^2 = \cdots = \sigma_m^2 = \sigma^2$.

4.4 Mean Square Controller Synthesis

In this section, we tackle the controller synthesis problem for the closed-loop system, $\mathcal{F}(\mathbb{G}, \frac{d\Delta}{dt})$. The controller is designed such that the closed-loop system can tolerate maximum uncertainty.

Using part (c) of Theorem 15 and Lemma 14, we pose the controller synthesis problem as an LMI-based optimization problem,

$$\inf_{\mathbb{K}-stab,LTI}\ \inf_{\theta>0,diag} \parallel \theta^{-1}\mathcal{F}(\mathbb{P},\mathbb{K})\theta \parallel^2_{MS} .$$

Moreover, the designed $\mathbb{K}$ satisfies Assumption 11a which is, the nominal system $\mathbb{G} = \mathcal{F}(\mathbb{P},\mathbb{K})$ is internally stable.

This optimization provides a robust optimal controller by searching in the space of linear time-invariant stabilizing controllers that minimizes the mean square norm. However, searching for a robust optimal controller is a nonconvex problem. This problem can be made convex by following the approach given in Scherer et al. (1997) along with fixing the variable θ. Later, in simulations, we solve the optimization problem for the controller by keeping the variable θ constant. The resultant controller formulation is given in the ensuing theorem.

Theorem 19. *Given a plant $\mathbb{P}$ and for any $\theta > 0$, the optimization problem:*

$$\inf_{\mathbb{K}-stab,LTI} \parallel \theta^{-1}\mathbb{G}\theta \parallel^2_{MS}$$

is equivalent to the following LMI optimization:

$$\inf_{\boldsymbol{X},\boldsymbol{Y},\boldsymbol{S},\hat{\boldsymbol{A}},\hat{\boldsymbol{B}},\hat{\boldsymbol{C}},\gamma} \gamma$$

$$\text{subject to}\ \ S_{\ell\ell} < \gamma, \quad \ell = 1,2,\ldots,m,$$

$$\begin{bmatrix} \mathcal{L}_1(\boldsymbol{X},\hat{\boldsymbol{C}}) & \hat{\boldsymbol{A}}^\top + A_p & \begin{pmatrix} 0 & B_p \\ \hat{\boldsymbol{B}} & \boldsymbol{Y}B_p \end{pmatrix}\theta \\ \hat{\boldsymbol{A}} + A_p^\top & \mathcal{L}_2(\boldsymbol{Y},\hat{\boldsymbol{B}}) & \\ \theta^\top \begin{pmatrix} 0 & \hat{\boldsymbol{B}}^\top \\ B_p^\top & (\boldsymbol{Y}B_p)^\top \end{pmatrix} & & -I \end{bmatrix} < 0,$$

$$\begin{bmatrix} \theta\boldsymbol{S}\theta & & C_p\boldsymbol{X} & C_p \\ & & \hat{\boldsymbol{C}} & 0 \\ (C_p\boldsymbol{X})^\top & \hat{\boldsymbol{C}}^\top & \boldsymbol{X} & I \\ C_p^\top & 0 & I & \boldsymbol{Y} \end{bmatrix} > 0,$$

where $\boldsymbol{X}, \boldsymbol{Y}, \boldsymbol{S}$ *are positive definite symmetric matrices of size* $n \times n, n \times n, m \times m$*, and* $\hat{\boldsymbol{A}}, \hat{\boldsymbol{B}}, \hat{\boldsymbol{C}}$ *are matrices of sizes* $n \times n, n \times q, d \times n$ *correspondingly. Furthermore,*

$$\mathcal{L}_1(\boldsymbol{X}, \hat{\boldsymbol{C}}) = A_p \boldsymbol{X} + \boldsymbol{X} A_p^\top + B_p \Lambda_I \hat{\boldsymbol{C}} + (B_p \Lambda_I \hat{\boldsymbol{C}})^\top,$$

$$\text{and } \mathcal{L}_2(\boldsymbol{Y}, \hat{\boldsymbol{B}}) = A_p^\top \boldsymbol{Y} + \boldsymbol{Y} A_p + \hat{\boldsymbol{B}} \Lambda_O C_p + (\hat{\boldsymbol{B}} \Lambda_O C_p)^\top.$$

A feasible solution to the above optimization is a controller of the order of the plant, $\mathbb{P}$*. Then, the system matrices of the controller can be uniquely obtained as follows:*

$$\begin{aligned}
C_k =& \hat{\boldsymbol{C}} \left(M^\top \right)^{-1}, \\
B_k =& N^{-1} \hat{\boldsymbol{B}}, \\
A_k =& N^{-1} \left(\hat{\boldsymbol{A}} - \boldsymbol{Y} A_p \boldsymbol{X} - N B_k \Lambda_O C_p \boldsymbol{X} - \boldsymbol{Y} B_p \Lambda_I C_k M^\top \right) \left(M^\top \right)^{-1},
\end{aligned}$$

where M, N *are invertible matrices satisfying* $NM^\top = I - \boldsymbol{Y}\boldsymbol{X}$*. One possible choice for* N *is* $NN^\top = \boldsymbol{Y} - \boldsymbol{X}^{-1}$ *and* M*, such that*

$$\begin{pmatrix} \boldsymbol{Y} & N \\ N^\top & I \end{pmatrix} \begin{pmatrix} \boldsymbol{X} & M \\ M^\top & * \end{pmatrix} = \begin{pmatrix} I & 0 \\ 0 & I \end{pmatrix}.$$

Proof. The result follows from Lemma 14 and applying congruence transformation as shown in Scherer et al. (1997). □

A similar result on controller synthesis in the case of a discrete-time system with uncertainty in feedback communication channels is given in Elia (2005). Furthermore, in Elia (2005), the author briefly mentions different ways to approach this type of nonconvex problem. One of the ways to solve the controller synthesis problem is by applying sub-optimal methods, such as the D-K iteration given in Dullerud and Paganini (2013). In this approach, first θ is fixed to solve for the controller matrices and then θ is updated by keeping the controller matrices constant. This process is continued until the update equation for θ converges. In general, this approach does not

guarantee a global optimal controller, but can always provide a local optimal controller. The D-step formulation in the D-K iteration is given as follows.

$$\inf_{\theta} \quad 1$$

subject to

$$\begin{bmatrix} \mathcal{L}_1(X,\hat{C}) & \hat{A}^\top + A_p & \begin{pmatrix} 0 & B_p \\ \hat{B} & YB_p \end{pmatrix}\theta \\ \hat{A} + A_p^\top & \mathcal{L}_2(Y,\hat{B}) & \\ \theta^\top \begin{pmatrix} 0 & \hat{B}^\top \\ B_p^\top & (YB_p)^\top \end{pmatrix} & & -I \end{bmatrix} < 0,$$

$$\begin{bmatrix} \begin{pmatrix} C_pX & C_p \\ \hat{C} & 0 \end{pmatrix} \begin{pmatrix} X & I \\ I & Y \end{pmatrix}^{-1} \begin{pmatrix} (C_pX)^\top & \hat{C}^\top \\ C_p^\top & 0 \end{pmatrix} & \theta \\ \theta^\top & \mathcal{S}^{-1} \end{bmatrix} < 0.$$

In the D-step of D-K iteration, only θ is the optimization variable.

We remark that dealing with fixed-order controllers is a difficult problem. The controller matrices can be extracted easily only when the controller is of the size of the plant. Similar formulations can be seen in Elia (2005) and Scherer et al. (1997).

Designing a static output feedback controller in general even for a deterministic system is a hard problem hence we expect that designing a mean square stabilizing output feedback controller will be a difficult problem. However, we agree that this will be an interesting problem to study in our future research.

In the subsection involving fundamental limitations result on a single input full state feedback case, we have designed a static state feedback controller. In this case, we applied the standard result from the robust control theory given in Rotea (1993), where the optimal $\mathcal{H}_2$ performance obtained from static and dynamic controllers are the same for systems with full state feedback.

We have now developed the mean square stability based analysis and controller synthesis results for continuous-time stochastic linear networked systems. In the next chapters, we apply these results

to study the impact of renewables on the mean square stability of stochastic power network and design a wide area controller robust to PMU measurement uncertainty.

CHAPTER 5. LOAD-SIDE FREQUENCY CONTROL WITH STOCHASTIC RENEWABLES

In this Chapter, we discuss two control strategies to achieve frequency regulation via load-side frequency control. The first one is a decentralized load-side frequency control as given in Zhao et al. (2014b) in the presence of stochastic uncertainty. Further, applying the results developed in Chapter 4, we show the fragility of decentralized load-side frequency controller in a stochastic environment. Lastly, we present the robust distributive control design algorithm to achieve frequency regulation robust to stochastic uncertainties.

5.1 Decentralized Control

Recall that, the primal-dual gradient system is the same as the dynamic network model for load-side frequency control, i.e., Eq. (2.9) except for the fact that the decentralized feedback control law for the controllable load is obtained as the solution of the optimization problem given in Eqs. (2.12) - (2.13). This implies that the dynamic power network model is essentially implementing the primal-dual gradient algorithm, where the feedback control law (2.18) needs to be implemented at each controllable load for decentralized load-side frequency regulation of power network. In Zhao et al. (2014b), the authors prove the existence of a unique equilibrium point for primal-dual gradient system which is globally asymptotically stable. Here, in the presence of a decentralized load-side frequency controller, we show that this asymptotically stable equilibrium point is very fragile to multiplicative stochastic uncertainty in the power network. We make following assumption on the cost function c_j corresponding to the controllable loads.

Assumption 20. *We assume that the cost function* c_j *is quadratic and hence of the form* $c_j(P_{C_j}) = \frac{{P_{C_j}}^2}{2\alpha_j}$ *for all* $j \in \mathcal{N}$. *Furthermore, we neglect the saturation constraints on the cost function and*

hence optimal decentralized control law at each controllable load is of the form $u_j = P_{C_j} = \alpha_j \omega_j$, *which is* $u = \hat{K}x$.

Using the Assumption 20 in the stochastic power network model, Eq. (2.33), we obtain,

$$\dot{x} = \hat{A}x + \sigma \sum_{\ell=1}^{m} \hat{B}_\ell x \xi_\ell + \sigma \sum_{\ell=1}^{m} H_\ell \xi_\ell, \tag{5.1}$$

where $\hat{A} := A + B\hat{K}$, $\hat{B}_\ell := B_1^\ell + B_2^\ell \hat{K}$. The appropriate notion of stability for this system is second moment stability. Next, consider the system (5.1) without the additive uncertainty.

$$\dot{x} = \hat{A}x + \sigma \sum_{\ell=1}^{m} \hat{B}_\ell x \xi_\ell. \tag{5.2}$$

The covariance propagation equation for the system given in (5.2) and (5.1) is given in Lemma 6. Let $Q(t)$ and $\bar{Q}(t)$ be the covariance matrices corresponding to systems (5.2) and (5.1). Then, they satisfy the following matrix differential equations (MDE's).

$$\dot{Q}(t) = Q(t)\hat{A}^\top + \hat{A}Q(t) + \sum_{\ell=1}^{m} \sigma_\ell^2 \hat{B}_\ell Q(t) \hat{B}_\ell^\top, \tag{5.3}$$

$$\dot{\bar{Q}}(t) = \bar{Q}(t)\hat{A}^\top + \hat{A}\bar{Q}(t) + \sum_{\ell=1}^{m} \sigma_\ell^2 \hat{B}_\ell \bar{Q}(t) \hat{B}_\ell^\top + \sum_{\ell=1}^{m} H_\ell H_\ell^\top + \sum_{\ell=1}^{m} \sigma_\ell H_\ell \mu(t)^\top \hat{B}_\ell^\top + \sum_{\ell=1}^{m} \sigma_\ell H_\ell \mu(t) H_\ell^\top. \tag{5.4}$$

The following equation shows the mean propagation equation for the system with additive noise given in (2.33).

$$\dot{\mu}(t) = \hat{A}\mu(t) \tag{5.5}$$

The mean square exponential stability of system (5.2) and second moment stability of (5.1) are related and is given in the following lemma.

Lemma 21. *The system (5.2) is mean square exponentially stable if and only if system (5.1) is second moment bounded.*

Proof. Using the operator ϕ, that transforms a matrix into a vector as defined in Costa et al. (2006)[Chapter 2], the MDE's given in Eq. (5.3) and Eq. (5.4) are written as linear differential

equations as given below.

$$\dot{q} = \quad \mathscr{A} q, \tag{5.6}$$

$$\dot{\bar{q}} = \quad \mathscr{A} \bar{q} + \mathscr{B}, \tag{5.7}$$

where $q = \phi(Q), \bar{q} = \phi(\bar{Q})$,

$$\mathscr{B} = \sum_{\ell=1}^{m}((H_\ell \otimes H_\ell) + ((\sigma_\ell H_\ell \mu^\top) \otimes \hat{B}_\ell) + (\hat{B}_\ell \otimes (\sigma_\ell \mu^\top H_\ell)))\phi(I) \in \mathbb{R}^{n^2},$$

$$\mathscr{A} = \hat{A} \oplus \hat{A} + \sum_{\ell=1}^{m} \sigma_\ell^2 (\hat{B}_\ell \otimes \hat{B}_\ell) \in \mathbb{R}^{n^2 \times n^2},$$

where I is the identity matrix of size $n \times n$ and $\otimes$ denotes the Kronecker product, $\oplus$ is the Kronecker sum.

Necessity: The mean square exponential stability of system (5.2) yields stability of system (5.6), that is, $\mathscr{A}$ is Hurwitz. Since $\mathscr{A}$ is Hurwitz, the steady state value of $\bar{q}$ is given by $\lim_{t\to\infty} \bar{q}(t) = \lim_{t\to\infty} \phi(\bar{Q}(t)) = -\mathscr{A}^{-1}(\sum_{\ell=1}^{m} H_\ell \otimes H_\ell)\phi(I)$. Now, taking the inverse ϕ operator, we obtain, $\lim_{t\to\infty} E[x(t)x(t)^\top] = -\phi^{-1}(\mathscr{A}^{-1}(\sum_{\ell=1}^{m} H_\ell \otimes H_\ell)\phi(I))$, which is finite. Further, the necessary condition for $\mathscr{A}$ to be Hurwitz is $\hat{A}$ being Hurwitz. This implies that the mean propagation system of (5.1), shown in Eq. (5.5) has a stable evolution. Therefore, system (5.1) is second moment bounded.

Sufficiency: If system (5.1) is second moment stable, then $\lim_{t\to\infty} \bar{Q}(t)$ is a finite value and the mean system (5.5) has a stable evolution. Taking the operator, it can be alternately written as, $\lim_{t\to\infty} \phi(\bar{Q}(t)) = \lim_{t\to\infty} e^{\mathscr{A}t}\phi(\bar{Q}(0)) - \mathscr{A}^{-1}(1 - e^{\mathscr{A}t}) \sum_{\ell=1}^{m}(H_\ell \otimes H_\ell)\phi(I) + e^{\mathscr{A}t}(\sum_{\ell=1}^{m}(\sigma_\ell H_\ell \mu^\top) \otimes \hat{B}_\ell)\phi(I) + e^{\mathscr{A}t}(\sum_{\ell=1}^{m} \hat{B}_\ell \otimes (\sigma_\ell \mu^\top H_\ell))\phi(I)$. The limit on the right-hand side is finite, if and only if $\mathscr{A}$ is Hurwitz. If $\mathscr{A}$ is Hurwitz, then the system (5.2) is mean square exponentially stable. □

Now, we can analyze the stochastic stability of the power network with decentralized load-side frequency controller. In particular, we study the mean square exponential stability of system (5.2). Later, in the next section, we consider the IEEE 68 bus system as a case study example and study its stochastic stability properties. It can be seen that the decentralized load-side control algorithm is very fragile in the presence of stochastic renewables. The variance that can be tolerated in the

voltages of renewable buses is very small, and hence, the decentralized control algorithm is termed fragile. Detailed discussion on this case study is discussed in subsection 5.3.1.

Next, to counteract the fragility of the decentralized controller, we discuss the design of a robust distributive control algorithm.

5.2 Robust Control

Here, we consider the stochastic system (2.33) and design a state feedback controller that is robust to the stochastic uncertainty entering the network because of considerable penetration of renewables. Again here, we consider the stochastic system without additive noise as follows.

$$\dot{x} = Ax + Bu + \sigma \sum_{\ell=1}^{m} B_1^{\ell} x \xi_{\ell} + \sigma \sum_{\ell=1}^{m} B_2^{\ell} u \xi_{\ell}. \tag{5.8}$$

Assume, the static state feedback controller is of the form, $u = Kx$. Then, similar to Lemma 21, we can establish the mean square stability of system (5.8) and second moment stability of system (2.33). However, for the sake of completeness of the analysis, we consider additive uncertainty that is independent of multiplicative uncertainty.

Then, we have the following closed-loop system by abusing the notation, H.

$$\dot{x} = (A + BK)x + \sigma \sum_{\ell=1}^{m} (B_1^{\ell} + B_2^{\ell} K) x \xi_{\ell} + H\eta \tag{5.9}$$

where $\xi_{\ell} = \frac{d\Delta_{\ell}}{dt}$ for $\ell = 1, \dots m$ with $\Delta_1(t), \dots, \Delta_m(t)$ being the standard independent Wiener processes, $H \in \mathbb{R}^n$, $\eta = \frac{d\zeta}{dt}$ is a Gaussian process and ζ is a standard Wiener process that is independent of the process, $\Delta_1(t), \dots, \Delta_m(t)$. The necessary and sufficient condition for the closed-loop stochastic system to be second moment bounded is there exists a $Q > 0$, such that, it satisfies (refer Pushpak et al. (2016)[Theorem 11]).

$$(A + BK)Q + Q(A + BK)^{\top} + \sigma^2 \sum_{\ell=1}^{m} (B_1^{\ell} + B_2^{\ell} K) Q (B_1^{\ell} + B_2^{\ell} K)^{\top} + HH^{\top} < 0. \tag{5.10}$$

A similar controller for the stochastic system is discussed in El Ghaoui (1995). The linear matrix inequality (LMI) for second moment bounded stability is used to solve for a robust K, such that

$Q > 0$ and the variance of uncertainty that can be tolerated by the stochastic system is maximum. To solve for the controller, rewrite inequality (5.10) as follows:

$$AQ + QA^\top + BKQ + QK^\top B^\top + HH^\top + \sigma^2 \sum_{\ell=1}^{m} (B_1^\ell Q + B_2^\ell KQ)Q^{-1}(B_1^\ell Q + B_2^\ell KQ)^\top < 0.$$

Solving the above LMI for a positive definite Q and K is in general a nonconvex problem. Hence, we consider the change of variables, $M := KQ$ and by taking Schur complements, we obtain the following inequality.

$$\begin{bmatrix} AQ + QA^\top + BM + M^\top B^\top + HH^\top & \sigma(B_1^1 Q + B_2^1 M) & \sigma(B_1^2 Q + B_2^2 M) & \dots & \sigma(B_1^m Q + B_2^m M) \\ \sigma(B_1^1 Q + B_2^1 M)^\top & -Q & 0 & \dots & 0 \\ \sigma(B_1^2 Q + B_2^2 M)^\top & 0 & -Q & \dots & 0 \\ \vdots & \vdots & \vdots & \ddots & \vdots \\ \sigma(B_1^m Q + B_2^m M)^\top & 0 & 0 & \dots & -Q \end{bmatrix} < 0. \tag{5.11}$$

The LMI shown in Eq. (5.11) is satisfied by multiple $Q > 0$. To get a meaningful solution to this LMI, rather than looking at this problem as a stability problem, we look at the $\mathcal{H}_2$ performance criterion of system. In doing so, we rewrite the closed-loop stochastic system (5.9) in the robust control form. The deterministic part of the closed-loop system with additive uncertainty is denoted by $\mathbb{G}$ and is shown below.

$$\mathbb{G} : \begin{cases} \dot{x} &= \mathcal{A}x + \mathcal{B}w + H\eta \\ z &= \mathcal{C}x \end{cases} \tag{5.12}$$

where $\mathcal{A} = A + BK$, $\mathcal{C} = \mathbb{1}_n \otimes I_n$, $\mathbb{1}$ is a column vector of size n with all entries as 1, I_n is an identity matrix of size n,

$$\mathcal{B} = \begin{bmatrix} B_1^1 + B_2^1 K & B_1^2 + B_2^2 K & \dots & B_1^m + B_2^m K \end{bmatrix}.$$

The variables w, z are the disturbance and control signals and they are related by

$$w = \xi z, \tag{5.13}$$

where $\xi = \text{diag}(\xi_1 I_n, \dots, \xi_m I_n)$. Note that, the feedback interconnection of Eqs. (5.12) and (5.13) gives the closed-loop stochastic system (5.9). The feedback interconnection of Eqs. (5.12) and

(5.13) is a multi-input multi-output (MIMO) system with number of uncertainties deciding the size of MIMO system.

The $\mathcal{H}_2$ norm for the system (5.12) can be interpreted as the output variance for white noise applied at the input (refer Dullerud and Paganini (2013) for more explanation). Therefore, the $\mathcal{H}_2$ norm of the system $\mathbb{G}$ is $\text{tr}(Q)$, where Q is the steady-state variance of x.

Now, we have the following optimization problem that gives a robust controller K while minimizing the steady state variance of states, i.e., minimizing the $\mathcal{H}_2$ norm of the system.

$$\begin{aligned} &\min_{Q>0,M} \quad \text{tr}(Q) \\ &\text{subject to} \quad \text{LMI (5.11)}. \end{aligned} \tag{5.14}$$

LMI (5.11) is still nonconvex in terms of M, K and σ. The robust controller, K is obtained by following the algorithm given below.

Robust state-feedback controller, K

1: Choose a range for $\sigma > 0$.

2: **for** $i = 1, 2, \ldots$

3: Fix $\sigma := \sigma(i)$

Solve (5.14) for M and Q

if problem is feasible

The controller, $K = MQ^{-1}$.

else

The robust controller, K is the one obtained from the previous iteration.

end **if**

4: end **for**.

5.3 Case Study: IEEE 68 Bus System

In this section, we consider the IEEE 68 bus network to analyze the decentralized and robust load-side primary frequency control strategies with stochastic load voltages. IEEE 68 bus New England/New York interconnection test system consists of 16 generator buses and 52 load buses.

The single-line diagram of the 68 bus test system is shown in Figure. 5.1. This system contains induction motor loads, constant power loads, and controllable loads. The relevant data for this system is obtained from the data files of power system toolbox (refer Chow and Cheung (1992)).

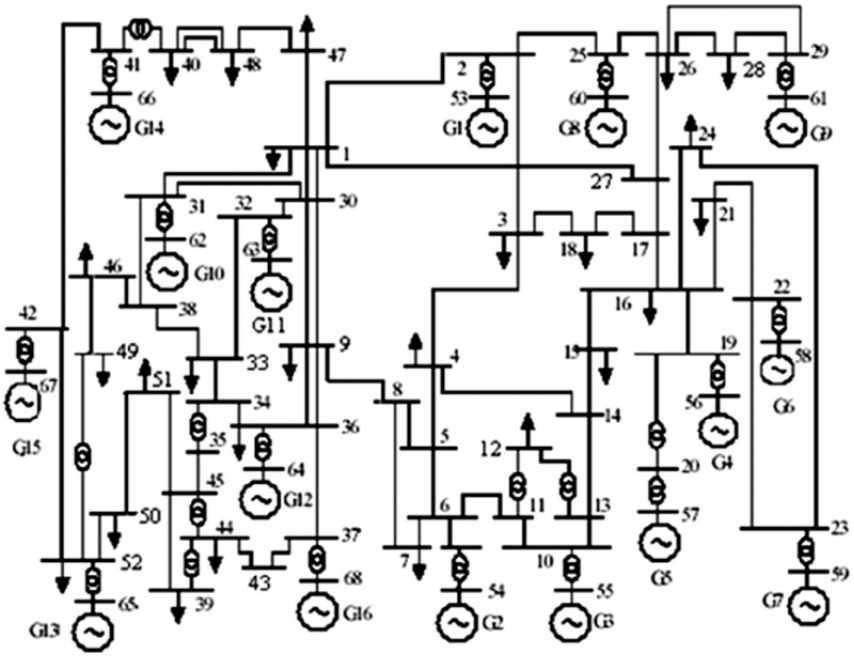

Figure 5.1 Single-line diagram of IEEE 68 bus system

As discussed in Section 2.3, we include the renewables in the power network, and the uncertain, intermittent nature of renewables is modeled into the power network by considering the voltages to be stochastic. Changing the controllable loads involves a cost measured in the form of aggregate dis-utility of loads, and it has to be minimized.

In this 68 bus system, there are 29 induction motor loads which are sensitive to frequency, 35 controllable loads and the remaining loads are uncontrollable frequency insensitive loads. Now, we replace few of the classical generators with renewable energy sources such as either solar or wind power. As there are no heavy moving parts at these renewables, the inertia values at these buses are relatively smaller, when compared to the classical generators (refer Gautam et al. (2009)).

Further, integration of renewables into the power network increases the damping slightly as shown in Slootweg and Kling (2003b). Therefore, we assume a relatively smaller value for inertia at renewables location and relatively bigger value for damping at those locations. For the simulation purpose, we assume the renewable energy source at buses $54, 55, 56, 60, 63, 64$ and 65 replacing the generator buses. Now, the buses connecting the renewable buses are $6, 10, 19, 25, 32, 36$ and 52 and hence, $s = 7$.

In the given data, the inertia values at generator buses lie between $1 - 5$, whereas, at the buses with renewable energy, we have considered it as 0.5. Similarly, the damping values at generator buses are in the range of $0 - 5$, and we consider the damping at renewable energy buses to be 6. The simulations results discussed below are consistent for the range of inertia values between $0.5 - 1$ and damping values between $5 - 6$.

Now, we first discuss the fragility of the decentralized frequency control on the power network in the presence of renewables.

5.3.1 Decentralized Control

We now analyze the effect of cost on controllable loads on the load-side primary frequency control with stochastic renewables. If the cost of controllable loads is high, then it is difficult to vary the controllable loads. Using the analytical framework discussed in section 4.3, we identify the critical variance that can be tolerated in the voltages while maintaining the mean square exponential stability of power network with a decentralized controller. The critical variance value, σ_*^2, is observed to be very small in the order of 10^{-3} with the maximum variance value of 1.9×10^{-3} which is obtained when the cost coefficient on the controllable load is equal to $\alpha = 0.5$ (Refer to Assumption 20). In Figure. 5.2, observe that, if the cost of controllable loads is further increased, the critical variance that can be tolerated by the stochastic power network reduces. It is important to notice that, for most of the cost values on controllable loads, the critical variance is very small. In generating Figure. 5.2, all the damping values at generator and load buses are kept constant.

Observe that, if the variance that can be tolerated by the system is small, then the system is on the verge of stability. This nature of the system can be seen, when we consider the stochastic voltages with a variance, $\sigma^2 > \sigma_*^2$, the frequencies grow out of bounds, and the power network becomes mean square unstable. This phenomenon is seen in Figs. 5.3 and 5.4. The stochastic voltage variation with respect to time is shown in Figure. 5.3.

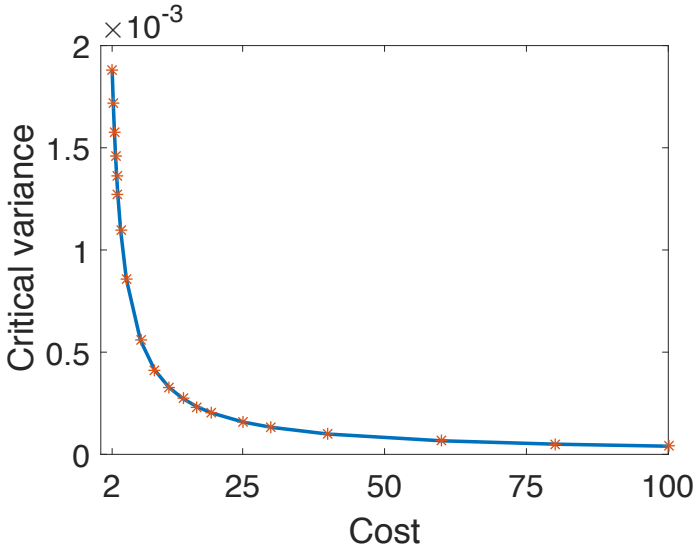

Figure 5.2 Impact of increase in cost on the critical variance

In Figure. 5.3, for the chosen $\sigma^2 > \sigma_*^2$, it is important to emphasize that although the voltages values lie within the safe operating limits of 0.95 pu to 1.05 pu, the frequencies violate the operating limits as seen in Figure. 5.4. This shows the fragility of the decentralized controller in the presence of renewables, as it is inadequate to regulate the frequency by means of controllable loads.

Consider a step change in the power network. For this step change in power, the decentralized frequency controller is ineffective in controlling the controllable loads to regulate the frequency. In Figure. 5.5, initially the system was in stable operating condition with frequencies with in the operating limits. We created a step change in power after 10 seconds, and then the frequencies

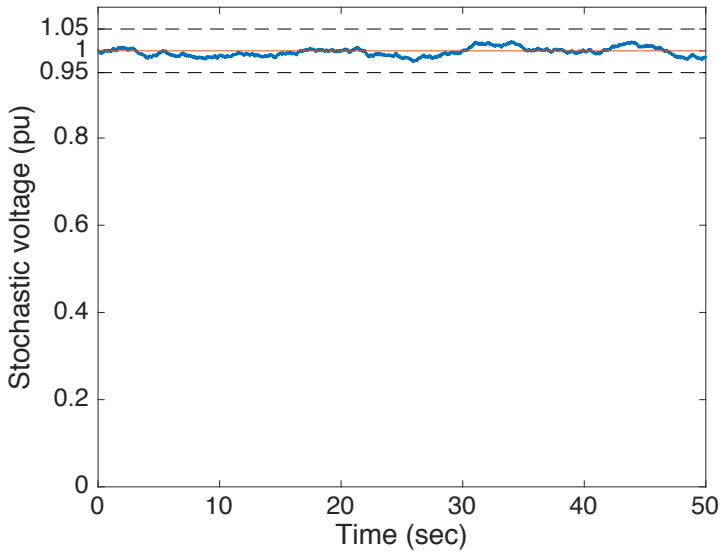

Figure 5.3 Voltage fluctuation at generator bus 56

oscillate and go out of the operating range and continue to oscillate. This phenomenon is not desirable, as it has the impact to damage the power system equipment.

Hence, to counteract the fragility of this decentralized controller, a modified robust distributive controller must be designed to regulate the frequency that can tolerate uncertainty in the renewables.

The higher penetration of renewables in the power network will make the decentralized frequency control algorithm more fragile. In particular, with the increase in the number of renewable energy resources, more bus voltages will become uncertain, and this has an adverse impact on the frequency regulation. Figure. 5.6 shows the impact of increasing the penetration of renewables in the power network. We notice, with the increase in penetration (i.e., with increase in the value of m) the critical variance that can be tolerated by the system decreases. Note that, this figure will change based upon which locations in the network are chosen for renewables. However, the trend of a decrease in the value of critical variance with the increase in the number of renewables will continue to hold true.

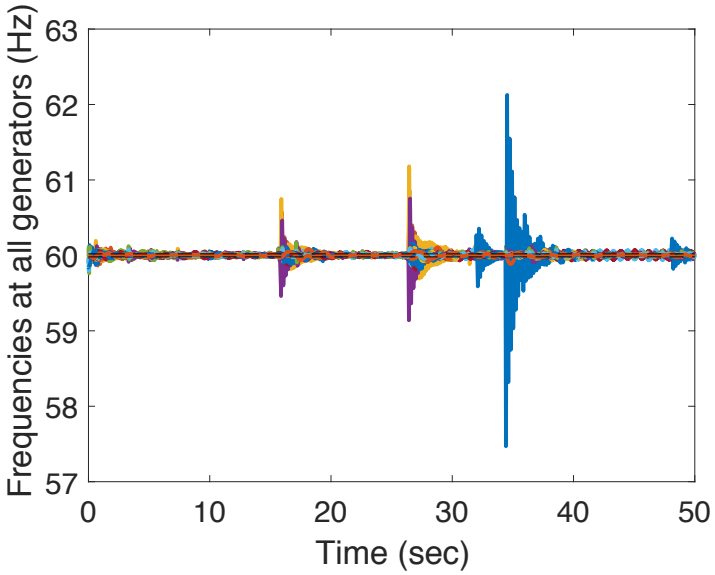

Figure 5.4 Mean square unstable behavior for frequencies at all generator buses.

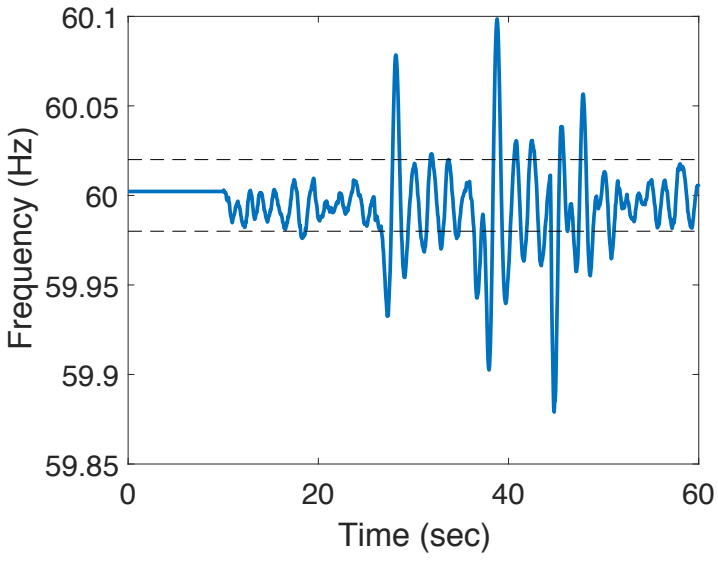

Figure 5.5 Frequency at generator bus 53 following a step change in power.

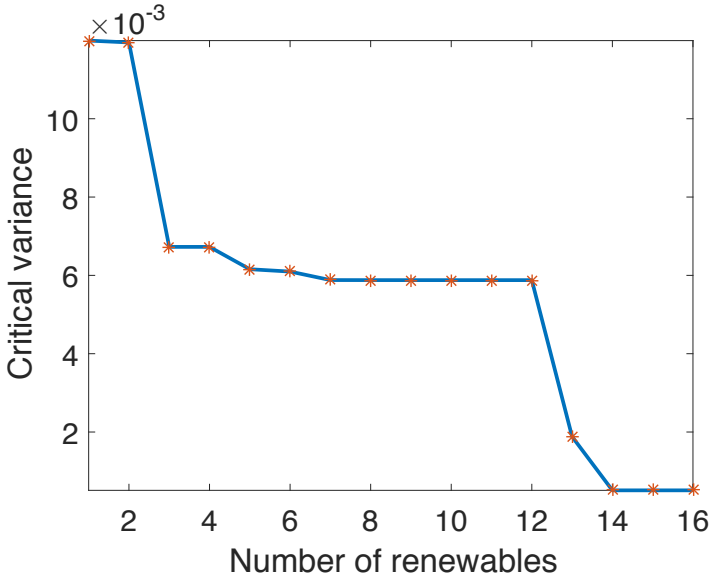

Figure 5.6 Critical variance with increase in number of renewables

CHAPTER 6. STOCHASTIC SMALL SIGNAL STABILITY OF POWER NETWORK WITH UNCERTAIN WIND

6.1 Simulation Study

We illustrate the proposed framework on an IEEE 39 bus system in this section. IEEE 39 bus system given in Information Trust Institute (2018); Chow and Rogers (2000) consists of 10 synchronous generators and for the purpose of our study, the SGs are replaced with DFIGs one by one. The system data for the simulation is obtained from Chow and Rogers (2000).

The DA description of the power network is elucidated in Chapter 2 and in particular in Section 2.1.5. The wind speeds to the DFIG are modeled stochastically to capture the intermittent nature of the wind as shown in Section 2.1.4. Cube of the wind speeds is modeled with a stochastic process rather than actual wind speed as discussed in Section 2.1.4. Finally, we arrive at the nonlinear stochastic DA equations as described in (2.4). These stochastic nonlinear DAEs are linearized around an operating point to obtain a linear stochastic DAE. The operating point at which the system is linearized can be obtained as described here. The network algebraic states are obtained from the power flow solution. The dynamic and algebraic states at SGs and DFIG are found from the steady-state solution of the reduced DA system. The implicit ode solver, *ode15i* in Matlab is used to solve the DA equations. Following this, we obtain the system matrices given in Eqs. (2.5) and (2.6). The system is then Kron reduced by expressing the algebraic states in terms of the dynamic states to obtain a stochastic ODE as shown in Eq. (2.7). The stochastic system is given in Eq. (2.7) where the wind speed uncertainty appears parametrically in the system matrix can now be expressed as a network system with stochastic uncertainty and control in the feedback as shown in Eq. (4.13) and Fig. 6.1.

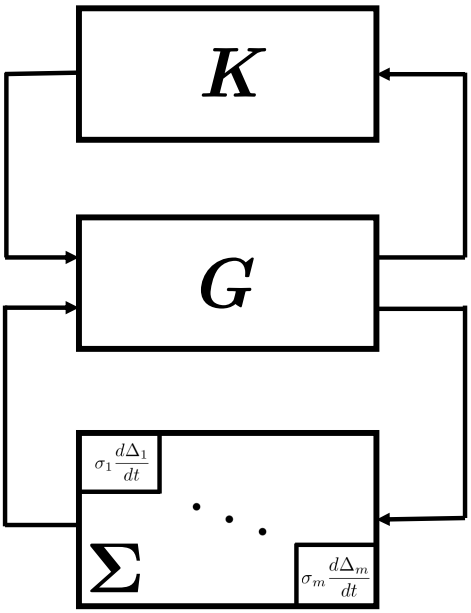

Figure 6.1 Dynamical system in (4.13) represented as the feedback interconnection of $\boldsymbol{G}$ with controller, K and $\boldsymbol{\Sigma}$.

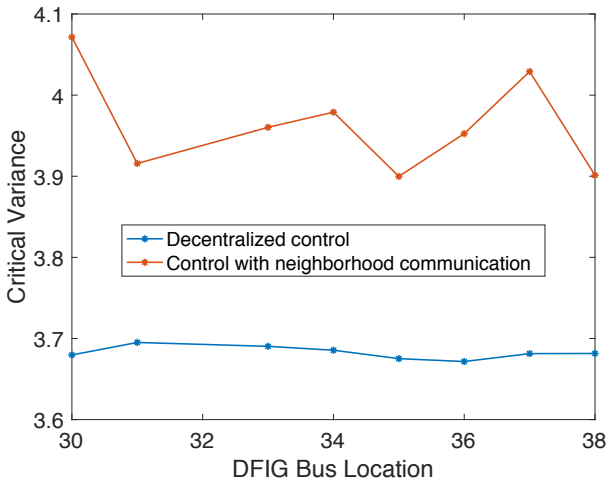

Figure 6.2 Critical variance that can be tolerated in wind speeds while maintaining the stochastic small signal stability with respect to the two load-side primary frequency control strategies.

6.1.1 Performance of Load-Side Primary Frequency Controller

The objective here is to study the performance of the load-side based frequency controllers in the presence of wind uncertainty. In so doing, we utilize the decentralized control and control with neighborhood communication from Section 2.4 and apply the Remark 16 to identify the critical variance that can be tolerated in the wind speed while maintaining the mean square exponential stability of the power network which essentially is the stochastic small signal stability of the power network. Buses $30-39$ contains the conventional SGs and one of the buses is replaced with a DFIG for the purpose of the simulation study. The process is repeated by replacing each of the SG with DFIG and the critical variance that the system can tolerate with wind uncertainty at that location is computed analytically using the decentralized control as well as control with neighborhood communication.

The control gains for the different controller strategies are chosen in such a way that, maximum 20% of the load is controllable at each load bus and they provide the frequency regulation in the range of 59.9-60.1 Hz. Utilizing these controller strategies, the critical variance that can be tolerated in the wind speeds while maintaining stochastic small signal stability are computed and

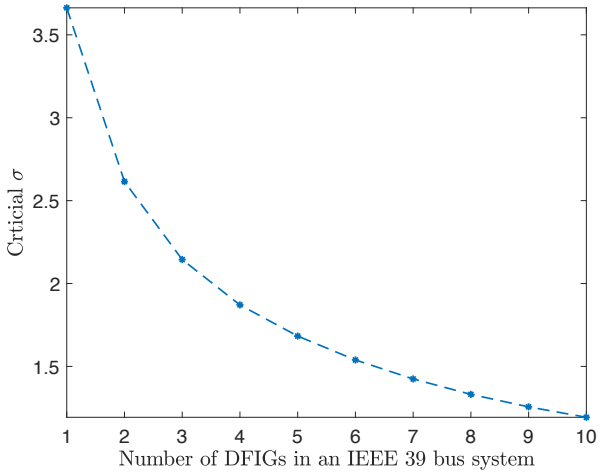

Figure 6.3 Increase in the penetration of renewables resulting in a reduced critical variance of the system.

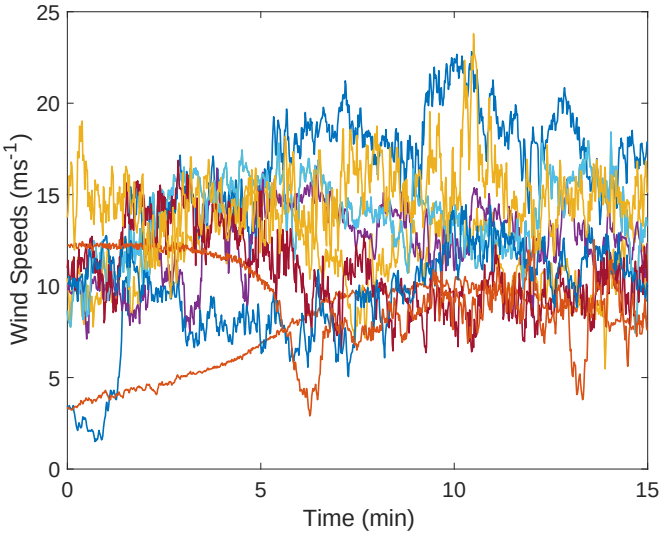

Figure 6.4 Actual wind speed data recorded near Ames, Iowa at different times/days (refer Takle et al. (2018)).

can be shown in Fig. 6.2. It can be observed that the control with neighborhood communication seems to be robust to wind uncertainties relative to decentralized load-side primary frequency control. Hereafter, we refer only to the control with neighborhood communication in the rest of the paper.

The effect of critical variance (σ_*^2) of the wind speeds thus obtained can be seen from the time-domain simulations of the power network. The nominal wind speed for the simulation study is chosen to be 8 ms^{-1} and when the uncertainty of the wind speeds is increased from a value smaller than critical variance to a value larger than the critical variance, the system transitions from mean square exponential stability to mean square instability. Figures 6.5 and 6.6 show the effect on frequency at the DFIG bus and the SG bus with increase in the critical standard deviation.

By modeling the wind speeds as a Wiener process, we study the impact of an increase in the number of DFIGs. In doing so, we make the assumption that when there is more than one DFIG in the network, then the variance of wind speeds at every DFIG is assumed to be the same. This assumption helps in understanding the overall effect of the stochastic wind speeds on the power network. Again, applying the Remark 16, the critical variance that can be tolerated by the power network while maintaining the stochastic small signal stability can be identified. It can be seen from Fig. 6.3 that increasing the number of wind turbine generators (DFIGs) in the power network leads to a reduction in the critical variance that the system can tolerate.

We next present stochastic small signal stability studies on the IEEE 39 bus system with statistics from the actual wind speed data collected from a wind tower located near Ames, Iowa. The actual wind speed data is available at a granularity of 1 sec and can be downloaded from Takle et al. (2018). By using the actual wind speeds and statistics from the actual wind speeds, we intend to study the maximum penetration of the renewables in the power network while maintaining the stochastic small signal stability.

The wind speed data from Takle et al. (2018) is considered for 15 min with 1 second granularity. These wind speeds are further interpolated to 1 millisecond for the purpose of using these wind speeds in the time-domain simulations. All the SGs can be replaced by DFIGs and to study such a

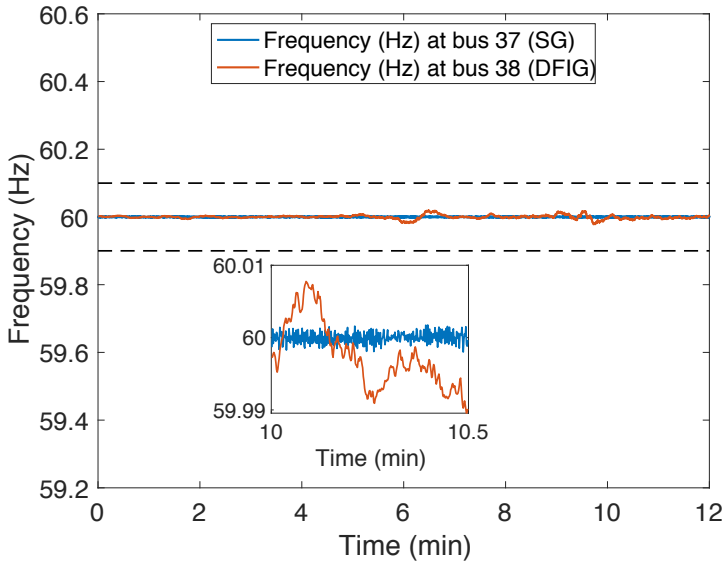

Figure 6.5 Frequencies at buses 37 (SG bus) and 38 (DFIG bus). The plots are derived with $\sigma = 0.4\sigma_*$ (stable scenario).

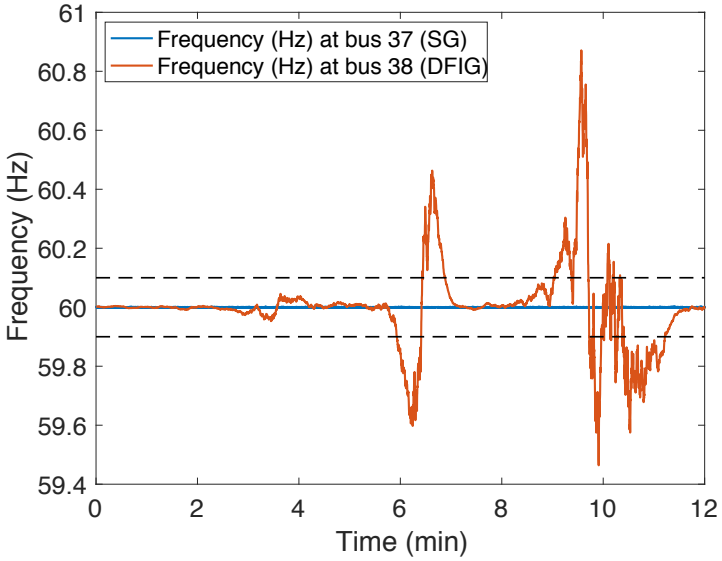

Figure 6.6 Frequencies at buses 37 (SG bus) and 38 (DFIG bus). The plots are derived with $\sigma = 2.2\sigma_*$ (unstable scenario).

system, ideally, we need 10 sets of wind speed data corresponding to 10 different locations. However, due to lack of unavailability of actual wind speed data at 1 second fineness, we consider the wind speed data at different time/day monitored at the wind tower near Ames as input to different DFIGs. Actual wind speed data corresponding to different time/day monitored at the tower near Ames, Iowa can be seen in Fig. 6.4.

6.1.2 Maximum Allowable Wind Generation

We now identify the maximum penetration of renewable wind energy by modeling the wind speeds as a stochastic process (with statistics from the actual wind speed data) in the presence of control with neighborhood communication.

6.1.2.1 Wind Speed Modeled as Wiener Process

Consider the wind speeds at each DFIG as a Wiener process whose variance is multiplied with the variance of the actual wind speed corresponding to the time-series data of the wind speeds as shown in 6.4. This process is repeated by increasing the penetration of wind generation and every time a DFIG is added, using the time-domain simulations, frequencies at each of the buses are monitored. It can be seen that, when the number of DFIGs are increased from 8 to 9, the power network turns to mean square unstable. In other words, the frequencies go out of tolerable bounds in similar as shown in Fig. 6.8 in the presence of control with neighborhood communication. Figure 6.7 shows the frequencies for 8 DFIGs. In particular, we identified the maximum penetration of wind generation which is 80% as there are a total of 10 generating sources and 8 can be replaced with DFIGs of equivalent capacity without loosing stochastic small signal stability.

We complement the above result with time-domain simulations of the reduced ode Eq. (2.8) where the stochastic wind speeds are now substituted with the actual wind speeds.

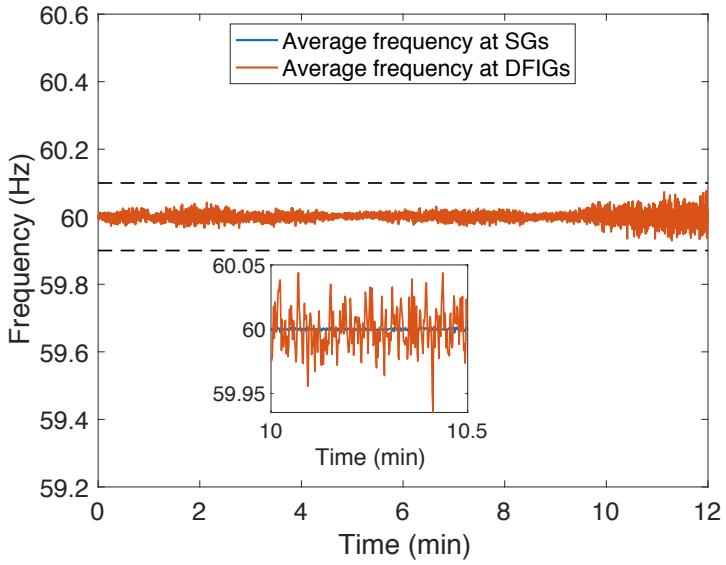

Figure 6.7 The wind speeds are modeled as a Wiener process. The plots are shown here for the case with utmost renewables (2 SGs and 8 DFIGs) while maintaining stochastic small signal stability.

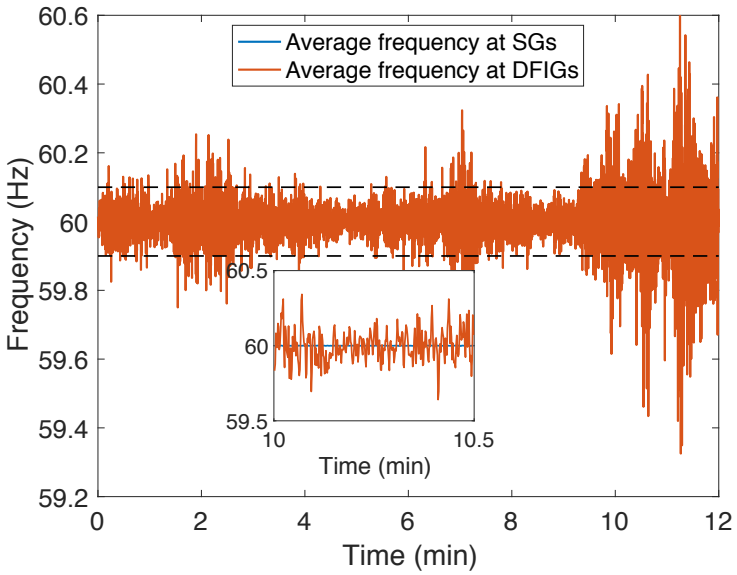

Figure 6.8 The wind speeds are modeled as a Wiener process. The plots are shown here for the case when the system turned mean square unstable with 1 SG and 9 DFIGs.

6.1.2.2 Linearized System with Real Wind Data

The small signal stability with linearized power system dynamics is studied using the actual wind speeds with power system time-domain simulations. In the case of linearized power system dynamics, it is seen that only 70% of penetration is allowed while maintaining the small signal stability. Figures 6.9 and 6.10 show the average frequencies of SGs and DFIGs when number of DFIGs are increased from 7 to 8.

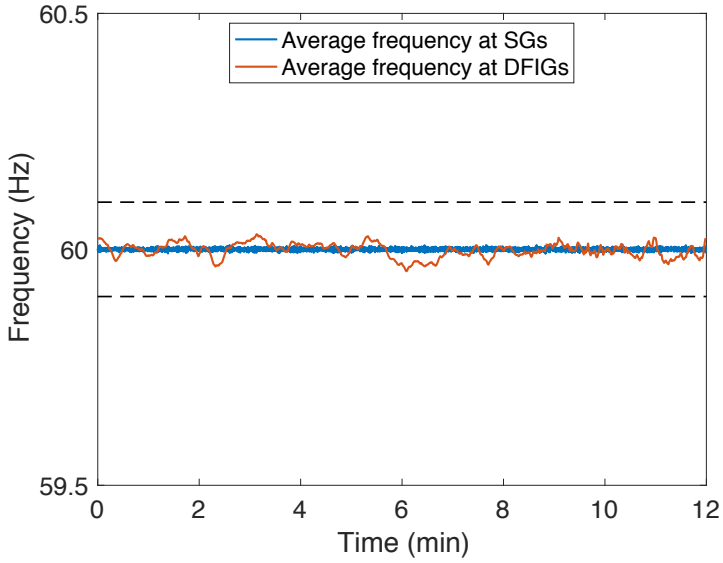

Figure 6.9 Linearized system simulations with real wind speed data. The plots are shown here for the utmost renewable energy sources (3 SGs and 7 DFIGs) while maintaining stochastic small signal stability.

We next intend to observe a similar phenomenon with nonlinear power system dynamics.

6.1.2.3 Nonlinear DAE System with Real Wind data

Nonlinear time-domain simulations of the system given in Eq. (2.4) are performed by considering actual wind rather than stochastic wind. Here, it is observed that when the number of DFIGs are increased from 5 to 6, the system turns unstable. The average frequencies of the SGs and DFIGs with 5 and 6 DFIGs can be seen in Figs. 6.11 and 6.12. Therefore, in this case, only 50% of wind generation is possible.

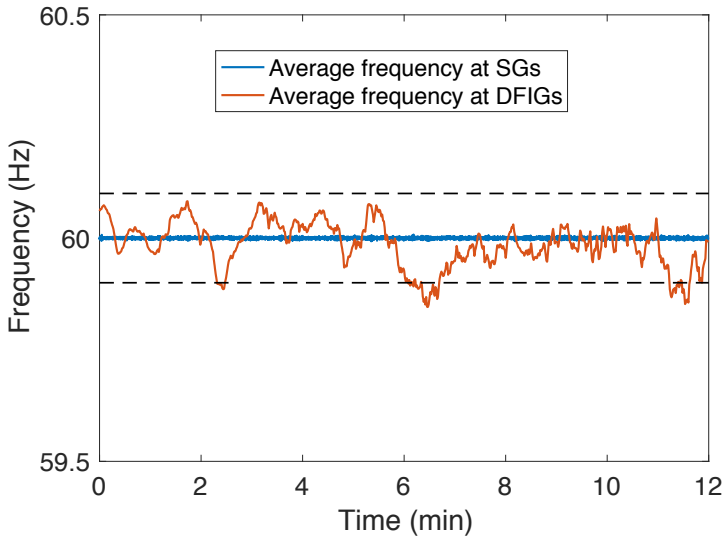

Figure 6.10 Linearized system simulations with real wind speed data. The plots are shown here when the system turned mean square unstable with 2 SGs and 8 DFIGs.

Note that, these results depend on the input wind speed data. In this work, we have considered the wind speed data with high variability (refer Fig. 6.4) and the results may vary if wind speeds are considered with low variability.

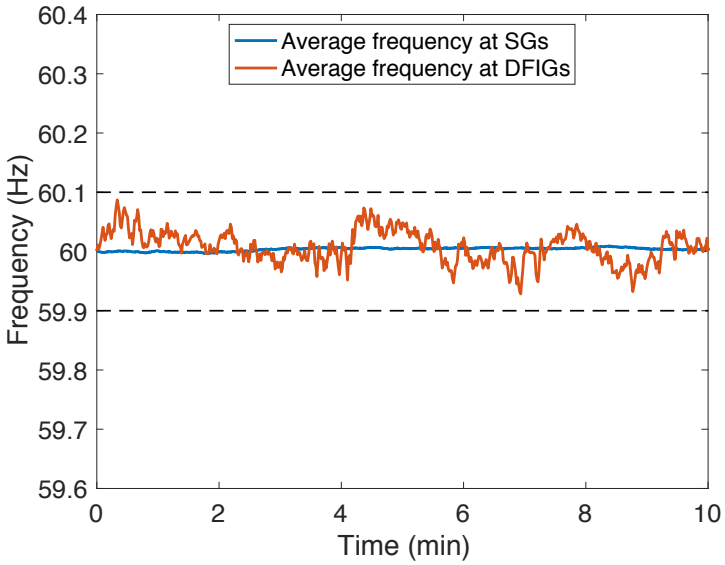

Figure 6.11 Nonlinear DAE simulations with real wind speed data. The plots are shown here with utmost renewable energy sources (5 SGs and 5 DFIGs) without any frequency violations.

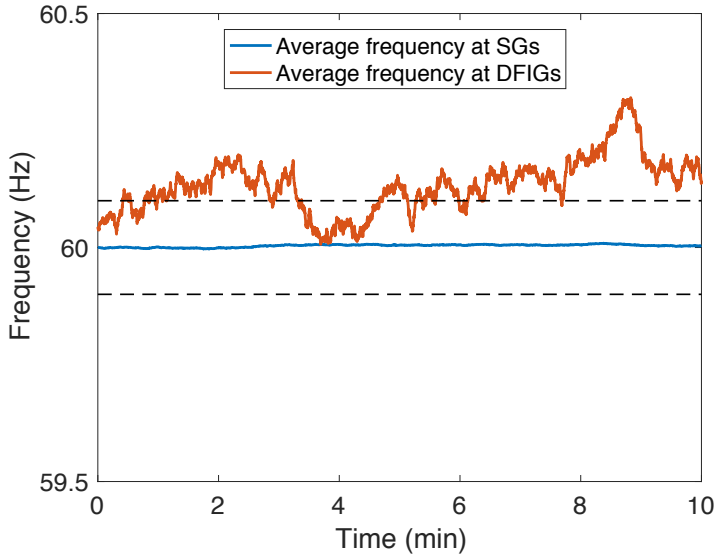

Figure 6.12 Nonlinear DAE simulations with real wind speed data. The plots are shown here when the average frequencies are violated with 4 SGs and 6 DFIGs.

CHAPTER 7. WIDE AREA CONTROL IN THE PRESENCE OF PMU MEASUREMENT UNCERTAINTY

We have described the problem of wide area control with communication channel uncertainty in subsection 3 of Chapter 2. The system (3.7) can be represented in the closed-loop form as shown in Eq. (4.2) and then, we invoke Lemma 7 to study the mean square stability analysis of Eq. (3.7). The mean square stability results and controller synthesis formulation for system (3.7) are developed in Sections 4.3 and 4.10 of Chapter 4. We now consider an IEEE 39 bus system and study the problem of damping of inter-area oscillations in the presence of uncertain PMU measurements and uncertain control inputs by applying the results developed in Chapter 4.

7.1 Case Study: IEEE 39 bus system

Consider the IEEE 39 bus system as shown in Figure. 7.1 which consists of 10 generators and 29 load buses. For the sake of simulation study, generator at bus 39 is considered as a reference bus. The power network model is obtained as discussed in Section 3.1 and includes the PSS controller (local) and SVC, a FACTS device. The PSS at each generator is designed using following parameter values from Jabr et al. (2010), $k_{pss} = 12, T_n = 0.1, T_d = 0.01, T_w = 3$ (please refer to Eq. (3.1) for parameter definitions).

7.1.1 Coherent Groups of Generators

The coherent groups of generators in the power network can be identified by eigen value analysis of linear power network model described in Eq. (3.2). The corresponding eigen vector plots are shown as polar plots in Figure. 7.2. There are 4 dominant inter-area modes and their oscillation frequency and damping coefficients corresponding to each mode are given in Table 7.1. A wide

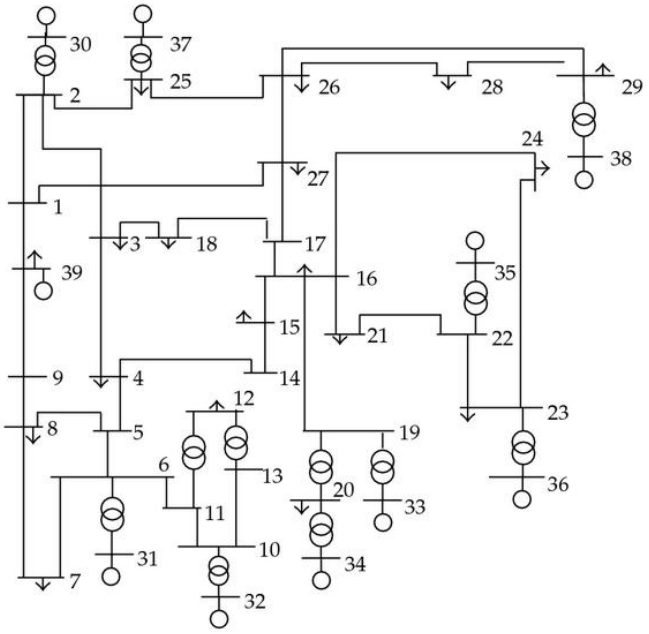

Figure 7.1 Single-line diagram of IEEE 39 bus system

area controller designed with the help of PMU measurements can induce additional damping in the power network and can damp the inter-area oscillations.

Table 7.1 Dominant inter-area modes

Eigen value	Coherent group	Frequency (Hz)	Damping
$-0.3192 \pm 4.9181i$	2,5 vs 1,3,4,6-9	0.7844	0.0648
$-0.4096 \pm 3.9581i$	6 vs 1-5,7-9	0.6333	0.1029
$-0.3153 \pm 3.0503i$	2-5 vs 1,6-9	0.4881	0.1028
$-0.2395 \pm 2.5276i$	8 vs 1-7,9	0.4041	0.0943

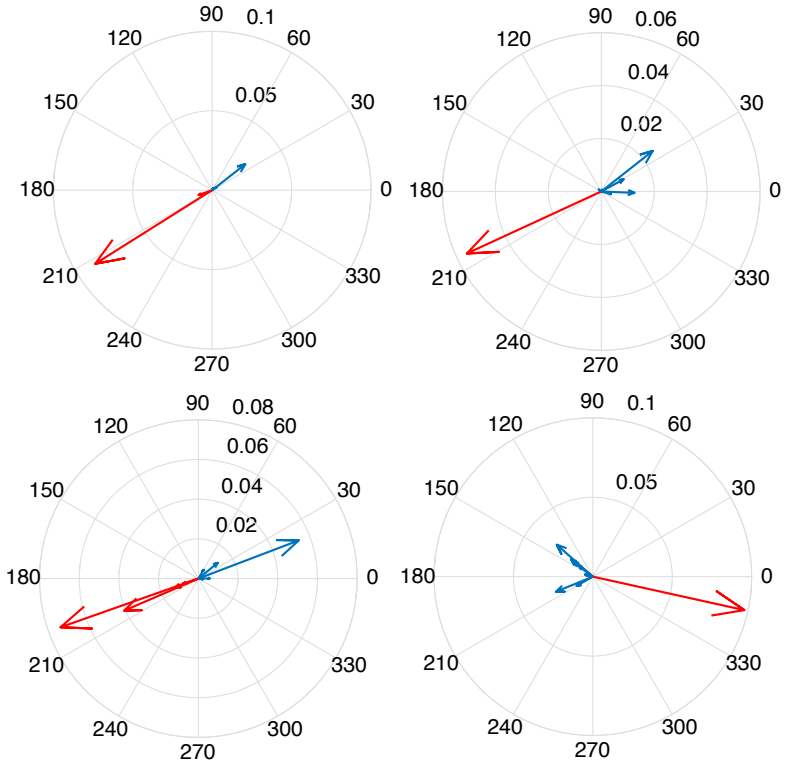

Figure 7.2 Inter area modes in NE 39 bus network

7.1.2 Critical PMU Measurements and Wide Area Control Inputs

Following the modeling of power network given in subsection 3.3, the PMU measurements and the wide area control inputs are modeled as stochastic uncertainty. Further, we make the assumption that the variance of uncertainty in all channels is the same and is equal to σ^2.

Now, applying the results from Section 4.3, we can find the critical measurements, critical control inputs and finally, we can compare their criticality based on identifying the critical variance that can be tolerated by stochastic uncertainty in each channel. We assume PMUs measure the angular velocity ω of generators and these measurements, wide area control inputs are modeled with stochastic uncertainty as shown in subsection 3.3.

To identify their criticality, we consider stochastic uncertainty in each measurement and each control input at a time and the critical variance, σ_*^2 corresponding to each channel is computed. The channel is termed most critical if it can tolerate least σ_*^2. Table 7.2 shows the normalized value of critical variance, σ_*^2 each PMU can tolerate. We notice that the PMU measurement at generator 32 is most critical. Similar simulations for the wide area control inputs yields, the control inputs to generator $31, 34$ and 37 are the most critical. Figure 7.3 show the location of critical PMUs and critical wide area control inputs on a single-line diagram of IEEE 39 bus. Further, Table 7.3 shows the normalized value of critical variance for control inputs to the generators.

Table 7.2 Critical variance tolerated by each PMU

PMU	30	31	32	33	34	35	36	37	38	39
Critical variance	0.1	0.04	0.01	0.14	0.04	0.07	0.05	0.18	0.08	1

Table 7.3 Critical variance tolerated by each control input

Control input	30	31	32	33	34	35	36	37	38	39
Critical variance	0.01	9×10^{-4}	0.02	0.01	7×10^{-4}	0.14	0.28	8×10^{-4}	0.006	1

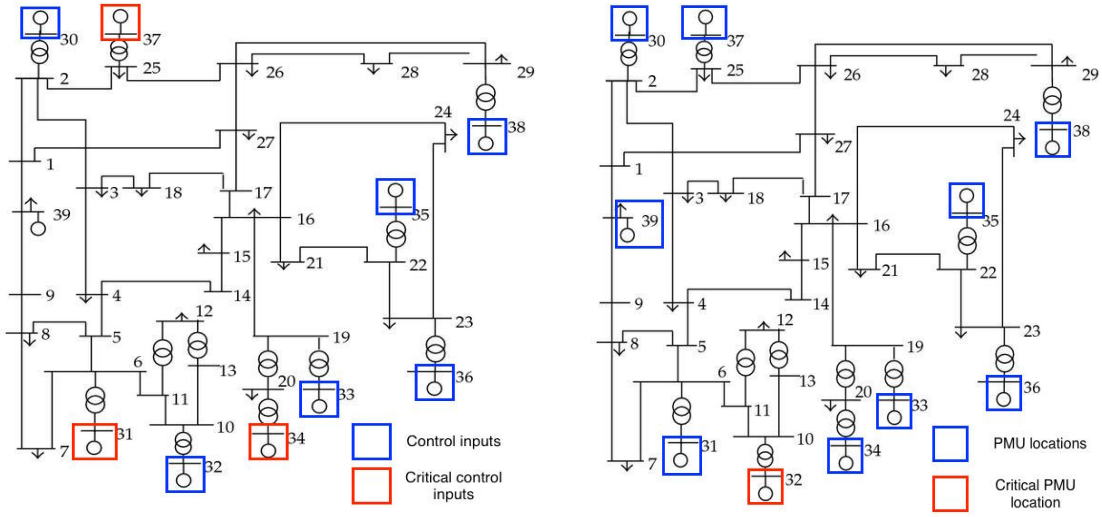

Figure 7.3 Critical PMU and wide area control input locations

7.1.3 Robust Wide Area Control

The PMU measurements from the power network and wide area control inputs to the power network are considered with stochastic uncertainty as it can model a malicious data attack or inherent communication channel noise. We model this uncertainty in input and output channels as a Gaussian distribution. The challenging part of the analysis is that the noise enters the system dynamics multiplicatively as well as additively. A dynamic controller of the size of the system is designed based on LMI-based optimization as shown in Theorem 19 such that the closed loop system is second moment bounded. The LMI-based optimization problem is solved in Matlab using Mosek solver and YALMIP (refer Löfberg (2004)). The outputs were chosen to be ω states of generators from PMU measurements. This dynamic controller is the wide area control that induces additional damping in the network to counteract the inter-area oscillations.

Furthermore, using the mean square stability results from Section 4.3, the critical variance is identified to be $\sigma_*^2 = 2.37$. Any value of σ^2 above the critical variance, σ_*^2, the system is mean square unstable. Figures 7.4(a) and 7.4(b), show the time domain simulation results with PSS and

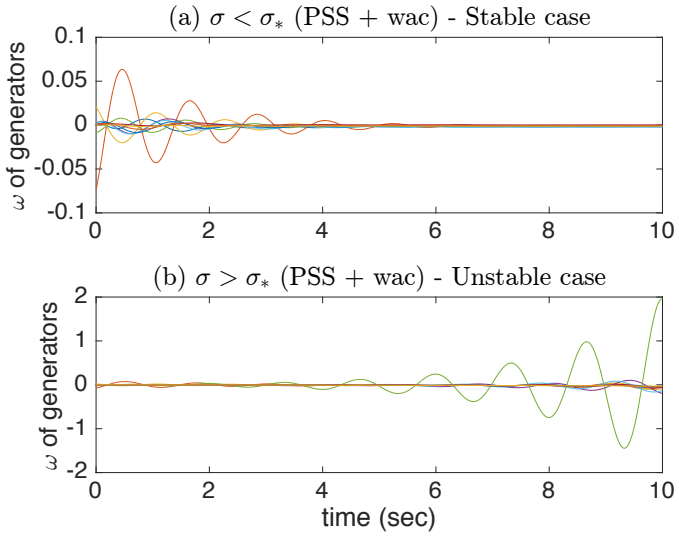

Figure 7.4 Time variation of generator angular velocities with different choice of uncertainties.

wide area controller for value of $\sigma^2 < \sigma_*^2$ and $\sigma^2 > \sigma_*^2$ respectively. From Figure. 7.4(b), we notice that the time domain trajectories grow unbounded for value of $\sigma^2 > \sigma_*^2$. In all these time-domain simulations, an additive noise of variance, 8×10^{-4} is added to amplify the effect of multiplicative noise on system dynamics. Further, these time-domain simulations are run over 25 realizations to obtain consistent results.

The LMI-based wide area controller designed here provides robustness to the uncertainty in measurements and control inputs. To verify the robustness of the proposed framework, we also design a non-robust controller based on the observer and compare the critical variance with respect to both the controllers. Figures 7.5(a) & 7.5(b) show the trace of steady state covariance against standard deviation for both the cases. The red dotted line in the plots corresponds to the critical standard deviation, σ_*. The value of σ_* for the robust controller is 1.5424 and for the non-robust controller, it is 1.2517. It is assumed that the variance in all channels is the same.

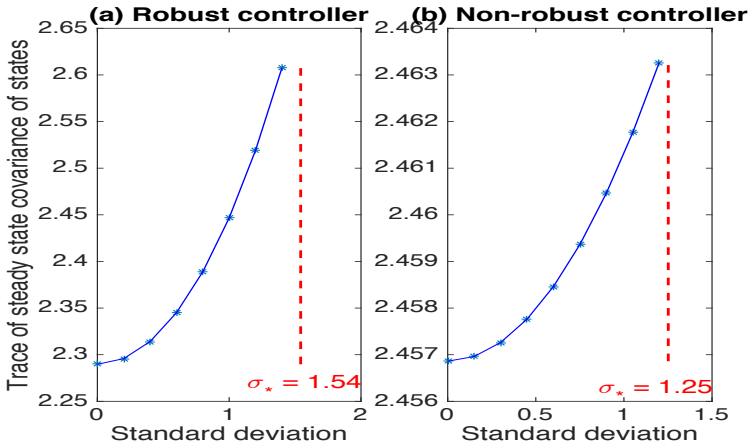

Figure 7.5 Variation of trace of steady state covariance with standard deviation (a) robust controller (b) non-robust controller

CHAPTER 8. CONCLUSION

8.1 Concluding Remarks

We have developed the stochastic power network model where the stochastic uncertainty arises due to the presence of intermittent and unreliable wind energy and communication channel uncertainties. Specifically, we have shown that, when the wind speed is uncertain, the resultant power network dynamics is stochastic and the stochastic uncertainty appears multiplicative in the system dynamics. We have also modeled the power network with uncertainty in PMU measurements to the control center and wide area control inputs to the power network. The challenging part of the stochastic stability analysis of the power network is that the uncertainty appears multiplicative as well as additive in the system dynamics. We have expressed the stochastic power network dynamics as a networked control system with uncertainty and then developed the mean square exponential stability analysis of such systems.

The developed framework is more general and can be applied to analyze the stability of any stochastic continuous-time linear stochastic networked systems. In particular, we developed the necessary and sufficient conditions for the mean square exponential stability that can also be expressed as a spectral radius condition. These results generalize the deterministic continuous-time small-gain theorem results to continuous-time stochastic systems. Further, these mean square exponential stability result can be equivalently represented as an LMI-based optimization problem minimizing the mean square norm of the stochastic system. This LMI-based optimization problem is leveraged to synthesize a robust controller of the size of the system. Further, we presented a fundamental limitation result which relates the unstable eigenvalues of the system with the critical variance that can be tolerated in the input channel for the special class of systems with single input full state feedback.

The system theoretic framework developed in this work is then applied to study the mean square exponential stability of stochastic power network where the stochastic uncertainty arises due to the presence of renewables or communication channel uncertainties. An IEEE 68 bus system is chosen as a test case to show the fragility of the decentralized load-side frequency controller in the presence of uncertain wind. We observe that the value of critical variance that can be tolerated in the bus voltages is very small and hence, the decentralized controller is very fragile. Also, we notice that with an increase in the cost of controllable loads and with the increase in penetration of wind farms, the critical variance value decreases. Finally, we propose a frequency controller that is robust to stochastic bus voltages.

Furthermore, we consider a detailed higher order nonlinear DAE model for the power network with stochastic renewables and apply the proposed framework of mean square exponential stability to study the stochastic small signal stability of the power network. The controllable loads are modeled into the power network to provide frequency regulation services in the presence of intermittent and unreliable wind. It is seen that the load-side primary frequency control based on the control with neighborhood communication outperforms the decentralized one. Furthermore, we studied the maximum allowable penetration of wind generation in an IEEE 39 bus system using the actual wind speed data. In particular, we show the stochastic small-signal stability of IEEE 39 bus system with maximum allowable penetration of renewables using the statistics of actual wind and validate them through linear and nonlinear time-domain simulations. Future work involves applying the proposed robust control strategy for load-side frequency controller which gives more robustness to uncertainty in comparison to control with neighborhood communication.

Finally, we considered the problem of damping the inter-area oscillations in the presence of noisy measurements from PMUs. Each generator in the power network is modeled with a third order model and power system stabilizer is used as a local control. An LMI-based optimization formulation is proposed to design a stabilizing wide-area controller robust to the noisy PMU measurements. The proposed framework is applied to identify the critical variance that can be tolerated in PMU measurement while maintaining the mean square exponential stability of the network. The

developed framework is applied to analyze the IEEE 39 bus power network. The critical variance the system can tolerate with uncertain PMU measurements is computed based on the proposed analytical framework. Finally, we identified the critical PMU measurements and wide area control inputs in an IEEE 39 bus system.

8.2 Publications

Journal Publications

1. Sai Pushpak Nandanoori, Amit Diwadkar, and Umesh Vaidya. "Mean Square Stability Analysis of Stochastic Continuous-time Linear Networked Systems." In preprint April 2018, IEEE Transactions on Automatic Control.

Conference Publications

1. Sai Pushpak Nandanoori, Umesh Vaidya, and Subhonmesh Bose. "On the Stochastic Small-Signal Stability of an Electric Power Network with Uncertain Wind." In Conference on Probabilistic Methods Applied to Power Systems (PMAPS), IEEE, June 2018.

2. Sai Pushpak Nandanoori, Keivan Ebrahimi, and Umesh Vaidya. "Distributed optimization via primal-dual gradient dynamics with stochastic interactions." In Indian Control Conference (ICC). 2018, pp. 18-23. IEEE, 2018.

3. Sai Pushpak Nandanoori, and Umesh Vaidya. "Fragility of decentralized load-side frequency control in stochastic environment." In American Control Conference (ACC), 2017, pp. 1079-1084. IEEE, 2017.

4. Sai Pushpak Nandanoori, and Umesh Vaidya. "Control of inter-area oscillation with noise corrupted wide area measurement." In American Control Conference (ACC), 2016, pp. 7498-7503. IEEE, 2016.

5. Sai Pushpak Nandanoori, Amit Diwadkar, and Umesh Vaidya. "Stability analysis and controller synthesis for continuous-time linear stochastic systems." In Decision and Control (CDC), 2015 IEEE 54th Annual Conference on, pp. 3792-3797. IEEE, 2015.

6. Sai Pushpak Nandanoori, Amit Diwadkar, and Umesh Vaidya. "Vulnerability analysis of dynamical power networks to stochastic link failure attacks." In Proceedings of the 18th International Conference on Hybrid Systems: Computation and Control, pp. 219-226. ACM, 2015.

7. Sai Pushpak Nandanoori, Hemanshu Pota, and Umesh Vaidya. "Power sharing in microgrids with minimum communication control." In Power & Energy Society General Meeting, 2015 IEEE, pp. 1-5. IEEE, 2015.

8. Sai Pushpak Nandanoori, Amit Diwadkar, Makan Fardad, and Umesh Vaidya. "Vulnerability analysis of large-scale dynamical networks to coordinated attacks." In Control Conference (AUCC), 2014 4th Australian, pp. 89-94. IEEE, 2014.

BIBLIOGRAPHY

Anderson, P. M. and Fouad, A. A. (2008). *Power system control and stability*. John Wiley & Sons.

Andreasson, M., Dimarogonas, D. V., Johansson, K. H., and Sandberg, H. (2013). Distributed vs. centralized power systems frequency control. In *2013 12th European Control Conference, ECC 2013; Zurich; Switzerland; 17 July 2013 through 19 July 2013*, pages 3524–3529.

Andreasson, M., Dimarogonas, D. V., Sandberg, H., and Johansson, K. H. (2014). Distributed control of networked dynamical systems: Static feedback, integral action and consensus. *IEEE Transactions on Automatic Control*, 59(7):1750–1764.

Arnold, L. (2013). *Random dynamical systems*. Springer Science & Business Media.

Bamieh, B. (2012). Structured stochastic uncertainty. In *Communication, Control, and Computing (Allerton), 2012 50th Annual Allerton Conference on*, pages 1498–1503. IEEE.

Bashash, S. and Fathy, H. K. (2013). Modeling and control of aggregate air conditioning loads for robust renewable power management. *IEEE Transactions on Control Systems Technology*, 21(4):1318–1327.

Berglund, N. and Gentz, B. (2003). Geometric singular perturbation theory for stochastic differential equations. *Journal of differential equations*, 191(1):1–54.

Bernstein, D. (1987). Robust static and dynamic output-feedback stabilization: deterministic and stochastic perspectives. *IEEE Transactions of Automatic Control*, 32:1076–1084.

Bian, X., Geng, Y., Lo, K. L., Fu, Y., and Zhou, Q. (2016). Coordination of psss and svc damping controller to improve probabilistic small-signal stability of power system with wind farm integration. *IEEE Transactions on Power Systems*, 31(3):2371–2382.

Bu, S., Du, W., Wang, H., Chen, Z., Xiao, L., and Li, H. (2012). Probabilistic analysis of small-signal stability of large-scale power systems as affected by penetration of wind generation. *IEEE Transactions on Power Systems*, 27(2):762–770.

Callaway, D. S. and Hiskens, I. A. (2011). Achieving controllability of electric loads. *Proceedings of the IEEE*, 99(1):184–199.

Chakrabortty, A. and Khargonekar, P. P. (2012). Introduction to wide area monitoring and control. http://people.engr.ncsu.edu/achakra2/wacs.pdf.

Chakrabortty, A. and Khargonekar, P. P. (2013). Introduction to wide-area control of power systems. In *American Control Conference*, pages 6758–6770. IEEE.

Chaudhuri, B., Majumder, R., and Pal, B. C. (2004). Wide-area measurement-based stabilizing control of power system considering signal transmission delay. *IEEE Transactions on Power Systems*, 19(4):1971–1979.

Chaudhuri, N. R., Chakraborty, D., and Chaudhuri, B. (2011). An architecture for facts controllers to deal with bandwidth-constrained communication. *IEEE Transactions on Power Delivery*, 26(1):188–196.

Chow, J. and Rogers, G. (2000). Power system toolbox. *Cherry Tree Scientific Software,[Online] Available: http://www. ecse. rpi. edu/pst/PST. html*, 48:53.

Chow, J. H. and Cheung, K. W. (1992). A toolbox for power system dynamics and control engineering education and research. *IEEE transactions on Power Systems*, 7(4):1559–1564.

Costa, O. L. V., Fragoso, M. D., and Marques, R. P. (2006). *Discrete-time Markov Jump Linear Systems*. Springer Science & Business Media.

Dasgupta, S., Paramasivam, M., Vaidya, U., and Ajjarapu, V. (2013). Real-time monitoring of short term voltage stability using pmu data. *IEEE Transactions on Power Systems*, 28:3702–3711.

Dasgupta, S., Paramasivam, M., Vaidya, U., and Ajjarapu, V. (2015). PMU-based model-free approach for real-time rotor angle monitoring. *IEEE Transactions on Power Systems*, 30(5):2818–2819.

De La Ree, J., Centeno, V., Thorp, J. S., and Phadke, A. G. (2010). Synchronized phasor measurement applications in power systems. *IEEE Transactions on Smart Grid*, 1(1):20–27.

Deng, H. and Krstić, M. (2000). Output-feedback stabilization of stochastic nonlinear systems driven by noise of unknown covariance. *Systems & Control Letters*, 39:173–182.

Deng, H., Krstić, M., and Williams, R. J. (2001). Stabilization of stochastic nonlinear systems driven by noise of unknown covariance. *IEEE Transactions of Automatic Control*, 46:1237–1253.

Diwadkar, A., Dasgupta, S., and Vaidya, U. (2014). Stochastic positive real lemma and synchronization over uncertain network. In *53rd IEEE Conference on Decision and Control (CDC)*, pages 4560–4565. IEEE.

Diwadkar, A., Dasgupta, S., and Vaidya, U. (2015). Control of systems in Lure form over erasure channels. *International Journal of Robust and Nonlinear Control*, 25(15):2787–2802.

Diwadkar, A. and Vaidya, U. (2011). Robust synchronization in nonlinear network with link failure uncertainty. In *50th IEEE Conference on Decision and Control and European Control Conference (CDC-ECC)*, pages 6325–6330. IEEE.

Diwadkar, A. and Vaidya, U. (2013). Limitations for nonlinear observation over erasure channel. *IEEE Transactions on Automatic Control*, 58(2):454–459.

Diwadkar, A. and Vaidya, U. (2014). Stabilization of linear time varying systems over uncertain channels. *International Journal of Robust and Nonlinear Control*, 24(7):1205–1220.

Diwadkar, A. and Vaidya, U. (2016). Limitations and tradeoffs in synchronization of large-scale networks with uncertain links. *Scientific reports*, 6:1–11.

Donnelly, M., Harvey, D., Munson, R., and Trudnowski, D. (2010). Frequency and stability control using decentralized intelligent loads: Benefits and pitfalls. In *Power and Energy Society General Meeting, 2010 IEEE*, pages 1–6. IEEE.

Dörfler, F., Simpson-Porco, J. W., and Bullo, F. (2016). Breaking the hierarchy: Distributed control and economic optimality in microgrids. *IEEE Transactions on Control of Network Systems*, 3(3):241–253.

Dotta, D., e Silva, A. S., and Decker, I. C. (2009). Wide-area measurements-based two-level control design considering signal transmission delay. *IEEE Transactions on Power Systems*, 24(1):208–216.

Dragan, V., Halanay, A., and Stoica, A. (1997). A small gain theorem for linear stochastic systems. *Systems & Control Letters*, 30(5):243–251.

Dullerud, G. E. and Paganini, F. (2013). *A course in robust control theory: a convex approach*, volume 36. Springer Science & Business Media.

Drfler, F., Jovanovi, M. R., Chertkov, M., and Bullo, F. (2014). Sparsity-promoting optimal wide-area control of power networks. *IEEE Transactions on Power Systems*, 29(5):2281–2291.

El Bouhtouri, A. and Pritchard, A. (1992). Stability radii of linear systems with respect to stochastic perturbations. *Systems & Control Letters*, 19(1):29–33.

El Bouhtouri, A. and Pritchard, A. (1993). A Riccati equation approach to maximizing the stability radius of a linear system by state feedback under structured stochastic Lipschitzian perturbations. *Systems & Control Letters*, 21:475–484.

El Ghaoui, L. (1995). State-feedback control of systems with multiplicative noise via linear matrix inequalities. *Systems & Control Letters*, 24(3):223–228.

Elia, N. (2005). Remote stabilization over fading channels. *Systems & Control Letters*, 54:237–249.

Elia, N., Wang, J., and Ma, X. (2013). *Mean Square Limitations of Spatially Invariant Networked Systems*, volume 499, pp 357-378. Control of Cyber-Physical Systems: Lecture Notes in Control and Information Sciences.

Fan, Z. (2012). A distributed demand response algorithm and its application to phev charging in smart grids. *IEEE Transactions on Smart Grid*, 3(3):1280–1290.

Florchinger, P. (1995). Lyapunov like techniques for stochastic stability. *SIAM Journal on Control and Optimization*, 33:1151–1169.

Gautam, D., Vittal, V., and Harbour, T. (2009). Impact of increased penetration of dfig-based wind turbine generators on transient and small signal stability of power systems. *IEEE Transactions on Power Systems*, 24(3):1426–1434.

Ghaoui, L. E. (1995). State-feedback control of systems with multiplicative noise via linear matrix inequalities. *Systems & Control Letters*, 24:223–228.

Han, X. and Kloeden, P. E. (2017). *Random Ordinary Differential Equations and Their Numerical Solution*. Springer.

Has'minskiĭ, R. Z. (1980). *Stochastic Stability of Differential Equations*. Sijthoff & Noordhoff, Germantown, MD.

Horn, R. A. and Johnson, C. R. (2012). *Matrix analysis*. Cambridge university press.

Imkeller, P. and Lederer, C. (2002). The cohomology of stochastic and random differential equations, and local linearization of stochastic flows. *Stochastics and Dynamics*, 2(02):131–159.

Information Trust Institute (2018). Illinois center for a smarter electric grid (icseg). http://icseg.iti.illinois.edu/power-cases/.

Jabr, R., Pal, B., Martins, N., and Ferraz, J. (2010). Robust and coordinated tuning of power system stabiliser gains using sequential linear programming. *IET generation, transmission & distribution*, 4(8):893–904.

Jiang, H., Liu, H., Wu, L., and Xu, H. (2016). Literature review of power system stochastic stability. In *Probabilistic Methods Applied to Power Systems (PMAPS), 2016 International Conference on*, pages 1–4. IEEE.

L. Schenato and B. Sinopoli and M. Franceschetti and K. Poolla and S. Sastry (2007). Foundations of control and estimation over lossy networks. *Proceedings of the IEEE*, 95(1):163–187.

Lasota, A. and Mackey, M. C. (1994). *Chaos, Fractals, and Noise: Stochastic Aspects of Dynamics*. Springer-Verlag, New York.

Lian, J., Marinovici, L., Kalsi, K., Du, P., and Elizondo, M. (2012). Distributed hierarchical control of multi-area power systems with improved primary frequency regulation. In *Decision and Control (CDC), 2012 IEEE 51st Annual Conference on*, pages 444–449. IEEE.

Liu, C., Thorp, J. S., Lu, J., Thomas, R. J., and Chiang, H. (1994). Detection of transiently chaotic swings in power systems using real-time phasor measurements. *IEEE Transactions on Power Systems*, 9:1285–1292.

Löfberg, J. (2004). Yalmip: A toolbox for modeling and optimization in matlab. In *Computer Aided Control Systems Design, 2004 IEEE International Symposium on*, pages 284–289. IEEE.

Lu, J. and Skelton, R. E. (2002). Mean-square small gain theorem for stochastic control: Discrete-time case. *IEEE Transactions of Automatic Control* , 47(3):490–494.

Mallada, E., Zhao, C., and Low, S. (2017). Optimal load-side control for frequency regulation in smart grids. *IEEE Transactions on Automatic Control*, 62(12):6294–6309.

Martin, K., Brunello, G., et al. (2014). An Overview of the IEEE Standard C37. 118.2–Synchrophasor Data Transfer for Power Systems. *IEEE Transactions on Smart Grid*, 5(4):1980–1984.

Mathieu, J. L., Koch, S., and Callaway, D. S. (2013). State estimation and control of electric loads to manage real-time energy imbalance. *IEEE Transactions on Power Systems*, 28(1):430–440.

Mclane, P. J. (1971). Optimal stochastic control of linear systems with state-and control-dependent disturbances. *IEEE Transactions on Automatic Control*, 16(6):793–798.

Molina-Garcia, A., Bouffard, F., and Kirschen, D. S. (2011). Decentralized demand-side contribution to primary frequency control. *IEEE Transactions on Power Systems*, 26(1):411–419.

N. Elia and J. N. Eisenbeis (2011). Limitations of linear control over packet drop networks. *IEEE Transactions on Automatic Control*, 56(4):826–841.

Naduvathuparambil, B., Valenti, M., Feliachi, A., et al. (2002). Communication delays in wide-area measurement systems. In *Southeastern Symposium on System Theory*, volume 34, pages 118–122. Citeseer.

Namerikawa, T. and Kato, T. (2011). Distributed load frequency control of electrical power networks via iterative gradient methods. In *2011 50th IEEE Conference on Decision and Control and European Control Conference*, pages 7723–7728. IEEE.

N.C. Martins, M.A. Dahleh, and N.Elia (2006). Feedback stabilization of uncertain systems in the presence of a direct link. *IEEE Transactions on Automatic Control*, 51(3):438–447.

Pan, Y., Mei, S., Liu, F., Wei, W., Shen, C., and Hu, J. (2016). Admissible region of large-scale uncertain wind generation considering small-signal stability of power systems. *IEEE Transactions on Sustainable Energy*, 7(4):1611–1623.

Pappala, V. S., Erlich, I., Rohrig, K., and Dobschinski, J. (2009). A stochastic model for the optimal operation of a wind-thermal power system. *IEEE Transactions on Power Systems*, 24(2):940–950.

Pulgar Painemal, H. A. (2011). *Wind farm model for power system stability analysis*. PhD thesis, University of Illinois at Urbana-Champaign.

Pushpak, S., Diwadkar, A., and Vaidya, U. (2015). Stability analysis and controller synthesis for continuous-time linear stochastic systems. In *2015 54th IEEE Conference on Decision and Control (CDC)*, pages 3792–3797. IEEE.

Pushpak, S., Diwadkar, A., and Vaidya, U. (2016). Stochastic stability analysis and synthesis of continuous-time linear networked systems. *arXiv preprint*.

Pushpak, S. and Vaidya, U. (2016). Control of inter-area oscillation with noise corrupted wide area measurement. In *American Control Conference (ACC), 2016*, pages 7498–7503. IEEE.

Rogers, G. (2012). *Power system oscillations*. Springer Science & Business Media.

Rotea, M. A. (1993). The generalized $\mathcal{H}_2$ control problem. *Automatica*, 29(2):373–385.

Rueda, J. L., Colomé, D. G., and Erlich, I. (2009). Assessment and enhancement of small signal stability considering uncertainties. *IEEE Transactions on power systems*, 24(1):198–207.

Sauer, P. W. and Pai, M. (1998a). Power system dynamics and stability. *Urbana*.

Sauer, P. W. and Pai, M. (1998b). Power system dynamics and stability. *Urbana*.

Scherer, C., Gahinet, P., and Chilali, M. (1997). Multiobjective output-feedback control via LMI optimization. *IEEE Transactions on Automatic Control*, 42(7):896–911.

Shayeghi, H., Shayanfar, H., and Jalili, A. (2009). Load frequency control strategies: A state-of-the-art survey for the researcher. *Energy Conversion and management*, 50(2):344–353.

Short, J. A., Infield, D. G., and Freris, L. L. (2007). Stabilization of grid frequency through dynamic demand control. *IEEE Transactions on power systems*, 22(3):1284–1293.

Singh, A. K., Singh, R., and Pal, B. C. (2015). Stability analysis of networked control in smart grids. *IEEE Transactions on Smart Grid*, 6(1):381–390.

Skogestad, S. and Postlethwaite, I. (2007). *Multivariable Feedback Control: Analysis and Design*, volume 2. Wiley New York.

Slootweg, J. and Kling, W. (2003a). The impact of large scale wind power generation on power system oscillations. *Electric Power Systems Research*, 67(1):9–20.

Slootweg, J. and Kling, W. (2003b). The impact of large scale wind power generation on power system oscillations. *Electric Power Systems Research*, 67(1):9–20.

staff report, F. E. R. C. (2006). Assessment of demand response and advanced metering. In *United States Department of Energy*.

Strand, J. (1970). Random ordinary differential equations. *Journal of Differential Equations*, 7(3):538–553.

Takle, G., Rajewski, D., Purdy, S., and Herzmann, D. (2018). Iowa Environmental Mesonet. https://mesonet.agron.iastate.edu/plotting/auto/?_wait=no&q=158&station=ETTI4. Online; accessed 10 June 2018.

Tatikonda, S. and Mitter, S. (2004). Control over noisy channels. *IEEE Transactions on Automatic Control*, 49:1196–1201.

Terzija, V., Valverde, G., Cai, D., Regulski, P., Madani, V., Fitch, J., Skok, S., Begovic, M. M., and Phadke, A. (2011). Wide-area monitoring, protection, and control of future electric power networks. *Proceedings of the IEEE*, 99(1):80–93.

Trudnowski, D., Donnelly, M., and Lightner, E. (2006). Power-system frequency and stability control using decentralized intelligent loads. In *2005/2006 IEEE/PES Transmission and Distribution Conference and Exhibition*, pages 1453–1459. IEEE.

V. Gupta and B. Hassibi and R. M. Murray (2007). Optimal LQG control across packet-dropping links. *System & Control Letters*, 56(6):439–446.

Vaidya, U. and Elia, N. (2010). Limitations of nonlinear stabilization over erasure channels. In *49th IEEE Conference on Decision and Control (CDC)*, pages 7551–7556. IEEE.

Vaidya, U. and Elia, N. (2012). Limitation on nonlinear stabilization over packet-drop channels: Scalar case. *Systems & Control Letters*, 61(9):959–966.

Vicente, W. B., Caire, R., and Hadjsaid, N. (2017). Stochastic simulations and stability to determine maximum wind power penetration of an island network. In *Power & Energy Society General Meeting, 2017 IEEE*, pages 1–5. IEEE.

Wang, S., Meng, X., and Chen, T. (2012). Wide-area control of power systems through delayed network communication. *IEEE Transactions on Control Systems Technology*, 20(2):495–503.

Wang, W., Xu, Y., and Khanna, M. (2011). A survey on the communication architectures in smart grid. *Computer Networks*, 55(15):3604–3629.

Wang, Z., Shen, C., and Liu, F. (2016). Probabilistic analysis of small signal stability for power systems with high penetration of wind generation. *IEEE Transactions on Sustainable Energy*, 7(3):1182–1193.

Willems, J. C. and Blankenship, G. L. (1971). Frequency domain stability criteria for stochastic systems. *IEEE Transactions on Automatic Control*, 16(4):292–299.

Willems, J. L. and Willems, J. C. (1976). Feedback stabilizability for stochastic systems with state and control dependent noise. *Automatica*, 12(3):277–283.

Willems, J. L. and Willems, J. C. (1983). Robust stabilization of uncertain systems. *SIAM Journal on Control and Optimization*, 21(3):352–374.

Wonham, W. M. (1967). Optimal stationary control of a linear system with state-dependent noise. *SIAM Journal on Control*, 5(3):486–500.

Xu, Z., Dong, Z., and Zhang, P. (2005). Probabilistic small signal analysis using monte carlo simulation. In *Power Engineering Society General Meeting, 2005. IEEE*, pages 1658–1664. IEEE.

Yan, J., Liu, C.-C., and Vaidya, U. (2011). Monitoring rotor angle stability based on phasor measurement units. *IEEE Transactions on Power Systems*, 26:2125–2133.

Yuan, B., Zhou, M., Li, G., and Zhang, X.-P. (2015). Stochastic small-signal stability of power systems with wind power generation. *IEEE Transactions on Power Systems*, 30(4):1680–1689.

Zhang, W., Lian, J., Chang, C.-Y., and Kalsi, K. (2013). Aggregated modeling and control of air conditioning loads for demand response. *IEEE transactions on power systems*, 28(4):4655–4664.

Zhao, C., Mallada, E., and Low, S. H. (2015). Distributed generator and load-side secondary frequency control in power networks. In *Information Sciences and Systems (CISS), 2015 49th Annual Conference on*, pages 1–6. IEEE.

Zhao, C., Topcu, U., Li, N., and Low, S. (2014a). Design and stability of load-side primary frequency control in power systems. *IEEE Transactions on Automatic Control*, 59(5):1177–1189.

Zhao, C., Topcu, U., Li, N., and Low, S. (2014b). Design and stability of load-side primary frequency control in power systems. *IEEE Transactions on Automatic Control*, 59(5):1177–1189.

Zhao, C., Topcu, U., and Low, S. H. (2013). Optimal load control via frequency measurement and neighborhood area communication. *IEEE Transactions on Power Systems*, 28(4):3576–3587.

NOTATIONS

Notations used in Chapter 2

The notations used in modeling the power network with uncertain wind speeds described in Chapter 2 are given here. The index i corresponds to either a SG or a DFIG.

E'_{q_i}, E'_{d_i} - quadrature and direct-axis transient internal voltage at SG i

δ_i, ω_i - phase angle and angular velocity of the SG i

E_{fd_i} - field voltage of SG i

R_{f_i} - rate feedback state of the voltage regulator at SG i

V_{R_i} - voltage regulator state at SG i

P_{m_i} - turbine/governor state at SG i

I_{q_i}, I_{d_i} - quadrature and direct-axis currents induced in the stator of SG i

T_{m_i} - mechanical input applied to the shaft at SG i

ω_s - rated synchronous speed of SG

H_i - inertia constant of SG i

T'_{d0_i}, T'_{q0_i} - quadrature and direct-axis transient time constant of SG i

X_{d_i}, X'_{d_i} - direct-axis salient and transient reactance of SG i

T_{G_i} - time-constant of the speed governor without droop

K_{A_i} - voltage regulator gain of the IEEE type-1 exciter

T_{A_i} - voltage regulator time constant of the IEEE type-1 exciter

K_{E_i} - IEEE type-1 exciter gain

T_{E_i} - time constant of the IEEE type-1 exciter

T_{F_i} - feedback time-constant of the IEEE type-1 exciter

K_{F_i} - IEEE type-1 exciter feedback gain

V_i, θ_i	-	voltage magnitude and angle at bus i
ω_{r_i}	-	angular velocity of DFIG i
z_{1_i}, z_{2_i}	-	state variables related to the speed controller at DFIG i
z_{3_i}, z_{4_i}	-	state variables related to the reactive power controller at DFIG i
V_{qr_i}, V_{dr_i}	-	quadrature- and direct- axis voltage induced in the rotor of DFIG i
I_{qr_i}, I_{dr_i}	-	quadrature- and direct-axis current induced in the rotor of DFIG i
I_{qs_i}, I_{ds_i}	-	quadrature- and direct-axis current induced in the stator of DFIG i
P_{gen_i}	-	total real power generated by DFIG i
Q_{gen_i}	-	total reactive power generated by DFIG i
V_{ref_i}	-	reference voltage at DFIG i
v_{wind}	-	velocity of the wind speed at DFIG i
s_i	-	slip of a DFIG i
K_{P1}, K_{I1}	-	proportional and integral gains of the speed controller's slow loop
K_{P2}, K_{I2}	-	proportional and integral gains of the speed controller's fast loop
K_{P3}, K_{I3}	-	proportional and integral gains of the reactive power controller's slow loop
K_{P4}, K_{I4}	-	proportional and integral gains of the reactive power controller's fast loop
R_{s_i}	-	stator internal resistance
X_{q_i}	-	quadrature-axis salient reactance

Notations used in Chapter 3

The following notations are used in describing the power network with communication uncertainty as shown in Section 3.1.

δ_i	-	generator phase angle
ω_i	-	angular velocity of the rotor
E_{q_i}	-	quadrature-axis induced emf
E_{fd_i}	-	emf of fast acting exciter connected to the generator
I_{d_i}	-	direct-axis currents induced in the generator
I_{q_i}	-	quadrature-axis currents induced in the generator
V_i	-	voltage magnitude at bus i
θ_i	-	voltage angle at bus i
T_{m_i}	-	mechanical input applied to the generator shaft
V_{ref_i}	-	reference voltage at bus i
ω_s	-	rated synchronous speed
M_i	-	inertia of the generator
R_{s_i}	-	stator internal resistance
X_{q_i}	-	quadrature-axis salient reactance
X_{d_i}	-	direct-axis salient reactance
X'_{d_i}	-	direct-axis transient reactance
K_{A_i}	-	exciter gain
T_{A_i}	-	time constant of the exciter